Master Thesis, Department of Geosciences

Mineralogy and petrology of the amazonite pegmatite at Bakstevalåsen, øvre Eiker

Øyvind Sunde

UNIVERSITY OF OSLO

FACULTY OF MATHEMATICS AND NATURAL SCIENCES

Mineralogy and petrology of the amazonite pegmatite at Bakstevalåsen, øvre Eiker

Øyvind Sunde

Master Thesis in Geosciences

Discipline: Geology

Department of Geosciences

Faculty of Mathematics and Natural Sciences

University of Oslo

July 2013

Supervised by associate prof. Rune S. Selbekk and prof. Tom Andersen

Cover picture: Hand specimen of the amazonite pegmatite at Bakstevalåsen measuring a 15 cm cross-section with amazonite matrix and abundant danalite.

This work is published digitally through DUO – Digitale Utgivelser ved UiO
http://www.duo.uio.no
It is also catalogued in BIBSYS (http://www.bibsys.no/english)

Acknowledgements

This thesis marks the end of a 5 –year period of time with relentless studies at the Department of Geosciences, University of Oslo. There are many people I have met during this 5-year ride who in various ways have contributed in shaping my interest for geology. I have never, ever, regretted my decision on setting sail onto this journey. You all know who you are and a huge thank you! My thesis would not have been possible without the help of several clever individuals, and I would like to aim a special appreciation to the following personnel:

Rune Selbekk: first of all, thank you for letting me volunteer at the natural History Museum during my infant years of studying. It brought more geology into a curriculum diluted with meteorology and philosophy. I never imagined I would end up working with this exciting pegmatite. During my work you have given me free hands and the opportunity to be as independent as possible. It pushed me to think for myself and test my own ideas. Your feedback and talks helped me navigate through a maze of geo-phantasy. I particularly enjoyed some of the discussions we had over a few beers.

Tom Andersen: thank you for always taking your time to explain and discuss confusing issues, and assisting the student seminars. It's been outstanding, and frankly, it was the only source of Proterozoic geology at the department. Your feedback during my time of writing helped clear up my cluttered literacy.

Muriel Erambert: thank you for excellent supervision during my microprobe analysis and the good company during very long hours of analysis. Also, thank you for taking your time with all my silly questions during my time at the department.

Henrik Friis: thank you for your invaluable help with calculations of structural formula, and feedback on several issues. I owe you a beer.

Salahalldin Akhavan: thank you for creating excellent thin sections which I never seem to finish staring at in the microscope.

Mufak Naoroz: for assistance with the crushing equipment at the Department of Geosciences.

Harald Folvik & Hans Jørgen Berg: thank you for assistance and good company on the SEM at the NHM.

My girlfriend Kjersti Jovik: thank you for all your continuous support and care during a hectic period of time. Not to forget; thank you for feeding me and keeping me alive during a frantic period of time when finishing this thesis. Also, thanks to my classmate Steinar Kleppe; you have been a good friend and monkey through our studies these 5 years. You have always challenged me to improve and I will always remember the summers we did fieldwork. Finally, but not least; a big thank you to my family for all your warm support in all my undertakings, and my dad for helping me figure out the old and wrong coordinates during fieldwork.

Abstract

An exotic pegmatite classified as a rare-element gadolinite type amazonite pegmatite is situated in Paleozoic sedimentary rocks, and associated with the peralkaline ekerite granites in the Permian Oslo Region. The amazonite pegmatite is approximately 16 meters long and consists of a coarse-grained, subhedral, green microcline feldspar (amazonite), quartz and danalite. Fine grained fabric with abundant sulphides intersect the coarse grained amazonite several places, and indicates a second generation of mineralization. The danalite has a strong reddish color with an intermediate composition of zinc and iron, i.e. composition along the danalite – genthelvite solid-solution series. Abundant pristine subhedral to euhedral phenakite coexist with danalite, and a boron zone in the pegmatite interior contains abundant danburite, tourmaline, and minor nordenskiöldine. Additional löllingite, gadolinite-(Y), biotite, zircon, columbite-(Fe), pyrochlore group minerals, and fluorite occur throughout the pegmatite body. Other pegmatites in the area contain primarily amphibole, pyroxene, microcline, and quartz. Major element variation of the amazonite pegmatite and its neighbor pegmatites correlate; however, trace-element evolution trends diverge in respect to REE, Nb, Y, and Ta. The amazonite pegmatite is clearly enriched in HREE relative to LREE, while Y, Nb, and Ta contents are significantly higher in the amazonite pegmatite than other pegmatites in the area. This evidence, in conjunction with the high boron- and sulphur-content, indicates an enrichment of the original NYF magma by circulating hydrothermal fluids, and chemical exchange with the sedimentary wall-rocks.

Contents

Introduction

Previous studies on alkaline plutonic rocks in the Oslo region suggest that elevated halogen (fluorine, chlorine) fugacity in magmas and associated fluids is important both for mineral stability (e.g. Andersen et al. 2010) and as a complexing agent promoting element mobility (e.g. Alderton et al. 1980; Salvi & William-Jones, 1996). Similarly, fluid inclusion studies in e.g. the Eikeren-Skrim alkaline complex in the Oslo Rift (Hansteen and Burke, 1990) have indicated high contents of Na, K, S, and Cl in sub-magmatic fluids, and observations of low fluorine content were attributed to leaching by circulating, post-magmatic fluids.

This work presents the results from a study of a rare-element class pegmatite of the NYF family (Černy & Ercit, 2005), and is associated with one of the major alkali granite intrusive complexes in the Oslo Rift, Norway. The aim is to investigate the mineralogy and petrogenesis of the amazonite pegmatite located at Bakstevalåsen in the øvre-Eiker district of Buskerud county. The pegmatite was discovered approximately 15 years ago (Hurum et al., 1998), but limited work has been done since its discovery. This study is based on mineralogy, geochemistry, and textural relations by the use of analytical instruments such as polarizing microscope, scanning electron microscope – energy dispersive (SEM-EDX), electron microprobe analysis (EMPA), and whole-rock chemistry analysis (XRF, ICP-MS).

Geological setting

The Oslo Region

The Oslo Region is a descriptive term referring to the area with well-preserved Palaeozoic rocks situated in a graben system stretching approximately from the Skagerrak in the south to the Brummundal area past lake Mjøsa in the north (Fig. 1). This graben system is related to extensional tectonics which occurred during the late Carboniferous to early Permian in northern Europe, and associated with the Sorgenfrei-Tornquist Zone (Neuman et al., 2004). The graben system consists of three main units; the Vestfold-, Akershus-, and Rendal-Graben, and have opposite polarity along the N-S fault axis; however, the latter is only associated with Permian rift tectonics and not magmatism (Larsen et al. 2008). The Oslo Rift has been studied for almost two centuries (Barth, 1945; Dons, 1978), but the major features and evolution of the Paleorift can be summarized through a succession of events (Larsen et al., 2008; Ramberg & Larsen, 1978; Neumann et al., 2004):

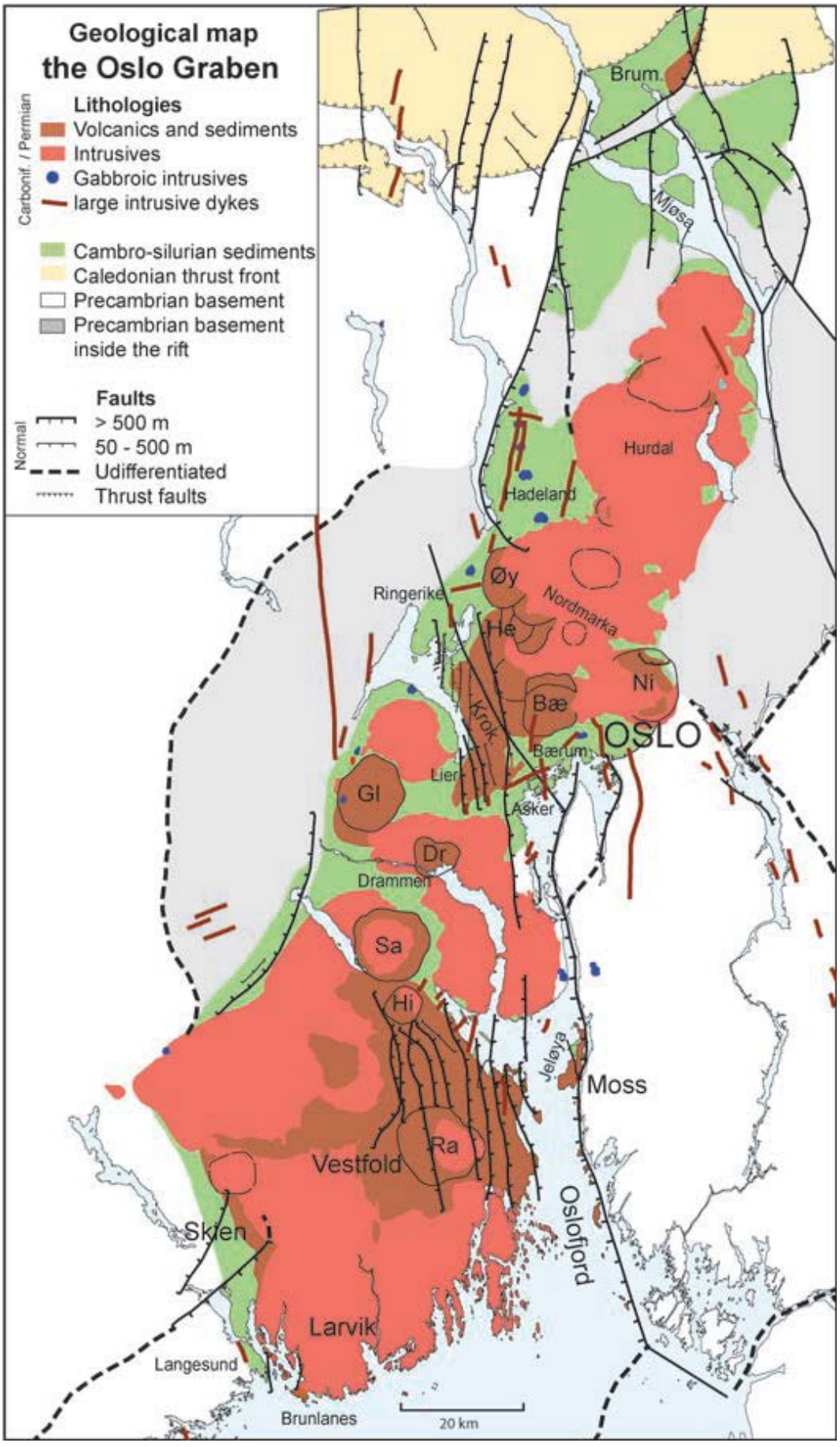

Figure 1 - Simplified geological map of the Oslo Region (Larsen et al., 2008).

Pre-rift stage

The pre-rift stage is marked by a thinning of the crust with subsequent basin formation in response to tensional stress. This led to sedimentation in a shallow lacustrine environment primarily in the SW region of Oslo, and led to sedimentation of the Asker group. The reader is referred to Henningsmoen (1978), Orlaussen et al., (1994), and Larsen et al., (2008) for review on the sedimentary units and basin formation. During stress build-up old Precambrian (Gothian) NE-SW striking fault-lines were probably rejuvenated, and to some degree, a controlling factor in the opening of the rift system (Ramberg & Larsen, 1978; Husbye & Ramberg, 1978). Early magmatic activity is marked by sill intrusions of primarily syenitic compositions (Larsen et al., 2008).

Initial rifting

The initial rifting introduced eruptions of basalt lavas with compositions ranging from silica under-saturation to quartz tholeiitic (Larsen et al., 2008). The early basalts are linked to fissure eruptions in pace with the opening of the Oslo rift, but they are limited to the southern area of the Vestfold Graben. The thickest basalt units are found in the Brunlanes- and Skien area (approximately 800 and 1500 m thickness respectively), while thin tholeiitic flows are found at Krokskogen (Ramberg & Larsen, 1978; Neumann et al. 2004; Larsen et al., 2008). The early basalt eruptions took place between 305 and 299 Ma with the oldest basalts in the south (Neumann et al., 2004).

Main rifting

The main rifting stage is marked by extensive fissure eruptions of primarily rhomb porphyry (RP) lavas and minor basalt. The basalt eruptions probably ceased in intensity and volume, but eruption continued towards the north (Neumann et al., 2004; Larsen et al., 2008). The pulses of RP lava flow form thick provinces and N-S striking dikes. These lava flows are characteristic of low viscosity flows and related to high temperature and fluorine fugacity (Larsen et al., 2008).

Central volcanoes and rift climax

Large central volcanoes formed along the main rift which had fully matured, and stretched from south to north in the Vestfold- and Akershus- Graben. Lava eruptions were primarily alkali-olivine basalts, and gradual depletion of the magma chambers led to caldera collapse which led to a decrease in eruption activity (Ramberg & Larsen, 1979; Neumann et al., 2004; Larsen et al., 2008). During this stage the biotite-granite of the Drammen batholith intruded

into the Vestfold Graben (Trønnes & Brandon, 1992; Larsen et al., 2008) and marks the entry of composite granitic intrusions.

Batholith, composite plutonic complexes

The large composite batholiths occur primarily within the Vestfold Graben and in the south-west of the Akershus Graben. During this stage the majority of plutonic rocks intruded the thinned crust and formed several composite plutonic complexes. The largest complexes are mapped as the Siljan-Mykle-, Eikeren-Skrim-, Finnemarka-Drammen-, and the Hurdal-Nordmarka batholiths (Fig. 2). Present day erosion level is approximately 3 km below the pre-existing Permian surface, and the deep-seated plutonic rocks make up most of the rocks we see in the Oslo Region today. Before solidifying at shallow crustal levels, the batholiths were a likely source of magma for the large central volcanoes before collapse. The lifespan of the Oslo Region in terms of magmatic activity ceased with the intrusion of minor, but separate plutonic bodies between 250 and 245 Ma (Larsen et al., 2008), hence lasting approximately 64 million years.

The Permian batholith complexes in the Oslo Region are made up by successions of plutonic intrusions which range in composition from monzonite and syenite to alkaline granites (e.g. the Grefsen syenite and ekerite). The Larvik plutonic complex (LPC) in the south of the Vestfold Graben ranges in composition through a succession of intrusions. The outer segment is quartz normative, with an intermediate section ranging from quartz and nepheline free, and late silica under saturated inner segments. The central Drammen – Finnemarka batholith are mildly peraluminous and high-silica granites (Trønnes & Brandon, 1992), while the Nordmarka – Hurdal batholith with its related intrusions are alkali-felsdspar syenite quartz alkali-feldspar syenite (Lutro & Nordgulen, 2004).

Basement rocks and intrusion interaction

Basement rocks in and around the Oslo Region consist primarily of Precambrian gneisses with Gothian and Sveconorwegian ages (1.60 – 0.90 Ga) (Andersen et al. 2004). A thick sequence of early Paleozoic (Cambrian, Ordovician, and Silurian) sedimentary rocks are well preserved overlying the basement in the Vestfold- and Akershus-Graben. These sediments consist mainly of marine calcic massive beds and shales, and contain a high amount of fossils (Owen et al., 1990). The sedimentary beds are strongly folded with a NE-SW axial plane, and part of the Caledonian foreland fold- and thrust-basin. Mineral deposits are abundant in the Oslo Region due to intrusion into the Paleozoic sedimentary rocks (e.g. Ihlen & Vokes, 1978).

Several historical important skarn deposits are associated with the biotite granites of the Finnemarka-Drammen pluton, and along the intrusion interface of the Nordmarka pluton. Petrogenetic studies indicate crustal contamination during partial melting and fractional crystallization of the rising magma (e.g. Neumann, 1976; 1977; Rasmussen et al., 1988). Fractionated anorogenic granites are important sources for rare-element pegmatites (Jahns & Burnham, 1969; Černy et al., 1985; London, 1990; Linnen et al., 2012).

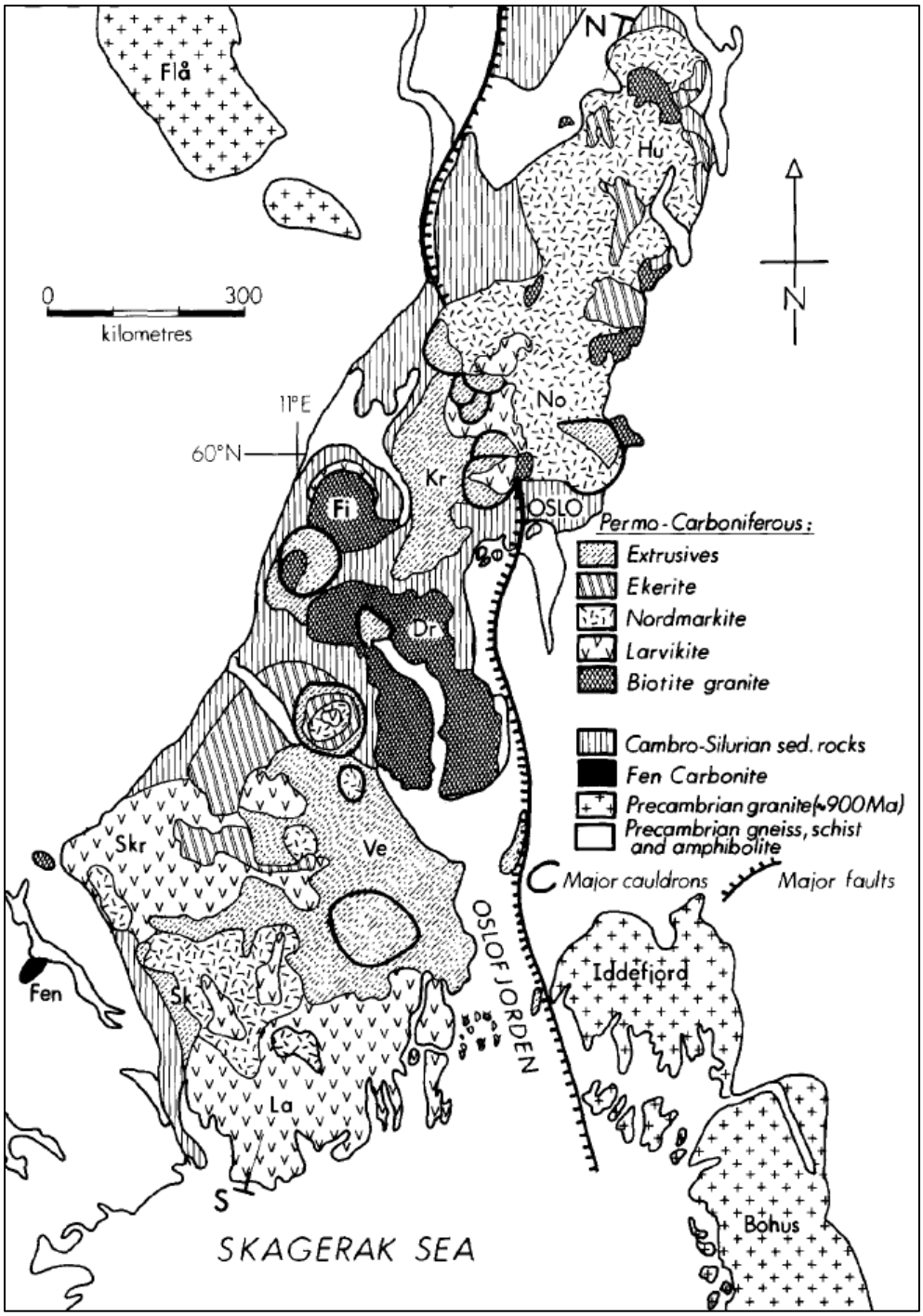

Figure 2 - Simplified geological map of some important plutonic rocks (larvikite, biotite granite, ekerite, and nordmarkite) within the Oslo Region (Trønnes & Brandon, 1991).

Alkaline rocks and their pegmatites

Alkaline granites are associated with the NYF-family (niobium, yttrium, and fluorine) classification of pegmatites (Černy & Ercit, 2005). They are typical poor in boron, tantalum, and phosphor, and the more evolved pegmatites belong to the gadolinite class (Černy 1997;

Černy & Novak, 2012). Fertilized A-type granites (e.g. by fenitization) introduce a host of incompatible elements with increasing alkalinity (e.g. London, 1990; Salvi & William-Jones, 1996). Granitic pegmatites thereby host a vast array of pegmatite compositions which promote a division based on petrogenetic relationship; the NYF family and LCT family (Lithium, Cesium, and Tantalum). The principle behind this classification is to maintain a concise classification based on a distinct chemical signature despite diversity in accessory minerals. However, complex pegmatites may carry mixed NYF + LCT signatures due to contamination and assimilation of sedimentary sources (e.g. I-type granite) (Černy & Ercit, 2005). However, Zagorsky and Shmakin have worked out analogous systematics, which are widely used in Russian literature (Zagorsky et al., 2003; Shmakin, 2008) and are based on the miarogenic evolution, which essentially is a set of classes and subclasses according to mineral assemblage (Zagorsky et al., 2003).

The amazonite pegmatite at Bakstevalåsen contain abundant Be-, Nb-, Y-, and REE-minerals. Fluorite and topaz are typical F- minerals related to NYF suite pegmatites (Černy & Ercit, 2005). However, the amazonite pegmatite also contains boron-, and a wide set of tantalum in primarily pyrochlore, which indicates LCT characteristics.

In Norway, the nepheline syenite pegmatites of the Langesund area with its type localities for mineral species have been extensively studied since the 19th century (Brøgger, 1890; Larsen, 2010 and references therein). However, pegmatites associated with the peralkaline granites have received much less attention. The alkali granite intrusion in the Eikeren district is the likely source of the numerous pegmatites that occur in the Cambro-Silurian limestones as dykes and sills. These pegmatites are mostly simple pegmatites with a mainly albite, quartz, amphibole, and zircon mineralogy. The amazonite pegmatite which is the target of this study was described briefly by Hurum et al. (1997) where a rare mineralogy is observed.

Geology within the study area

The Eikeren – Skrim complex are the youngest of several pluton complexes in the southern part of the paleorift where magmatic activity is believed to have culminated around a mean age of 270±1 Ma (Rasmussen et al., 1980). The intrusion consists of a relatively monotonous, medium- to coarse grained alkali feldspar granite with sodic amphibole and / or pyroxene as characteristic mafic silicate minerals. The rock is thus an alkali granite in modern terminology (LeMaitre et al., 2002), but was given the name ekerite by Brøgger in 1880 after lake Eikeren ("Ekeren" in pre 1930s spelling). The peralkalinity index classifies these rocks as peralkaline

granites carrying riebeckite and arfvedsonite amphiboles. Miarolitic cavities and minor aplite are abundant throughout the ekerite complex and indicate a high volatile content. The miarolitic cavities range in size from small interstices (0.05 – 1 cm) to larger veins and cavities up to ≤ 5 cm (Hansteen and Burke, 1990). Raade (1972; 1980) described the mineralogy and rare fluorides in miarolitic cavities of syenites and alkali granites (although the fluorides are from a separate ekerite intrusion further north).

The study-area is approximately a 1 km^2 between the amazonite pegmatite and ekerite (Fig. 3). The Ekerite massif intrudes into Cambrian - Silurian sedimentary country rocks in the west, and form a sharp and well-defined boarder. The sedimentary rocks in this area are composed of several successions of marine sediments, where the amazonite pegmatite at Bakstevalåsen has intruded into the upper Ordovician limestones as a sill. The sedimentary rocks in the area are heavily contact metamorphosed, and classify as feldspar-cordierite hornfels (Goldschmidt, 1911; Hurum et al., 1997). A large normal fault with a NNE-SSW fault plane offsets the sedimentary sequence adjacent to the ekerite and exposes augen-gneisses of the Proterozoic basement (Jahren & Hurum, 1997).

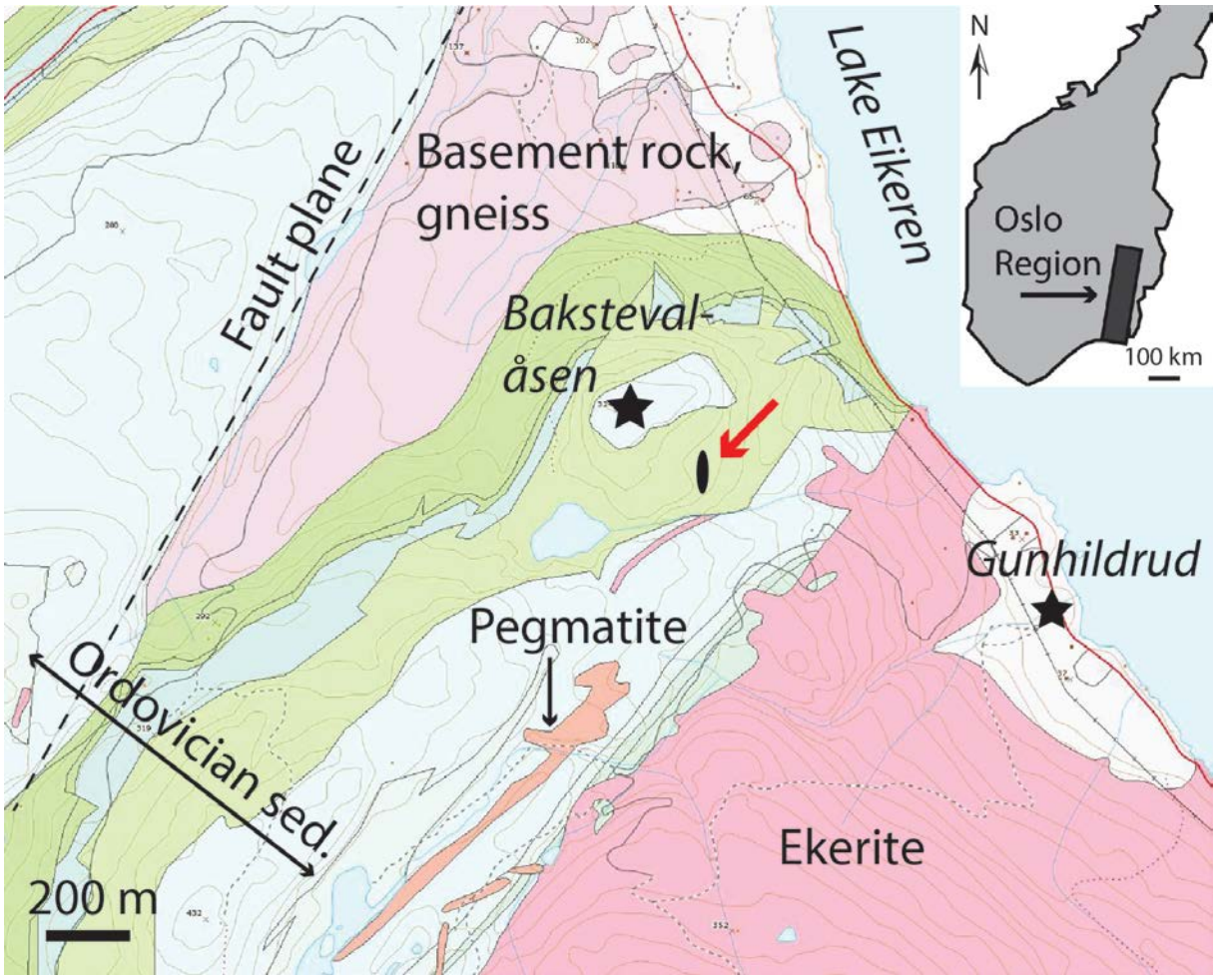

Figure 3 – Simplified geological map of the study area. The amazonite pegmatite at Bakstevalåsen is indicated by the red arrow and oval circle (size exaggerated). The sedimentary units are primarily upper Ordovician massive limestones and shales (Owen et al., 1990).

Pegmatites in the area

There are numerous pegmatite bodies in the bedrock adjacent to the ekerite intrusion, forming sill and dyke intrusions. These bodies vary in thickness from ~0.5 m and up to approximately 3 m, and are composed of a simple mineral assemblage dominated by coarse subhedral to euhedral crystals of quartz, feldspar, and amphibole. The feldspar appears to be dominated by microcline with some minor albite. All the pegmatites appear to follow a general NE-SW strike, which also coincides with the major fault plane uplifting the local sedimentary units. The fault is likely related to the half graben fault system of the Vestfold Graben as an anti-tectic faultplane in respect to the main fault. Texturally, the pegmatites display a thin zone with graphic granite where quartz and microcline intertwine, and grades into the pegmatite body where the amphiboles occur with a random orientation. However, in two pegmatites situated in close proximity to the studied amazonite-pegmatite, additional minerals to the

normal assemblage in the area can be observed. Astrophyllite was observed during fieldwork as fibrous and sheeted crystals up to 2 cm in length. Helvite occur in at least one other fragmented pegmatite as fine grained (mm) euhedral crystals (Hurum, pers. Comm.).

Amazonite pegmatite field-observations

The amazonite pegmatite that has been the target for this study occurs as a sill intruded into the upper Ordovician limestones of the Fossum formation, and partly in calcareous shales of the Elnes formation. The main body of the pegmatite extends approximately 16 meters with an alternating thickness along its NNE strike. The core of the body, where the most diverse mineralogy occur, is estimated to a lens roughly 30 – 40 cm thick by 2 meters long, while the peripheral part of the pegmatite ranges from 15 cm to 5 cm in thickness. However, the pegmatite is not exposed along the inferred 16 meter profile, but is partly covered by overburden. Smaller veins (2 - 5 cm thick) are observed to break off towards the east under the soil. The core of the pegmatite is exhausted by extensive sampling by mineral collectors, and only a trace of the amazonite can be observed along the wall rock. Because of cover, the total extent of the pegmatite cannot be determined precisely, and it is possible that additional linked veins exist under overburden.

Texture and microstructure of the pegmatite

The pegmatite consists of fine grained and coarse grained zones; however, the grain size of the coarsest grains is relatively small compared to what is commonly observed in pegmatites (London, 2008; 2009). The largest amazonite grains range between 2 – 5 cm and the largest danalite grains do not exceed 1 cm. The amazonite coloring appears as both a crisp green and pale blue to grey variety. Within the fine grained material white albite is consistently appearing in varying amounts, and in the northern part of the pegmatite cleavelandite, a bladed variety of albite, is present and replacing amazonite primarily along grain boundaries.

The southern end of the pegmatite body has a well-developed layered structure, which contain different minerals. The bottom layer contains magnetite, astrophyllite, and microcline. Faint grey microcline and smoky quartz form the middle layer, while strong green amazonite dispersed as coarse grains, up to 1.5 cm is limited to the top layer. Magnetite is abundant and limited in the bottom layer, and makes a sharp transition into the middle layer which is free of magnetite. Individual large grains of astrophyllite are scattered in the bottom and middle layer of this section of the pegmatite and can easily be recognized without a hand lens. Minor crystals of helvite group minerals (2 - 5 mm) appear with amazonite. Northwards the layered

structure disappears, and the pegmatite vein becomes homogenous with amazonte as matrix mineral.

The mineralogy in the amazonite pegmatite contains some exotic minerals which occur only a few other places in Norway. A short list and description is presented in Table 1 below. Columbite and gadolinite group minerals are relative common in evolved pegmatites, and löllingite is found a common accessory mineral in the plutonic rocks in the Oslo region.

Table 1 - List of some rare minerals found in the amazonite pegmatite at Bakstevalåsen.

Mineral	**System**	**Chemical formula**	**Occurrence in Norway**
Danalite	Isometric	$(Fe,Zn,Mn)_4Be_3Si_3O_{12}S$	Høgtuva, Nordland
Danburite	Orthorombic	CaBSiO8	Kragerø, Telemark
Nordenskiöldine	Trigonal	$CaSn[BO_3]_2$	Arøya, Langesund, Telemark
Phenakite	Trigonal	Be_2SiO_4	Høgtuva, Nordland
Löllingite	Orthorombic	$FeAs_2$	Common in the Oslo Region
Columbite-(Fe)	Orthorombic	$FeNb_2O_6$	Stetind, Nordland
Gadolinite-(Y)	Monoclinic	$(Y,REE)_2FeBe_2Si_2O_{10}$	Evje-Iveland, Aust-Agder

Methods of study

Analytical methods

Electron microprobe analysis

Analysis was carried out on a Cameca SX 100 microprobe fitted with 5 wavelength dispersive spectrometers. Each analyzed thin-section was coated with a thin carbon layer by a vacuum evaporator. Due to several unknown minerals and uncommon mineral compositions (in respect to solid solution series) among the samples, analysis could not be carried out by standard procedures for silicate mineral analysis. In order to set up analytical protocols suitable for minerals such as the helvite- and gadolinite-group, full wavelength dispersive spectrum (WDS) were acquired from each mineral to be investigated. Major- and minor-elements were identified by their $K\alpha_1$ peaks as well as their recurring lower energy peaks (i.e. $L\alpha_1$, $L\beta_1$ et cetera). After all the major and minor elements were identified qualitatively in each mineral, background positions had to be found for all elements in each of the minerals. This was done by partial WDS to select the positions where to count background on both sides from the selected X-ray line for each element, and thus avoid interference with peaks of

other elements. Element peak to background ratio were quantified by calibrating the intensity of the selected x-ray line on both natural and synthetic standard samples (see list below).

Calibration standards and the respective X-ray lines used were: wollastonite (Si Kα, Ca Kα, Kβ), synthetic Al_2O_3 (Al Kα), albite (Na Kα), pyrophanite (Mn Kα, Ti Kα), synthetic MgO (Mg Kα), galena (Pb Mα), gallium arsenide (As Lα), ZnS (Zn Lα, S Kα), Fe metal (Fe Kα), SnO_2 (Sn Lα), glass with 15 wt% Th (Th Mα), Nb-metal (Nb Lα), Sb_2O_3 (Sb Lα), glass with 15 wt% UO_2 (U Mα), Ta (Mα), W (W Mβ), synthetic orthophosphates for REE and Y (Y Lα, La Lα, Pr Lβ, Nd Lβ, Tb Lα, Er Lβ, Dy Lα, Gd Lβ, Yb Lα) (Jarosewich and Boatner, 1991). Peak to background ratios were accepted if the average of 7 measurements was within reasonable 3σ values. A quantitative analytical procedure then followed with beam parameters as seen in table 2.

Table 2 - Beam parameters and counting times during EMP analysis.

Beam parameters			Counting time (s)		
Acceleration voltage (kV)	Current (nA)	Size	Element	Background	Mineral
15	15	Focused	10	2x5	Danalite
15	15	Focused	10	2x5	Sulphide
20	15		20	2x5	Columbite-(Fe)
20	15	Focused	10	2x5	Gadolinite-(Y)

Helvite group minerals; Si, S, Fe, Zn, Mn, and Be

Beryllium was not analyzed, but estimated based on stoichiometry. Background positions for major elements were selected on a partial spectrum: Si (+/- 800), S (+/- 700), Zn (+/- 750), Fe (+/- 900), Mn (+/- 800), and Zn (+/- 750).

Sulphides; Fe, Pb, As, and S

The main sulphides that were identified for analysis were galena, pyrite, arsenopyrite, and löllingite. Background position for major elements were selected on a partial spectrum: Fe (+/- 800), Pb (+/- 700), As (+1000/-600), and S (+1600/-800).

Oxides; Sn, Ca, and B

Boron was not analyzed, but estimated based on stoichiometry. Background positions were selected as: Sn (+/- 600) and Ca (+460/-550).

Rare-earth rich mineral

One of the major occurring minerals had not been successfully identified, and a full spectrum analysis revealed several heavy rare earth elements in the composition. The identified REE were further tested and verified by running a partial spectrum for each element and identifying the peaks near the theoretical peak position. However, the REE X-ray lines are close to each other and multiple order lines were removed by using pulse height analysis. These elements were important to measure as accurately as possible due to a significant contribution to the total sum weight-%, and acceleration voltage was increased to 20 kV in order to activate better HREE X-ray lines. Background positions were set to; Nd (+400/-450), Gd (+/- 600), Tb (+/-400), Er (+450/-650), Pr (+500/-450), Dy (+1000/- 605), and Mn (+850/-815).

Scanning electron microscope (SEM)

Additional qualitative analysis was carried out on a Hitachi S-3600N SEM-EDX with a low-vacuum (15 Pa) setting at the Natural History Museum, UiO. These analyses were primarily used for qualitatively mineral identification and to efficiently study various mineral paragenesis and relationships.

Fieldwork and samples acquired for the study

Prior to the current study, approximately 15 years ago, the Natural History Museum University in Oslo acquired approximately 50 kg worth of samples shortly after the discovery of the pegmatite. These samples were mostly collected from the middle segment of the pegmatite; however they were not catalogued or mapped according to sampled-position within the pegmatite. Since the time of discovery, the middle segment of the pegmatite has been exhausted due to severe sampling by private collectors. In order to create a frame of reference on the existing material a sketch of the pegmatite was made, and additional samples collected and mapped according to origin. Additional samples were collected from the neighboring pegmatites and ekerite granite (Fig. 4). The majority of pegmatites in the area are situated in the country rock between the amazonite pegmatite and ekerite intrusion.

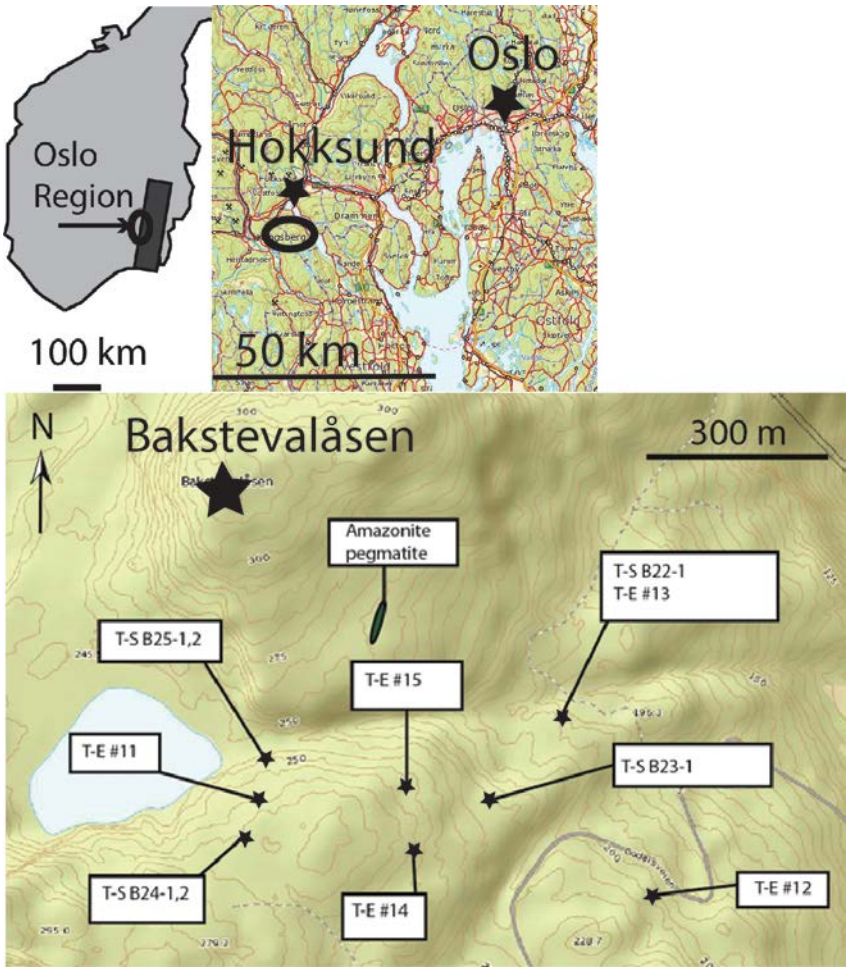

Figure 4 – Topographic map of additional samples gathered from neighboring pegmatites and ekerite. T-E = trace-element sample analysis, T-S = thin-section sample. Scale of amazonite pegmatite exaggerated for visibility on topographic placement.

Thin section preparation

Thin sections were prepared at the Department of Geosciences, UiO. A total of 20 samples from the amazonite pegmatite, and 5 samples from neighboring pegmatites were used as material. Samples and a short description are listed in Table 3 below.

Table 3 – Overview of thin-sections used in the study. Sample code = [BX1-X2]; B = Bakstevalåsen, X1 = Sample number, X2 = sample sub-specie. A = amazonite pegmatite, N = neighbor pegmatite. Thin section images supplied in appendix 3.

Sample	Description
B-0	A; cross section of coarse grained and fine grained domain in middle segment.
B1-1	A; 3 cm wide vein with a reaction rim towards the wall-rock
B1-2	A; same sample as the above
B1-3	A; same sample as the above
B2-1	A; pegmatite and wall-rock
B3-1	A; Danalite rich zones
B3-2	A; same as the above

B4-1	A; danalite crystals overgrowing phenakite
B5-1	A; specimen near overlying wall-rock, fine grained and coarse grained zones.
B5-2	A; specimen near overlying wall-rock, large zones of fluid textures
B5-3	A; coarse grained zone with interstitial albite
B9-1	A; pegmatite and wall-rock interaction, fine grained xenoliths and albite rich domains
B10-1	A; bleached amazonite in vicinity of tourmaline
B10-2	A; subhedral tourmaline with a reaction rim into the amazonite matrix
B11-1	A; Sharp interface between coarse grained domain and fine grained domain containing danalite
B12-1	A; Bleached amazonite with interstitial albite
B13-1	A; fine grained bleached amazonite matrix with albite and danalite
B14-1	A; sample from northern segment of the pegmatite, substantial albite both interstitial and along wall-rock interface. Little modal danalite and phenakite.
B16-1	A; fine grained matrix
B21-1	A; danalite with epitaxial tourmaline and minor nordenskiöldine.
B22-1	N; Microcline with interstitial quartz, and cm large amphiboles.
B23-1	N; zoned pegmatite with two zones, quartz with interstitial microcline, and hornblende with interstitial microcline.
B24-1	N; pyroxene, amphibole, microcline, and quartz.
B24-2	N; same as the above
B25-1	N; fine grained microcline matrix with interstitial amphibole and pyroxene.
B25-2	N; interface between coarse grained domain and fine grained domain. Coarse grained domain contains amphibole, pyroxene, and quartz. Fine grained domain contains primarily interstitial amphibole.

Trace-element analysis

A total of 15 samples (Table 4) were crushed at the Department of Geosciences to fine grained powder and sealed for shipment to Act Labs Ltd (Activation Laboratories, Canada) which performed trace-element analysis. These analyses were conducted according to a pre-defined program “Lithogeochemistry for Exploration and Research”, which involves a lithium metaborate/tetraborate fusion ICPMS and XRF whole rock analysis. Contamination from the

crushing device is expected at trace amount of chromium, nickel, and iron, and the apparatus was cleaned out with ethanol between each sample.

Table 4 - Overview of samples prepared for trace-element analyses.

Sample	Description	Type of pegmatite
1	Pegmatite core, boron influx	Amazonite
2	Fine grained and bleached amazonite matrix	Amazonite
3	1 cm reaction zone between pegmatite and wall-rock	Amazonite
4	Wall-rock	Amazonite
5	Amazonite matrix with danalite and danburite	Amazonite
6	Fine grained danalite and löllingite veins	Amazonite
7	Amazonite, quartz, and danalite with overgrowth of tourmaline aggregates	Amazonite
8	Same material as in sample B-4 (Table 3)	Amazonite
9	Same material as in sample B-10 (Table 3)	Amazonite
10	Fine grained amazonite matrix with danalite, löllingite, and tourmaline	Amazonite
11	Quartz, microcline, and amphibole pegmatite	Neighbor pegmatite
12	Ekerite	Host granitic intrusion
13	Same material as in sample 22-1 (Table 3)	
14	Quartz, microcline, and amphibole	Neighbor pegmatite
15	Quartz, microcline, and amphibole	Neighbor pegmatite

Petrology

In the following chapter a description of the mineral assemblage, textural- and petrogenetic-relationship is made based on mineral identification by microscopy and SEM-EDX, and chemical EMP analysis. However, due to the wealth of primary and secondary minerals, the study is limited to a selection of mineral species.

General features of the amazonite pegmatite

The amazonite pegmatite at Bakstevalåsen is not homogenous in mineralogy or texture along its N-S profile. The pegmatite is zoned in respect to the geochemical composition and matrix mineral. As a frame of reference the pegmatite is subdivided into three segments based on different mineralogical compositions; the south segment, middle segment, and north segment (Fig. 5). One striking difference between the amazonite pegmatite and neighboring pegmatites

(besides the amazonite), is the lack of amphibole which is an important mineral in the other pegmatites in the area.

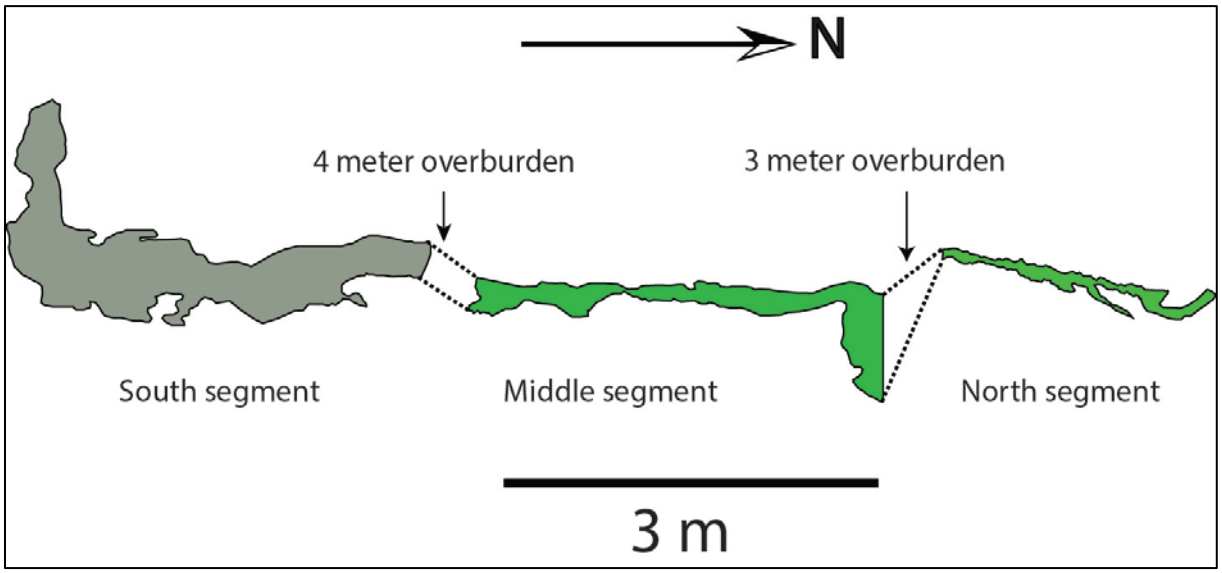

Figure 5 - Simplified sketch of the amazonite-pegmatite at Bakstevalåsen. Dashed lines represent overgrown portions of the body and are not included in the scale. Point of view located above the pegmatite looking down. Coloring represents a difference in modal compositions. Green areas indicate amazonite as matrix mineral. The total length of the pegmatite body including overburden is approximately 16 m.

The texture of the pegmatite is dominated by two features (Fig. 6 and 7);

1) Coarse grained zones where the size of the amazonite matrix crystals is in the range of cm large grains (up to 2 cm).
2) Fine grained zones where crystal sizes range in mm (up to 0.5 mm).

Within large samples the textural relationship of coarse- and fine-grained zones are randomly ordered in the pegmatite body (Fig. 6c, 7a). The transition between coarse- and fine-grained zones is abrupt and sharp, as opposed to a chilled margin along the contact of an intrusion. Samples containing small veins (approximately 5 cm in thickness) have fine grained zones confined towards the bottom-side of the pegmatite margin (Fig. 6e, 7b). Minerals within the coarse grained zones are subhedral to euhedral, while anhedral to subhedral in the fine grained zones. The spatial distribution of coarse- and fine-grained zones appears random where several samples contain bodies of coarse grained microcline, which is outlined by crystallization of smoky quartz along the interface between coarse- and fine-grained zones. The fine grained zones are associated with masses of fine grained biotite ($\geq$ 1 mm), albite, and sulphides. The coarse grained zones contain primarily microcline and quartz.

The amazonite pegmatite shows signs of interaction with the wall-rock, which is observed by two features in the pegmatite body; wall-rock dilution into the pegmatite body and an intense alteration zone of the wall-rock. The alteration zone is approximately 0.5 – 1 cm thick, and contains primarily quartz, biotite, and clay minerals. In small veins (3-5 cm thickness) the interface between pegmatite and wall-rock is sharp (Fig. 7b). These samples show the same feature as described above where approximately 1 cm of the inner wall-rock contains a reaction-rim (Fig. 6e, 7b). The opposing pegmatite margin of such alteration rims is in all observed samples covered by a broad zone of fine-grained material with interstitial sulphides (primarily pyrite, galena, löllingite, arsenopyrite, and minor chalcopyrite), and only observed in contact with such fine grained zones (Fig. 6e, 7b). The largest samples which have a 10 - 20 cm cross-section contain slabs of wall-rock material diluted into the amazonite body. The diluted wall-rock material contain fine grained quartz and biotite (≥1 mm), but mineralization of danalite, tourmaline, and albite can be intense along the diluted wall-rock interface.

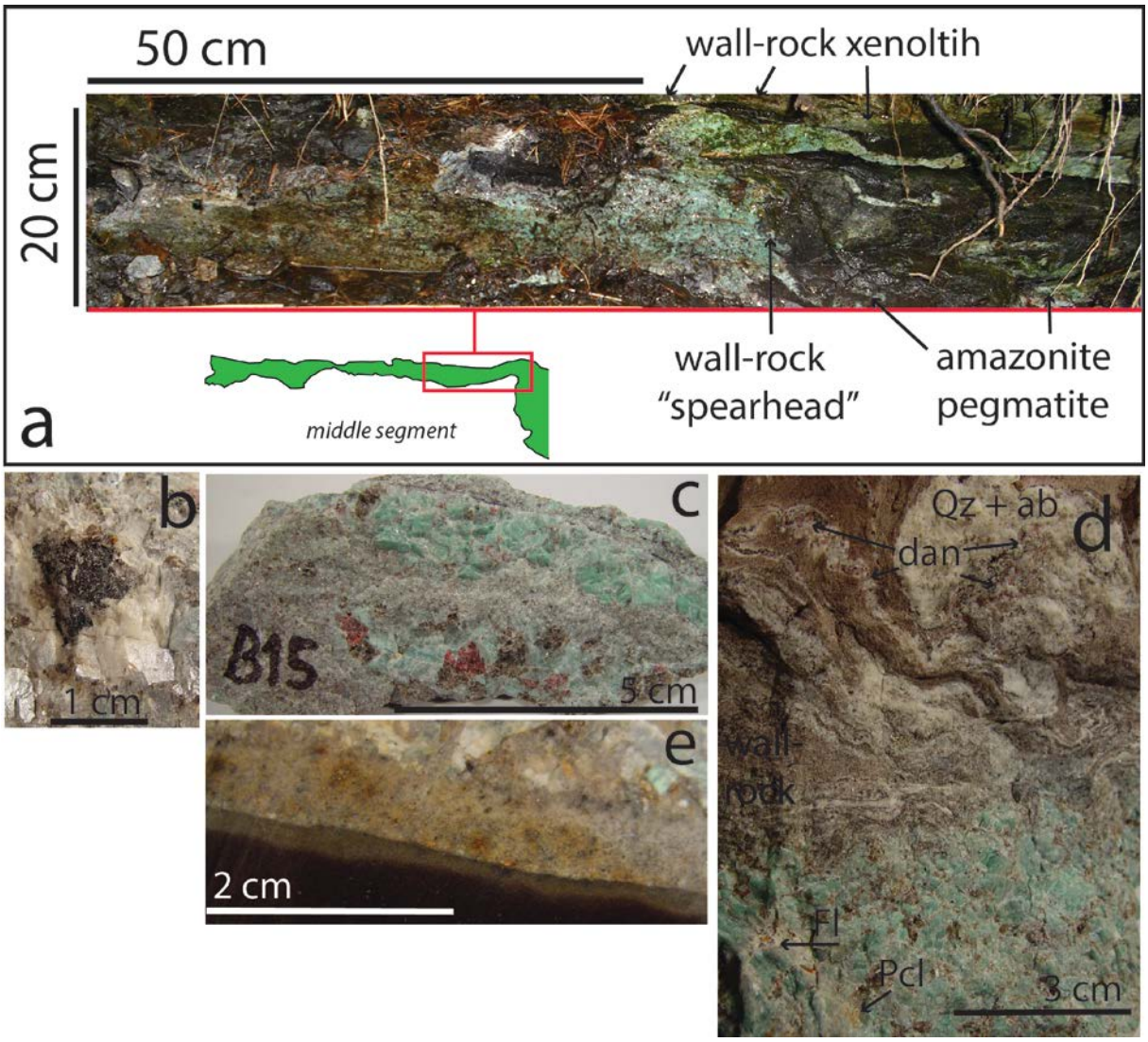

Figure 6 - Photographs of the amazonite pegmatite. A: Field picture of the middle segment with wall-rock xenoliths and dilution into the pegmatite body. B: Tourmaline masses and apparent bleaching of the amazonite. C: Hand-specimen with coarse grained microcline enclaved in fine grained fabric. D: Dilution of wall-rock into pegmatite body in hand-specimen. Note mineralization of danalite along the wall-rock material and dominantly quartz + albite composition in white zones. Minor fluorite (Fl) and pyrochlore group minerals (Pcl) can be seen in the amazonite. E: Alteration zone, approximately 0.5 cm thick, towards the wall-rock.

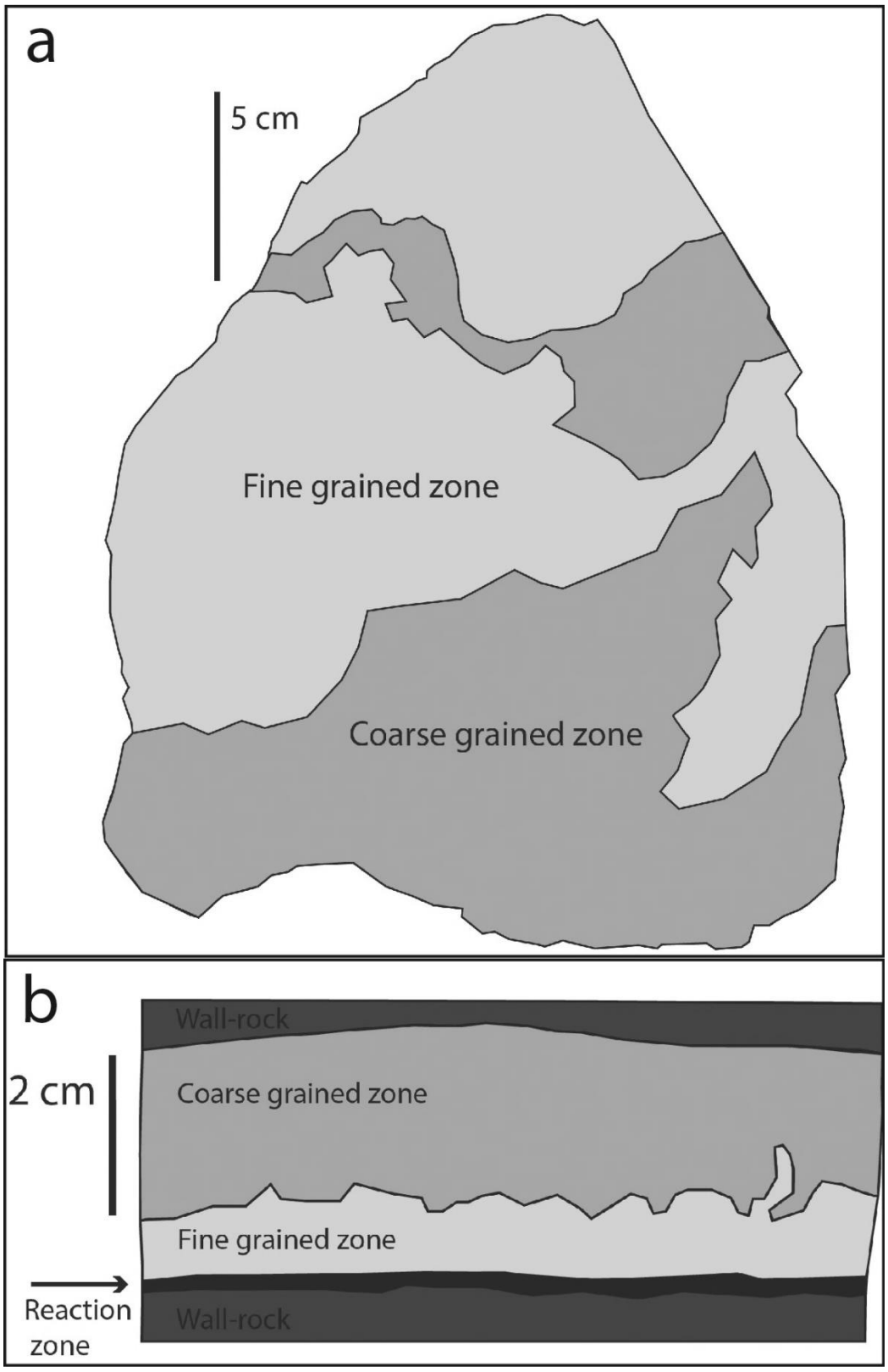

Figure 7 – A: simplified sketch of alternating coarse- and fine-grained zones in large specimens. B: Off-branching secondary veins average in 3 cm thickness, with a local zone of fine-grained material along the bottom interface. These zones contain a 1 cm thick reaction zone towards the wall-rock.

South segment

The south segment is dominated by two key features; 1) a matrix dominated by perthitic microcline with minor albite, and 2) a layered structure which contains specific minerals in each layer (Fig. 8). The layered structure is continuous (along the strike of the pegmatite) in the south segment and consists primarily of three distinct layers with different mineral composition. The bottom layer is dominated by magnetite (0.5 cm), microcline (1 cm), quartz (0.5 cm), and scattered aggregates of astrophyllite (sheets up to 0.5 cm). The middle layer contains primarily grey to faint-green colored microcline, abundant smoky quartz, and minor astrophyllite. The top layer is dominated by albite with local grains of crisp-green colored amazonite and dark red helvite group minerals (have not been analyzed). The content of amazonite in the upper layer increases progressively towards the north where it becomes the dominant feldspar. The south segment transitions into the middle segment when the layered structure is homogenized such that amazonite is the dominant matrix mineral. Figure 6 shows an overgrown area between the south- and middle- segment, which cover most of the transition.

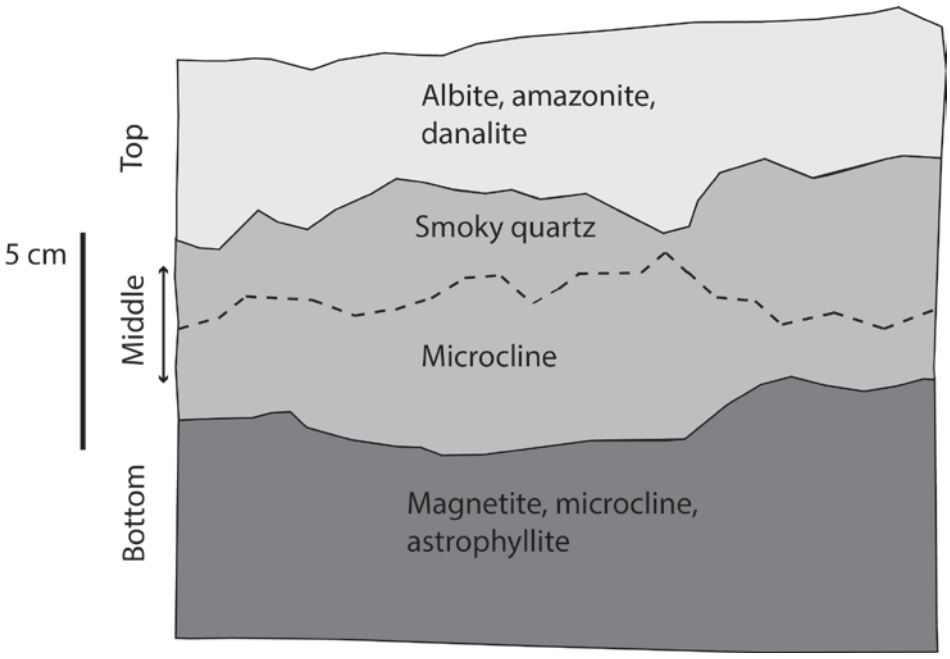

Figure 8 - Simplified sketch of the layered texture in the south segment. Important modal minerals highlighted for each layer. Dashed lines indicate slight segregation between masses of quartz and microcline in the middle layer.

Middle segment

This segment is characterized by amazonite with a crisp green color as the matrix mineral. The main difference from the south segment is that magnetite and perthitic microcline are no longer present and astrophyllite is accessory. Danalite, phenakite, danburite, tourmaline, gadolinite-(Y), pyrochlore group minerals, columbite-(Fe), and sulphides are abundant in the middle segment. The texture alternates between coarse- and fine-grained zones as seen in figure 7a. The coarse grained amazonite is several places intersected by veins of fine grained material, which creates a fabric with coarse microcline segments enclaved by fine grained zones. Amazonite occurs as average 2 cm large crystals in the coarse grained zones, but local crystals up to 5 cm have been observed. The fine grained material average approximately 0.5 cm in size. There is a sharp transition between the fine grained and coarse grained zones, and the interface in between is defined by a sharp and abrupt change. Biotite, albite, and abundant sulphides (i.e. pyrite, galena and löllingite) are associated with the fine grained zones and appear to nucleate along grain-boundaries between amazonite and quartz. Phenakite occurs as subhedral to anhedral pristine grains, and is distinguished from quartz in hand-specimen with its high luster and distinctive crystal habit. A majority of the phenakite crystals are overgrown with danalite.

The coloring of amazonite is not uniform throughout the middle segment. In the vicinity of boron minerals (tourmaline and danburite) the color grades from grey to faint blue. Danburite occurs primarily along the wall-rock interface and as interstitial aggregates in the matrix enclosing individual amazonite grains. Tourmaline accompanies danburite and is observed primarily as masses of small grains (0.1 – 0.2 mm) and larger crystals (up to 1 cm) inside cavities.

The thickness of the pegmatite body alternates between 20 and 30 cm in the middle section and it contains visible wall-rock xenoliths up to 10 cm (Fig. 6a). There are also pieces of wall-rock which spearheads and partly pierces the pegmatite body. As seen in figure 6 the middle segment dives under thick overgrowth; however, by digging holes into the overburden it appears that the middle segment continues at least another meter. Furthermore, it is unknown if there are additional veins which spread off in other directions under the overburden.

North Segment

The north segment is characterized by the amazonite pegmatite narrowing into one thin vein, which alternates between 5 and 10 cm thickness and eventually wedges out. The composition is dominated by amazonite as matrix mineral, with albite along microcline grain boundaries, and cleavelandite intersecting and enclosing the amazonite several places. Danalite is present in minor amount as 1 mm large scattered grains. Albite forms a thin, outer zone between the pegmatite and wall-rock (approximately 5 mm). The north segment is not spatially aligned with the middle segment and due to overburden it is not possible to determine whether the displacement is induced by a fault or a natural kink in the pegmatite.

Deformation features in the pegmatite

The amazonite pegmatite occurs with a straight profile in the stratigraphy. However, the middle segment is displaced approximately 1 meter east relative to the south and north segment, but it is not clear if this displacement is induced by deformation or the emplacement itself. A NW-SE striking fault plane exposes the south segment (Fig. 5). Hand specimens of the amazonite pegmatite show lineations where mineralization of e.g. tourmaline and biotite are localized. These lineations are in cm scale and cut into the pegmatite body from the wall-rock at various angles, and are interpreted as fractures which were mended by later mineral growth.

Mineralogical description

The mineralogy in the amazonite pegmatite at Bakstevalåsen contains a broad assemblage of different minerals. The minerals are abundant as both primary and secondary phases as well as microscopic crystals which can only be identified with SEM-EDX. Many of these minerals are not common rock-forming silicates, and not listed with standardized abbreviation (Whitney & Evans, 2010). Table 5 provides a list of additional abbreviations used in this study.

Based on Figure 6 and the apparent change in modal composition of the pegmatite along a northward trend, a general crystallization sequence is shown in Figure 9. The majority of analyzed (EMPA) samples originate from the middle segment of the pegmatite. However, several additional samples from the periphery of the body have been studied with a low vacuum scanning electron microscope (SEM-EDX). This approach was adapted to ensure that major mineralization trends were not overlooked in respect to important modal compositions. The following mineral description is a summary of observations made with a polarizing

microscope, scanning electron microscope (SEM-EDX), and high powered optical microscope.

Table 5 –List of mineral abbreviation of minerals not included in Whitney & Evans (2010).

Mineral	Abbreviation
Danalite	Dan
Danburite	Dab
Phenakite	Phe
Columbite-(Fe)	Col-(Fe)
Nordenskiöldine	Nörd
Gadolinite-(Y)	Gad-(Y)

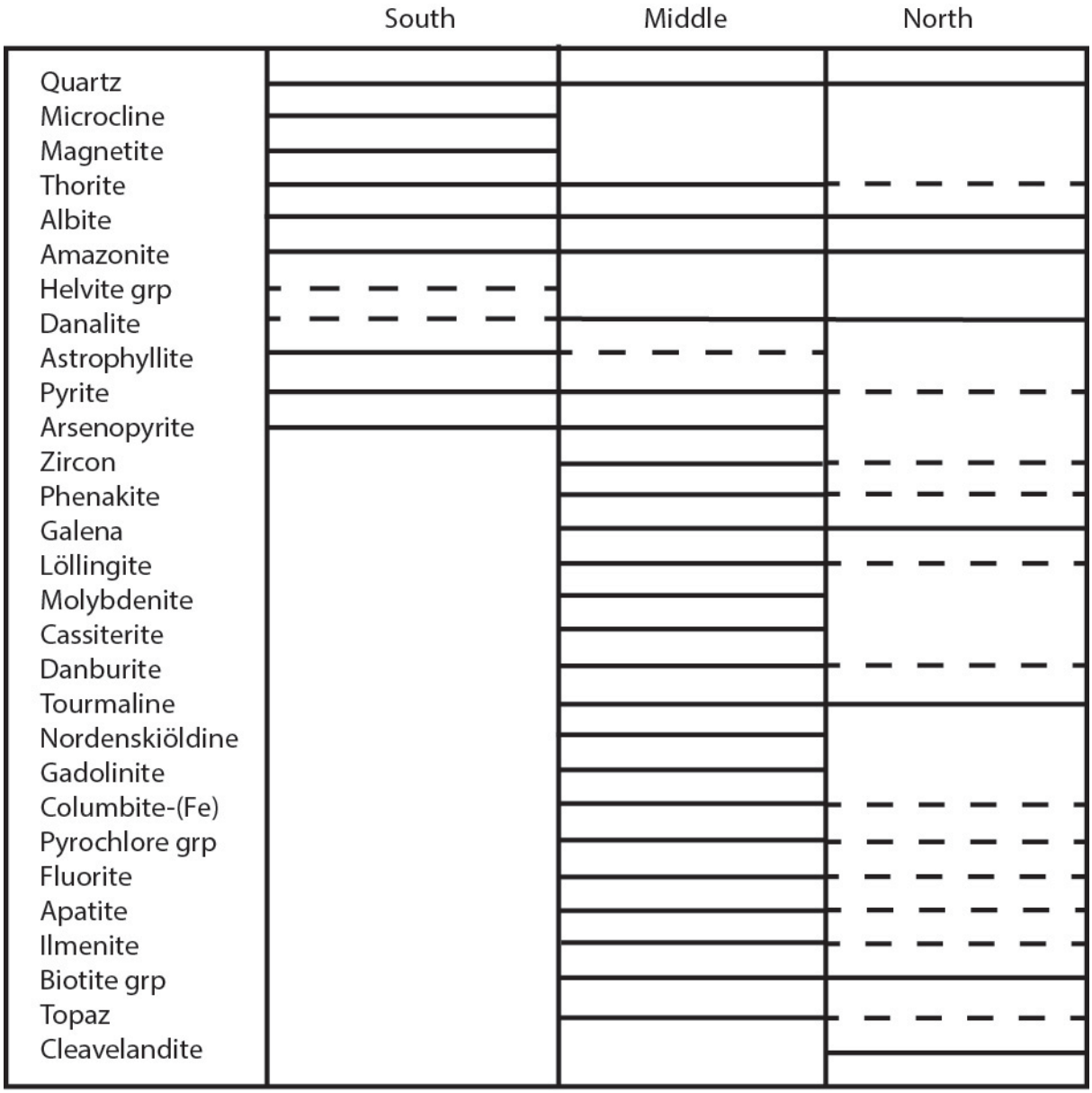

Figure 9 – Observed crystallization sequence based on mineral occurrence and abundance throughout the pegmatite body. Solid lines = observed mineral occurrence in abundance, dashed lines = minor occurrence and uncertainty.

Quartz, SiO_2

In hand-specimens quartz occurs as two generations of subhedral crystals up to 1 cm. The quartz crystals vary between a transparent and smoky variety, where the latter is abundant throughout the pegmatite body and the former as minor masses in fine grained zones. In thin-section quartz occurs as subhedral to euhedral crystals with varying sizes (0.2 mm – 1 cm). Near the wall-rock quartz grows perpendicular to the contact into the pegmatite and comprises the coarse grained zones in the pegmatite with microcline. The large grains are mostly pure without mineral inclusions, but some grains contain a large amount of small (≤1 mm) mineral inclusions. These inclusions are oval in shape and have parallel extinction in XPL (crossed polarized light). Along the grain-boundary of such quartz grains, secondary muscovite is crystallizing.

Feldspar: Microcline and variety amazonite, $KAlSi_3O_8$; albite, $NaAlSi_3O_8$

The primary K-feldspar occurs as two different generations with an early microcline and a late amazonite variety. Microcline comprises the matrix in the south segment of the pegmatite (Fig. 5). The crystals range from 2 mm and up to 5 cm in size, while the early stages of the pegmatite (south segment, Fig. 6) contain the coarsest microcline crystals in the center of the pegmatite body. In the field, the margin along the wall-rock contains fine grained (mm) microcline similar to a chilled margin. Amazonite is the dominant variety in approximately 2/3 (middle and north segment) of the pegmatite and occurs in association with albite. In the south segment where amazonite is scarce, microcline occurs exclusively in albite rich zones along the top layer of the pegmatite. The amazonite color is mostly crisp green, but appears changes to a grey and blue variety in the vicinity of albite and boron minerals.

Additionally, the feldspar has two distinguishing features. Microcline is confined to coarse grained zones and exhibit diffusive perthite-lamella and Carlsbad twinning in XPL. In several places along the grain boundaries between individual microcline grains albite occurs as <1 mm subhedral masses. However, feldspar within the fine grained zones is exclusively albite with polysynthetic twinning and in most cases euhedral crystals (0.1 -0.5 mm). In thin section albite also forms euhedral mineral inclusions within quartz grains that are larger than 2 mm. In hand-specimens albite and quartz form a cryptocrystalline zone between pegmatite margin and wall-rock.

Thorite, $(Th,U)SiO_4$

Thorite is common in all samples as subhedral grains associated with zircon and pyrochlore group minerals. Thorite is a common mineral within fine grained domains, and in some cases overgrown with aggregates of subhedral pyrochlore crystals. Energy dispersive spectrum (EDS) qualitative analysis indicates primarily thorium with little to no uranium in the crystals.

Biotite, $K(Mg,Fe)_3(AlSi_3O_{10})(OH)_2$

Biotite occurs exclusively within fine grained zones as interstitial growth between quartz and microcline grains. The biotite crystals are anhedral and never exceed crystal sizes greater than 1 – 2 mm. Biotite is observed in both hand-specimens and thin-section to accumulate along the interface between coarse grained zones and fine grained zones. This biotite "front" can be observed as both sharp and alternating interface between the two different textures. Biotite is abundant in the wall-rock with quartz and clay minerals.

Muscovite, $KAl_2(AlSi_3O_{10})(OH)_2$

Muscovite is observed in thin-sections as subhedral grains up to 2 mm and associated with secondary mineralization in alteration zones. This alteration appears as serisitization along microcline and albite grain-boundaries.

Astrophyllite, $(K,Na)_3(Fe,Mn)_7Ti_2Si_8O_{24}(O,OH)_7$

Astrophyllite occurs in minor sheeted masses with a light brown color in the south segment of the pegmatite, as well as scattered grains up to 5 mm in the middle segment. However, in the transition-zone between the south- and middle segment (Fig. 5), astrophyllite is abundant as sheets confined along microcline grain-boundaries. These astrophyllite sheets are darker in color with a metallic lustre opposed to what is observed in the southern segment. Larger quartz crystals (approximately 0.5 – 1 cm) also contain several inclusions of mm sized astrophyllite needles. The astrophyllite in the transition zone between the south and middle segment is observed with growth of zircon, and the amazonite matrix appear with a dark to black color.

Titanite, $CaTi(SiO_4)O$

Titanite is observed locally in minor amounts as anhedral grains between approximately 0.1 – 0.4 mm large crystals. Titanite is observed in some thin-sections along the margin between coarse- and fine-grained zones.

Oxides and sulphides

Magnetite, Fe_3O_4

Magnetite appears as both aggregates and as scattered euhedral to subhedral grains, and ranges from mm and up to cm large clusters within parts of the pegmatite. Most notable is the strong presence of magnetite in the early southern part of the pegmatite, but into the transition where amazonite defines the groundmass magnetite is no longer present in noticeable amounts.

Hematite, Fe_2O_3

Hematite occur as minor grains scattered in a few samples and appear to be localized to grain-boundaries between quarts and albite within fine grained domains, and in some cases individual grains may be found with secondary muscovite or sericitization.

Galena, PbS

Galena is observed as both subhedral crystal aggregates of ≤1 mm and individual euhedral crystals up to 1 cm. In hand-specimens galena is observed as large masses along the margin of the amazonite pegmatite body and up to 2 cm into the wall-rock. In thin-sections galena is abundant in fine grained zones and as interstitial growth between microcline and quartz. Most notably are clustering of microcrystalline anhedral grains (approximately 10 – 20 µm) in several fine grained zones (Fig. 10). These masses of microcrystalline galena appear in some samples to follow possible relict microcline grain boundaries, where the material has recrystallized to albite.

Pyrite, PbS_2

Pyrite is observed in approximately equal abundance as galena, and found as subhedral to euhedral masses up to 1 cm in hand-specimens. Thin section studies reveal that pyrite is abundant within fine grained zones as scattered euhedral crystals and adjacent to galena.

Cassiterite, SnO_2

Cassiterite occurs in thin-sections as anhedral grains up to 200 µm and has not been identified in hand-specimens. These crystals are primarily associated with masses of galena and löllingite.

Chalcopyrite, CuS_2

Chalcopyrite is observed in minor amount as masses up to 1 cm in hand-specimens with purple to metallic luster.

Arsenopyrite, FeAsS

Arsenopyrite is observed in thin-sections as minor interstitial phases (up to 50 µm) and related with pyrite löllingite, and galena.

Molybdenite, MoS_2

Molybdenite is primarily observed in hand-specimens as scattered local subhedral grains up to 5 mm. These grains have a bright grey color and metallic luster and can be scratched by a finger nail.

Löllingite, $FeAs_2$

Löllingite is common in all samples and occur both as scattered and as clustered euhedral crystals. Fe and As is stable and does not change significantly in the analyzed specimens.

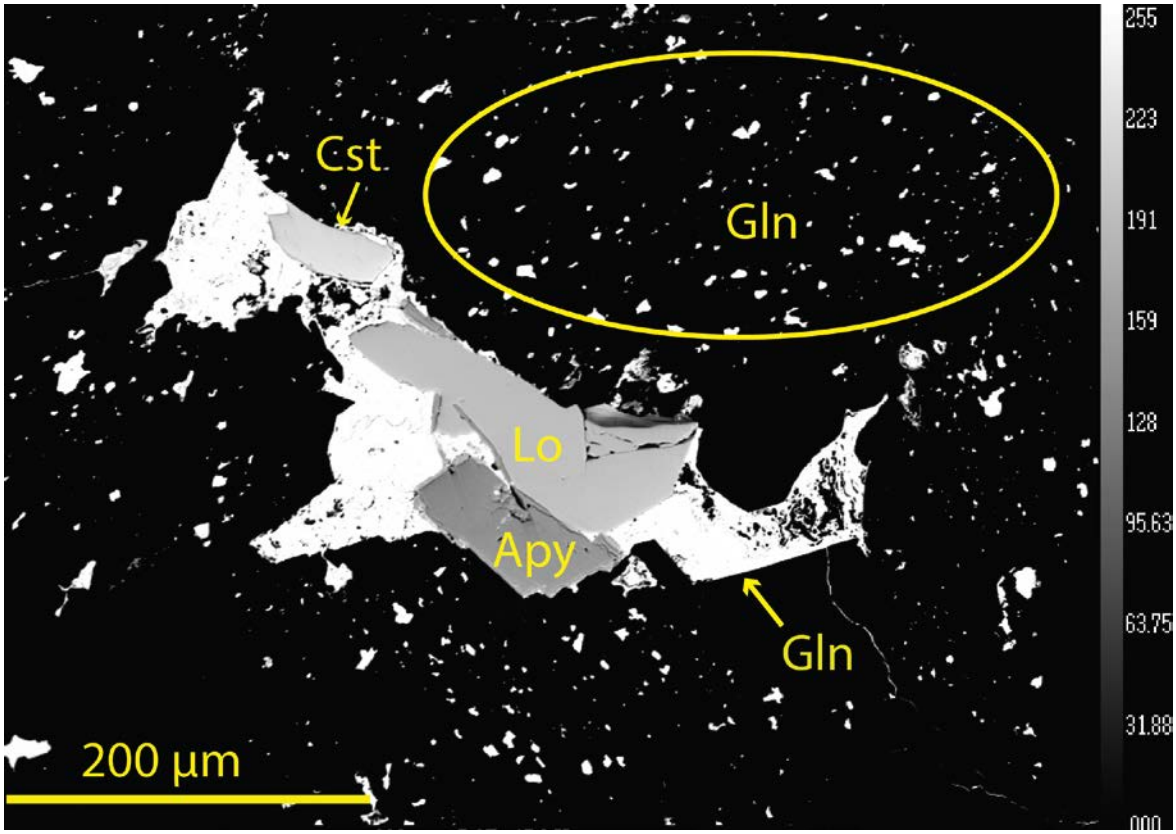

Figure 10 - BSE image of löllingite (Lo), cassiterite (Cst), and arsenopyrite (Apy) with a later growth of galena (Gln). Interstitial and subhedral galena radiate outwards from the cluster. Such clustering of fine grained galena is found in all thin-sections, and galena is also commonly found as laths inside fractures. Quartz and microcline are not seen in the matrix due to low brightness.

Fluorine-rich minerals

Fluorite, CaF_2

Fluorite is observed in all thin-section and occurs as anhedral crystals up to approximately 0.2 mm. The fluorite crystals are scattered with no apparent affinity to other minerals. In large hand-specimens fluorite is observed as cryptocrystalline masses up to 0.5 cm.

Topaz $(Al_2SiO_4)(F,OH)_2$

Topaz is primarily found in thin-sections sampled from smaller veins (approximately 5 cm thick), and found as subhedral grains up to 5 mm within coarse grained zones. Topaz occurs both as individual grains and masses of several grains adjacent to fine-grained zones.

Beryllium minerals

Helvite group, $(Zn,Fe,Mn)_4Be_3Si_3O_{12}S$

In the amazonite pegmatite at Bakstevalåsen the helvite group is abundant. Several analyses were carried out on helvite group minerals and found to be confined to the solution series between zinc and iron (end-member genthelvite and danalite respectively), with an average 12 % of the manganese component. Large crystals of genthelvite – danalite appear heterogeneous in respect to zinc and iron ratios when measuring large grains. Particularly large grains have in some cases higher zinc concentrations near the core, while iron increases relative towards the rim. However, this relationship is not linear and varies locally throughout the grain interface. Such crystals also differ from sample to sample in respect to how well defined the crystal habit appears, i.e. some samples contain well defined and massive euhedral crystals with inclusions, whereas other samples contain crystals with only an external subhedral to euhedral crystal shape (Fig. 11). These subhedral crystals appear mainly in two physical configurations; 1 - a subhedral crystal shape where the rim is continuous while the core contains a substantial amount of the matrix minerals quartz and microcline. 2 - The core is continuous while the rim is poorly defined with inclusions of quartz and microcline. Inclusions are common within all analyzed crystals and appear mainly as both small inclusion material (>mm), and secondary mineralization and alteration (≤mm).

This means that for all the analyzed large grains the composition is not uniform, but covers a range between genthelvite (Zn>Fe>Mn) and danalite (Fe>Zn>Mn). However, the average composition appears to be dominated by danalite (Fig. 12). Large crystal aggregates show a

general trend with higher iron ratios along the margin with even zinc and iron ratios within the core, but local variations occur with no systematic zonation. 179 measurements were conducted in total on danalite crystals, with an average of 6 measurements in a cross-section over large crystals (~500 µm). From these measurements danalite appear as the dominating composition with the exception of local variations in the Zn to Fe relation (Fig. 12 and 13).

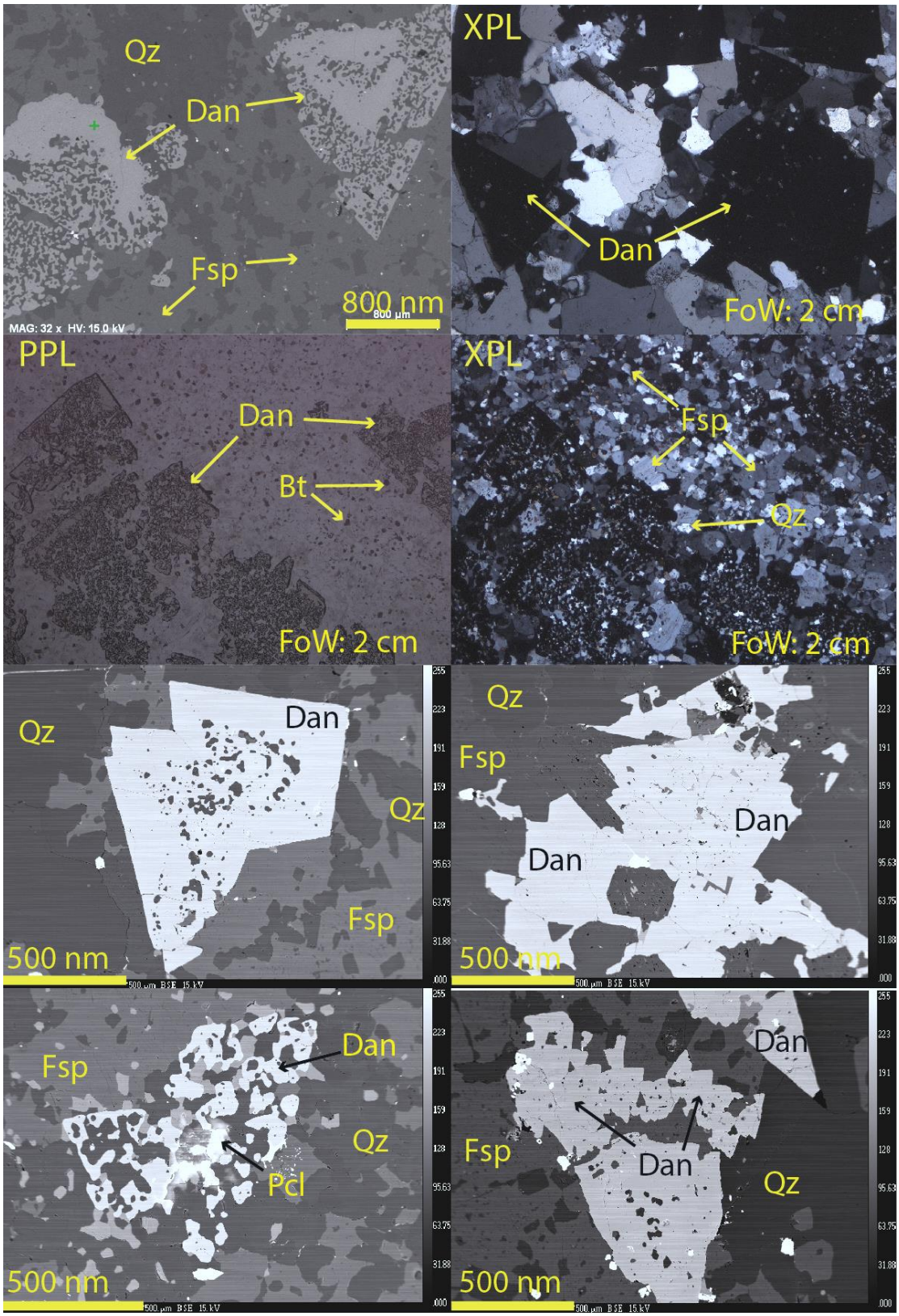

Figure 11 - BSE and microscope images (plane polarized and cross polarized) of different danalite crystal textures. Note the fine grained matrix occurs with the less defined danalite (Dan) crystals, while the coarse grained feldspar (Fsp) and quartz (Qz) matrix is observed with massive danalite crystals. Note the XPL images of coarse- and fine-grained matrix; abundant albite and biotite occur in the latter, while the former contains primarily microcline and quartz.

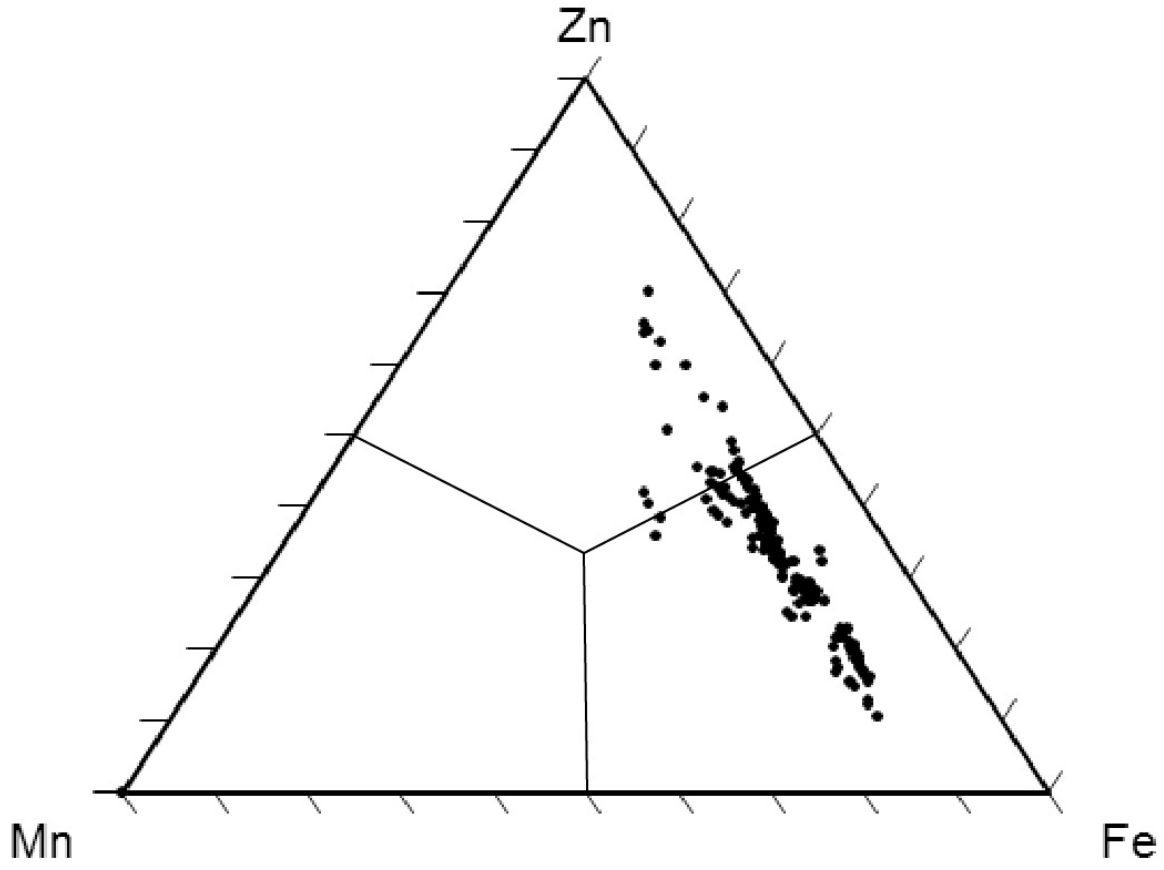

Figure 12 – Helvite (Mn), danalite (Fe), and genthelvite (Zn) composition triangular diagram. Diagram includes all analysis and plots along the genthelvite – danalite solid solution series. Manganese is relatively consistent with an approximately 15% helvite component. Atoms per formula unit (apfu) calculated assuming 13 anions. All data listed in appendix 1.

Sample-specific plots of danalite crystals

Figure 12 show a considerable spread between Zn and Fe in the measured danalite crystals. Each sample viewed with BSE shows different danalite crystal texture as seen in Figure 11. These variations not only occur between the different samples, but also over a short distance in each thin section (i.e. over a distance of approximately 3.0 cm). Sample specific plots from different thin sections show a minor spread between Zn and Fe as seen in Figure 13. A considerable spread can be seen in sample B-0 and B3-2, and analysed grains are highlighted in Figure 14 and 15 respectively.

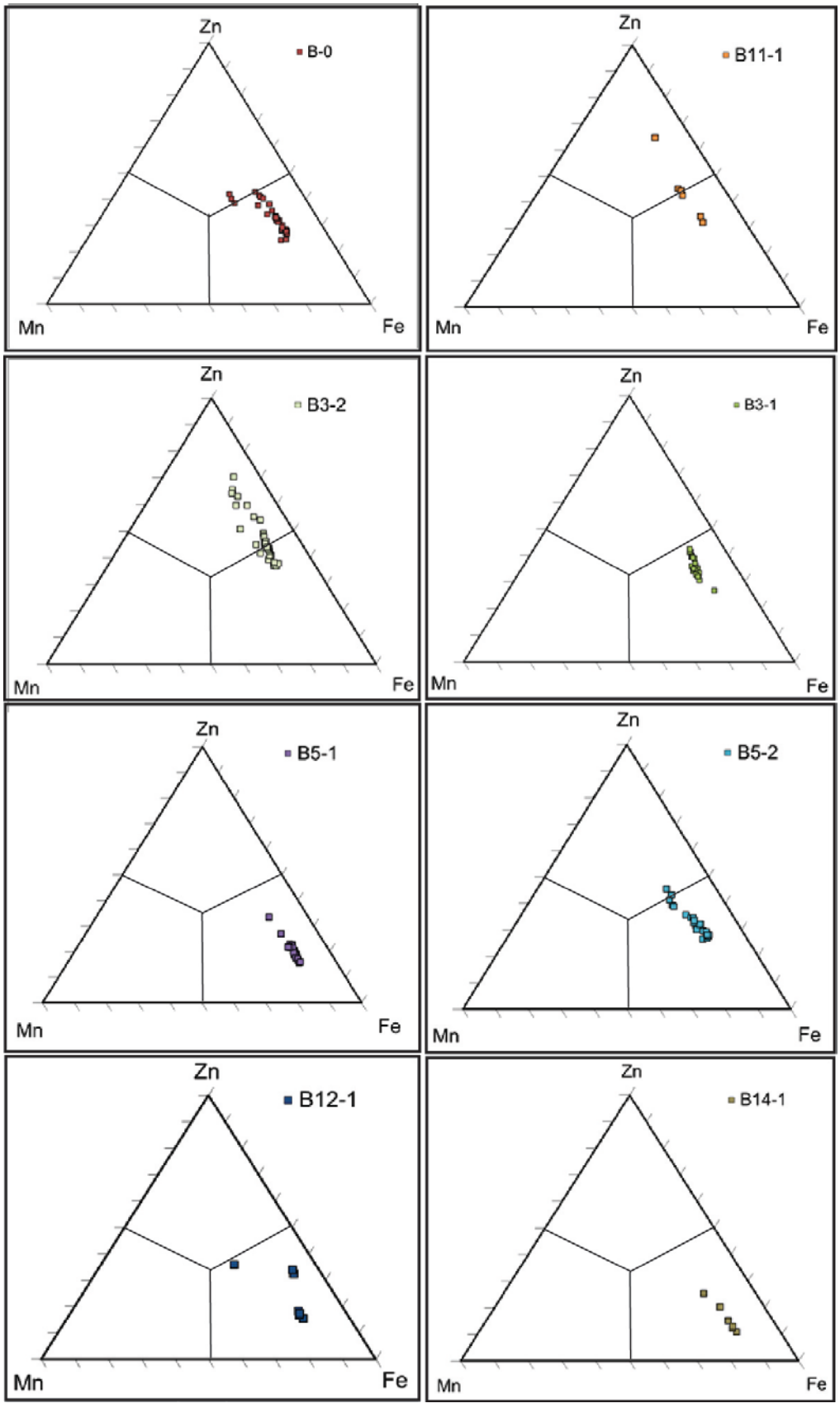

Figure 13 – Helvite-danalite-genthelvite composition diagram. Each diagram represents genthelvite – danalite plot from each analyzed sample (thin section). Sample B11-1 contains grains of ilmenite ($FeTiO_3$) partly overgrowing the danalite crystals. Sample B3-2 contains dense genthelvite – danalite crystals and consequently a higher frequency of analysis.

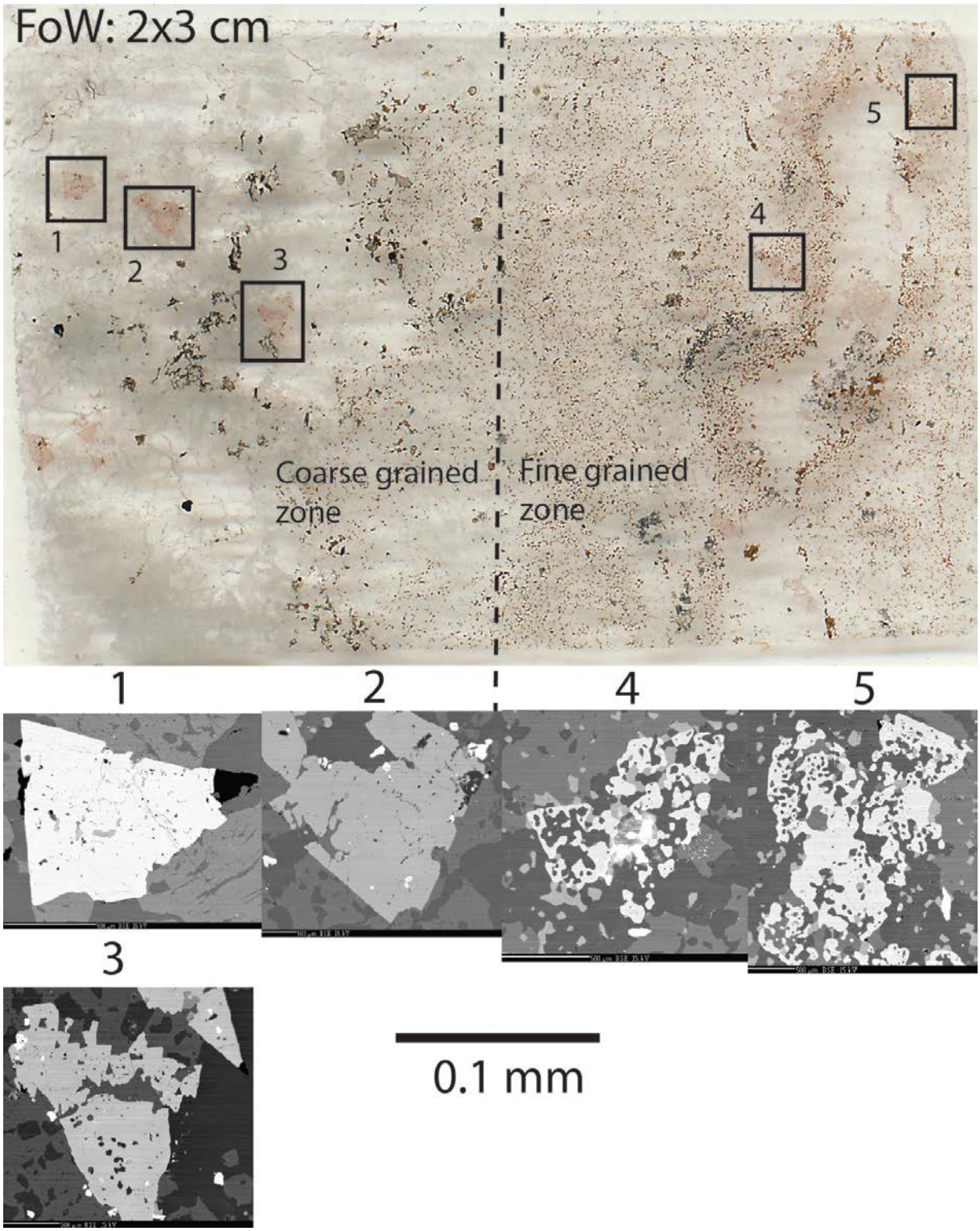

Figure 14 - Thin-section scan of sample B-0 and BSE images of analyzed danalite grains (1 - 5). Each grain is approximately 0.1 mm in diameter, and the sample consists of a coarse- and fine-grained zone as indicated by the dashed lines. A trend in crystal habit is observed across the thin-section. Massive crystals dominate in the coarse-grained zone, while masses of smaller crystals dominate in the fine-grained zone. Figure 13 shows 4 plots in the genthelvite field which originate from grain 1 and 2 between crystal core and rim. BSE image 4 and 5 are the most iron-rich measurements. Note the grey zones in thin section scan (underneath box 4), which are clusters of anhedral galena similar to figure 10.

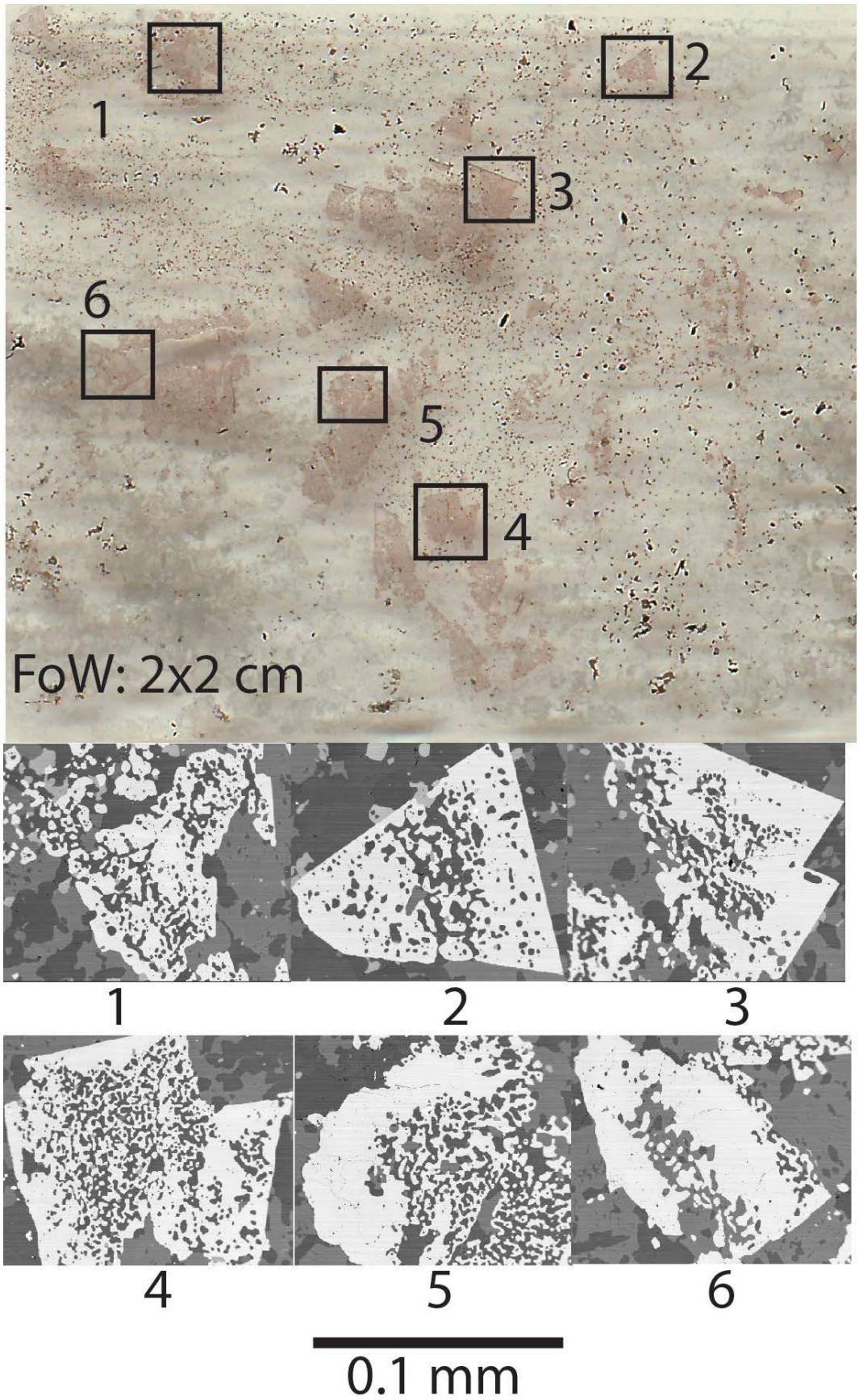

Figure 15 – Scan of thin section sample B3-2 and associated BSE image of analyzed danalite grains. Compositions are plotted in Figure 13 and several plots are in the helvite field. These plots originate from the margin of danalite grain 2, 3, 5, and 6. Majority of plots are concentrated within the danalite field and originate from the crystal core in grain 1 – 6.

Phenakite, Be_2SiO_4

Phenakite occurs as subhedral to euhedral transparent grains up to 1 cm in the amazonite pegmatite. In hand-specimens phenakite is distinguished from quarts by its high refractive index and transparent luster. The most abundant occurrence of phenakite is in the middle segment of the pegmatite where magnetite leaves the system, and several phenakite grains are overgrown by danalite. Due to beryllium passing below the detection limit of SEM-EDX, phenakite is not as easily distinguished from quartz. Some hand-specimens contain fractured phenakite crystals (approximately 0.5 cm) were fractures are annealed by quartz growth.

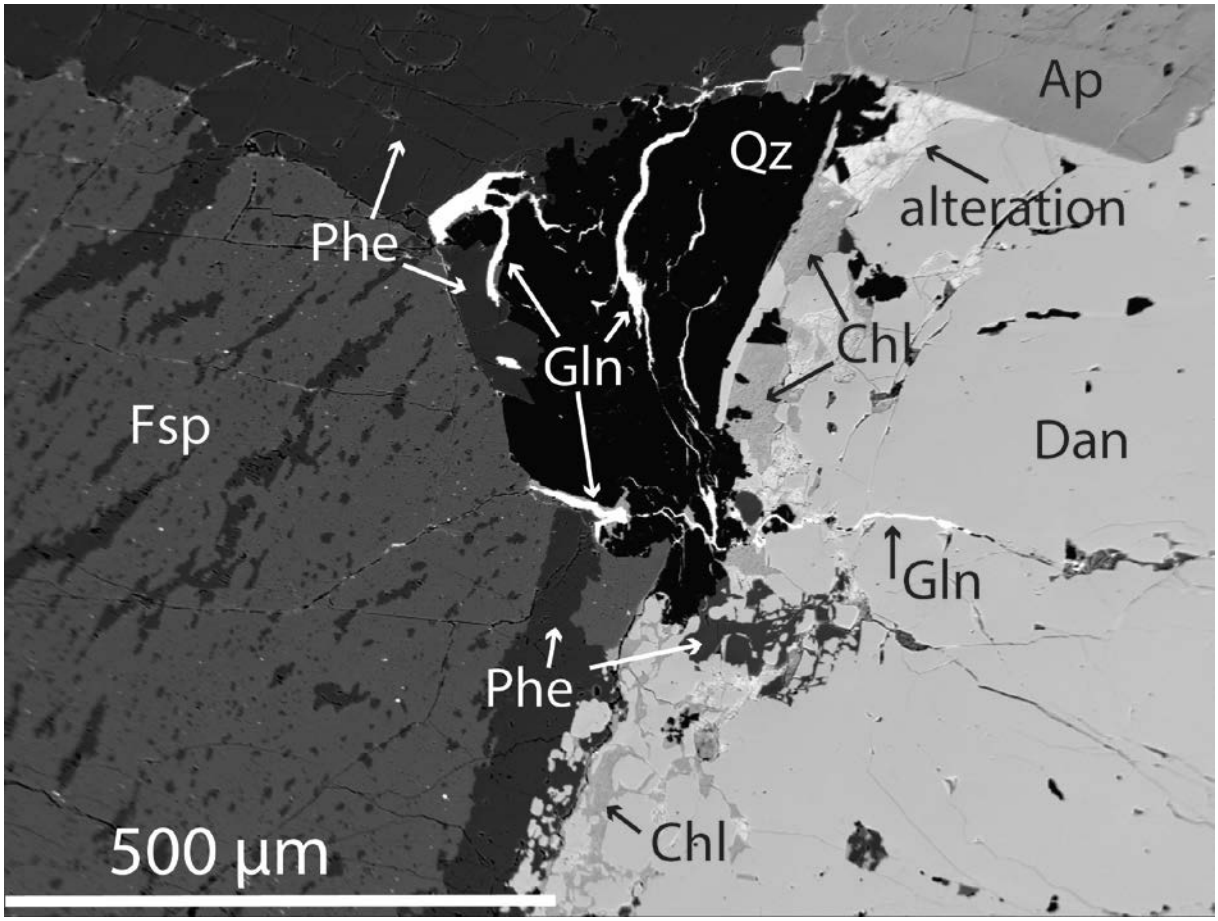

Figure 16 - BSE image of danalite (dan) and phenakite (phe) in sample B21-1. Minor alteration and chlorite (Chl) along the grain boundary between danalite and phenakite, and galena (gln) appears to fill cracks in quartz and danalite. Apatite (ap) in the top right corner, and is one of the larger observed grains.

Boron minerals

Tourmaline, $Na(Fe_3)Al_6(Si_6O_{18})(BO_3)_3(OH)_3(OH)$; $Na(Mg_3)Al_6(Si_6O_{18})(BO_3)_3(OH)_3(OH)$

Tourmaline have not been extensively analyzed in this study, however Jahren et al (1998) identified the species as primarily schorl with minor dravite. The former appear as fine grained masses up to 5 cm primarily along the margin – wall-rock zone, and as larger crystals

(up to 1 cm crystals) in cavities. Amazonite crystals adjacent to tourmaline appear discolored with a grey to blue color. Figure 17c and d shows interstitial tourmaline associated with danburite.

Danburite, $CaB_2Si_2O_8$

Danburite primarily appear in the middle section as anhedral to subhedral crystals up to 1 cm. The crystals are typical pale yellow with a slightly greasy luster, and are abundant along the margin of the pegmatite body and in some specimens in the wall-rock. Danburite occur both as masses up to 3 cm and as aggregates along amazonite grain-boundaries in the matrix. The amazonite crystals adjacent to danburite, as observed in relation with tourmaline, are always discolored with a grey to blue color. Inside cavities danburite grows interstitial with tourmaline as mm large crystals (up to 6 mm).

Nordenskiöldine, $CaSn[BO_3]_2$

Nordenskiöldine has been identified by chemistry with EMPA analysis as masses up to 100 µm in thin-sections. Nordenskiöldine occur as epitaxial overgrowth on cassiterite and interstitial $CaCO_3$ (Fig. 18). However, nordenskiöldine has not been found as grains visible in hand-specimens.

Other minerals

Zircon, ($ZrSiO_4$)

Zircon shows no particular affinity to any minerals and covers all samples persistently as subhedral to euhedral millimeter large grains. These grains are present in all thin-sections as masses of several grains and often accompanied by pyrochlore group minerals (nomenclature after Hogarth, 1977). However, qualitative SEM-EDX analysis indicates slight variation between zirconium and oxygen ratio, and when viewed with crossed nicols some zircon grains show minor differentiation in birefringence. In most hand-specimens zircon crystals are not visible, but samples from the transition zone of the pegmatite contain euhedral light colored zircon crystals up to 0.2 mm.

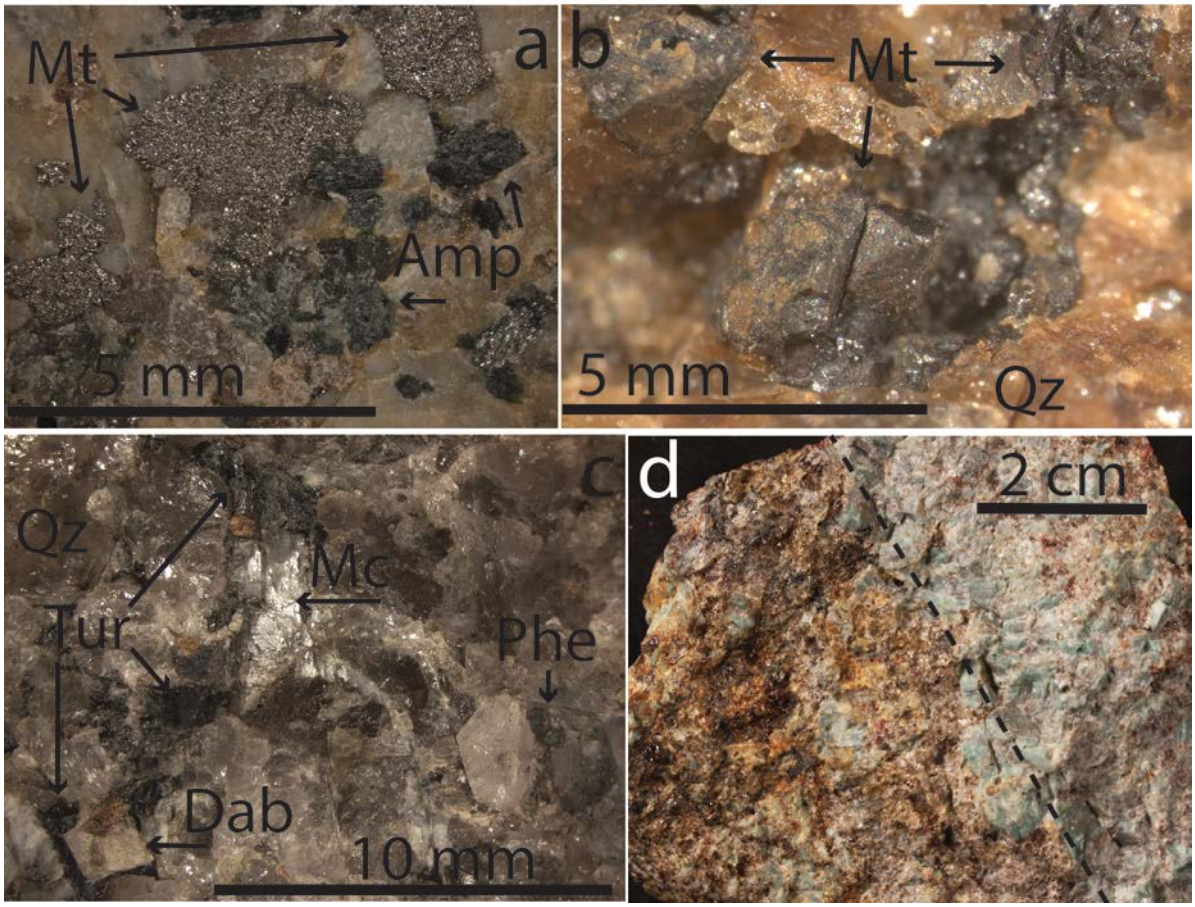

Figure 17 - Photograph of mineral appearance in hand-specimens. A: Observed relationship of magnetite and amphibole in some neighboring pegmatites, magnetite is interstitial to quartz and amphibole. B: euhedral magnetite in the south segment of the amazonite pegmatite. C: Masses of tourmaline, danburite, and phenakite in amazonite (Mc) and quartz (Qz) matrix. Note the phenakite (Phe) depression into the amazonite (bottom right). D: Hand-specimen showing a boron-saturated side and relative boron-free side. Left side of dashed line contains abundant interstitial tourmaline and danburite with local grains of phenakite, danalite, and sulphides. Right side of dashed line contains primarily amazonite, quartz, phenakite, danalite, and local grains of danburite.

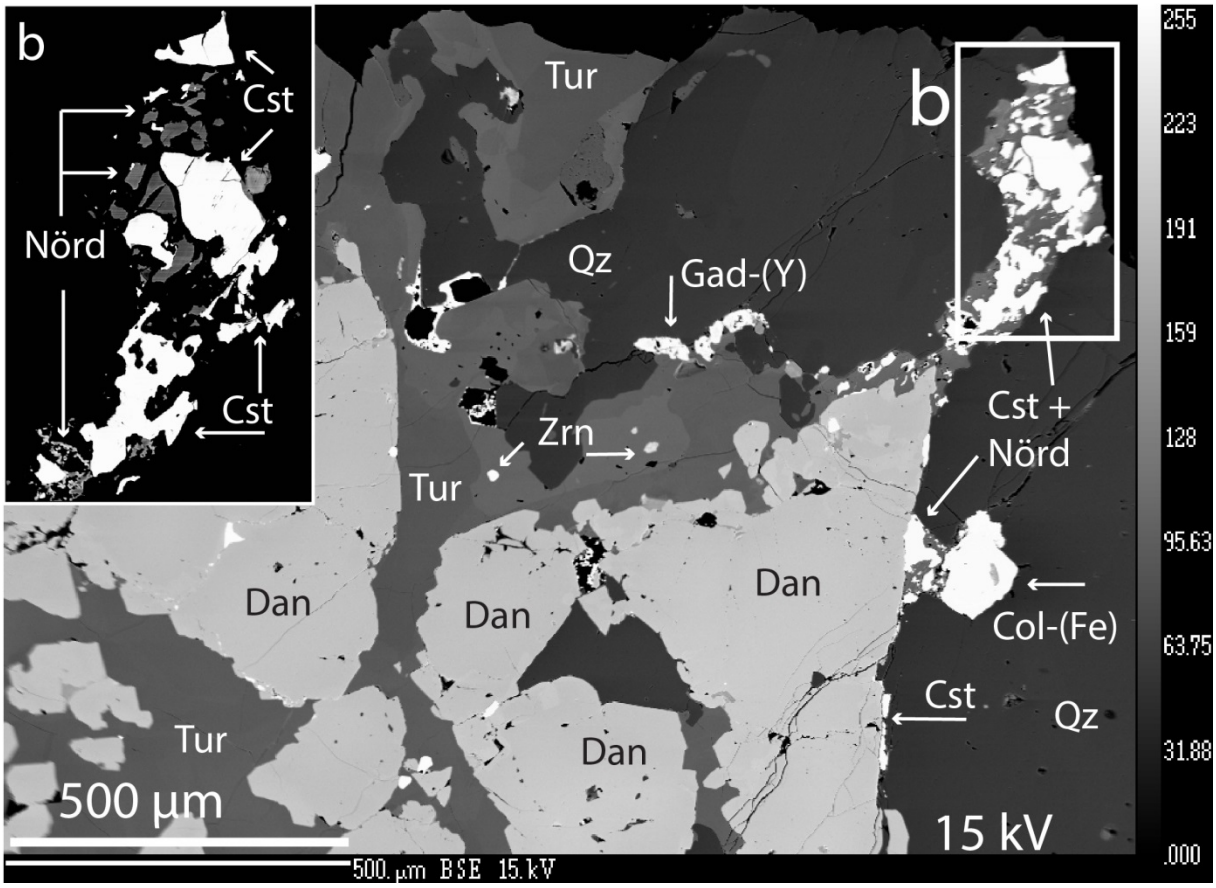

Figure 18 - BSE image of sample B21-1; masses of danalite crystals with interstitial tourmaline and minor inclusions of zircon and gadolinite. Columbite-(Fe) is adjacent to cassiterite with minor nordenskiöldine. Upper right corner is saturated with masses of cassiterite, minor nordenskiöldine, and interstitial calcite. B: close-up view of nordenskiöldine and cassiterite, calcite is not seen due to low brightness.

Apatite, $Ca_5(PO_4)_3(OH,F,Cl)$

Apatite is observed in thin-sections with BSE as scattered and limited subhedral grains up to approximately 50 µm, and associated with masses of pyrochlore, zircon, and thorite. However, these grains have not been analyzed and the exact composition is unknown.

Calcite, CaCO3

Calcite is observed in as minor interstitial grains primarily in relation with cassiterite and nordenskiöldine.

Carbon, amorphous C

In several thin-sections some opaque minerals are amorphous when analyzed with EDS, and are carbon material. Hand specimens contain abundant carbon nodules (approximately 1 mm) along the pegmatite margin, and the dark luster resembles fine grained subhedral tourmaline.

Gadolinite-(Y), $(Y,REE)_2FeBe_2Si_2O_{10}$

The gadolinite group consists of the solution series gadolinite – datolite; however, there are additional species in the group depending on chemistry (i.e. minasgerasite, hingganite, and homilite species). The ideal formula for gadolinite can be expressed by $A_2XZ_2Si_2O_{10}$ where in gadolinite-(Y) A = yttrium and rare earth element, Z = beryllium; and in datolite A = calcium and Z = boron (Miyawaki et al., 1984; Demartin & Minaglia, 2001; Cámara et al., 2008). In the amazonite pegmatite gadolinite has not been observed with confidence in hand-specimens, but occurs in several thin sections as subhedral to euhedral large crystals up to 2 mm. These crystals are to an individual extent metamict where a few crystals are near pristine while others are completely metamict. When viewed under polarized light the near pristine crystals show distinct zonation with alternating positive and negative interference. The metamict crystals are clearly fractured and covered with large metamict zones (Fig. 19). Several relict crystal shapes can be observed in thin section where all the material is metamict. These crystals are in most cases associated with aggregates of thorite and pyrochlore group minerals. 13 grains were analyzed with 46 measurements to investigate the composition in the most apparent zonation. The chemistry (Table 6) shows high calcium content relative to iron, while some zones are dominated by calcium (Fig. 20). The analysis also indicates a variety of HREE where the calcium content is low. Most notably is the relationship between calcium, iron, and HREE in the zonation. Figure 21 shows REE chondrite normalized pattern indicating enrichment of HREE relative on LREE. On BSE images dark zones contain elevated calcium weight percent relative to iron and HREE, while bright zones contain higher iron and HREE weight percent relative to calcium (Fig. 22). A relationship between the thorium content (wt. %) and the extent of metamictization can be observed where near pristine crystal contain little thorium, and severe metamict crystals contain elevated thorium wt. % (Table 6).

Table 6 – Selected chemical analysis of gadolinite-(Y) in the amazonite pegmatite. Apfu (atoms per formula unit) recalculated assuming 10 oxygen atoms. Iron is treated as Fe^{2+}, and low total weight percentage is related to metamict crystals. BSE images of analyzed grains displayed in Figure 19. Measurement B5-1 #1 contains low thorium values and the crystal is near pristine. Measurement B5-1 #2 contains elevated thorium values and is severely metamict.

	B5-1 #1					B5-1 #2		
Wt. %	core	inter	core	Inter	rim	rim	inter	rim
CaO	2.80	2.45	2.38	1.92	5.36	7.04	8.07	7.62
SiO_2	24.47	23.99	24.03	23.46	25.36	25.29	25.96	25.49
FeO	9.96	10.32	10.35	10.74	10.11	9.75	9.17	9.69
$Y2O_3$	27.178	26.527	26.522	24.498	27.864	20.964	19.466	19.272
La_2O_3	0.496	0.558	0.525	0.446	0.702	1.530	2.327	1.969
Ce_2O_3	2.967	2.982	3.024	2.804	2.146	2.902	4.319	3.226
Dy_2O_3	4.972	5.230	5.222	6.863	2.518	2.960	2.591	2.769
Gd_2O_3	2.857	2.761	3.041	3.399	1.424	1.668	1.388	1.471
Yb_2O_3	2.282	2.671	2.345	3.071	2.911	3.107	2.970	2.987
ThO_2	1.621	2.169	2.503	1.777	2.743	5.297	3.658	5.880
Pr_2O_3	0.377	0.450	0.415	0.439	0.179	0.238	0.299	0.253
Nd_2O_3	1.467	1.4	1.494	1.186	0.480	0.733	0.849	0.676
Tb_2O_3	0.487	0.494	0.425	0.673	0.171	0.115	0.174	0.202
Er_2O_3	3.191	3.117	3.089	3.970	2.439	2.761	2.449	2.463
MnO	0.41	0.37	0.40	0.32	0.38	0.21	0.22	0.25
BeO	10.2	10.0	10.0	9.7	10.5	10.5	10.8	10.7
Total	95.75	95.52	95.80	95.29	95.32	95.09	94.75	94.95
Formula proportions based on 10 oxygen atoms								
Ca	0.26	0.23	0.22	0.18	0.48	0.64	0.72	0.68
Si	2.09	2.08	2.08	2.07	2.11	2.13	2.16	2.14
Fe	0.71	0.75	0.75	0.79	0.70	0.69	0.64	0.68
Y	1.24	1.22	1.22	1.15	1.23	0.94	0.86	0.86
La	0.02	0.02	0.02	0.01	0.02	0.05	0.07	0.06
Ce	0.09	0.09	0.10	0.09	0.07	0.09	0.13	0.10
Dy	0.14	0.15	0.15	0.20	0.07	0.08	0.07	0.07
Gd	0.08	0.08	0.09	0.10	0.04	0.05	0.04	0.04
Yb	0.06	0.07	0.06	0.08	0.07	0.08	0.08	0.08
Th	0.03	0.04	0.05	0.04	0.05	0.10	0.07	0.11
Pr	0.01	0.01	0.01	0.01	0.01	0.01	0.01	0.01
Nd	0.04	0.04	0.05	0.04	0.01	0.02	0.03	0.02
Tb	0.01	0.01	0.01	0.02	0.00	0.00	0.00	0.01
Er	0.09	0.08	0.08	0.11	0.06	0.07	0.06	0.06
Mn	0.03	0.03	0.03	0.02	0.03	0.02	0.02	0.02
Be	2.09	2.08	2.08	2.06	2.10	2.12	2.15	2.15

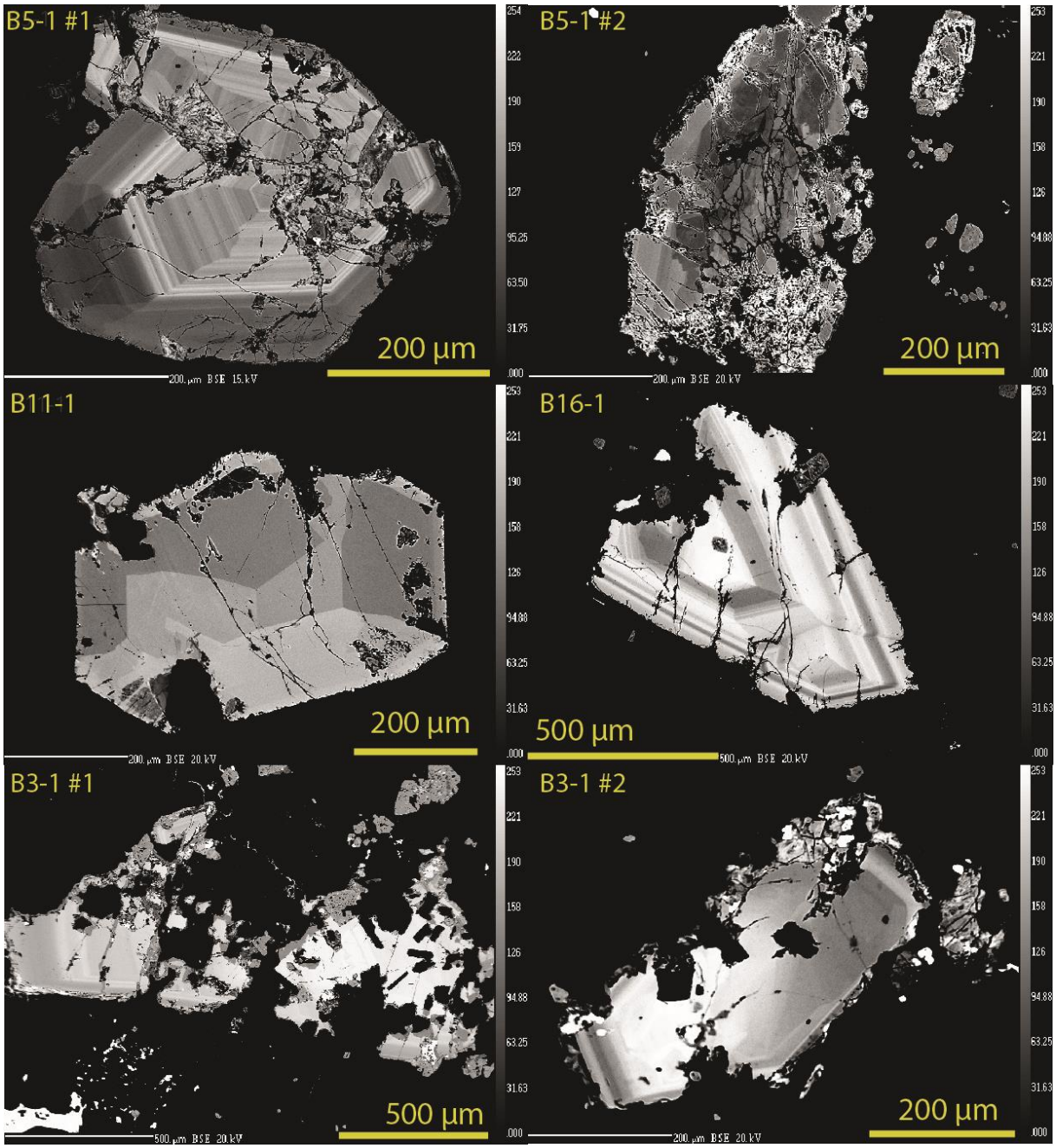

Figure 19 – Selection of BSE images of gadolinite crystals with varying degree of zonation. Higher calcium content is associated with dark bands while REE is associated with the brighter bands. Due to varying thorium contents (wt. %) the gadolinite crystals are partly metamict, which is seen as extensive cracks and altered zones.

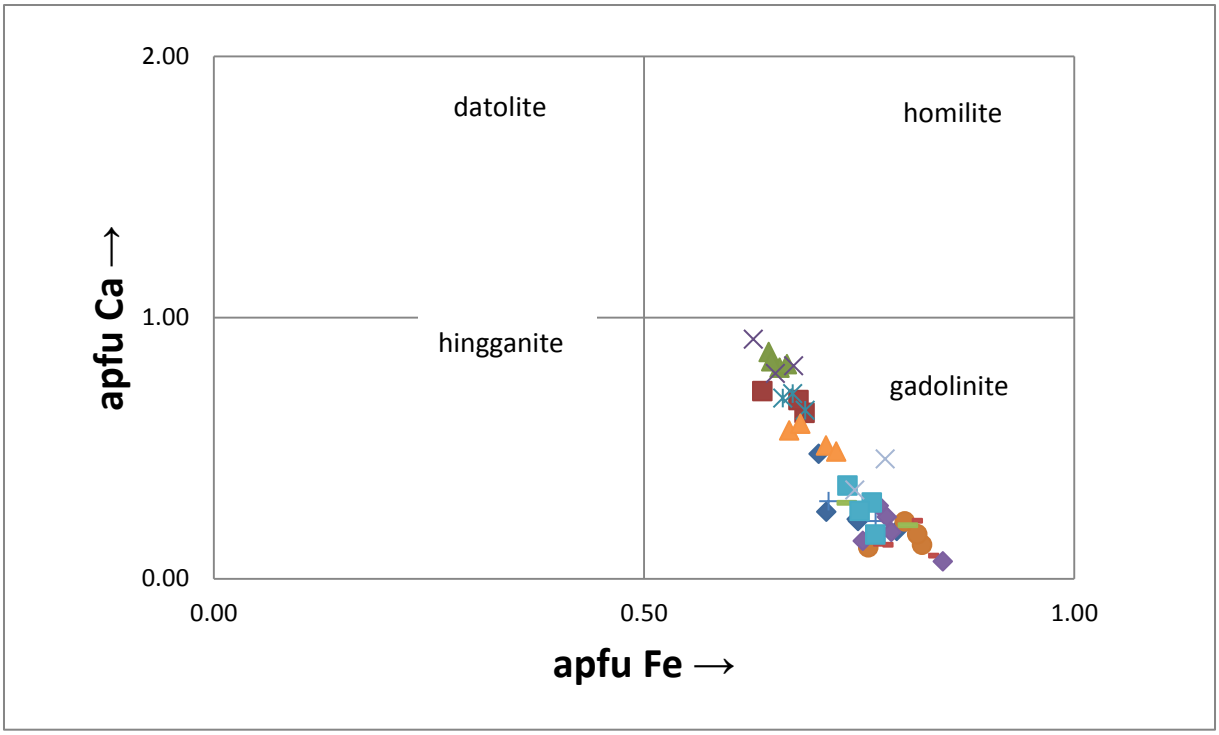

Figure 20 – Diagram showing the gadolinite – datolite compositional relationship. Diagram contains every analyzed gadolinite grains, and plots a linear relationship with datolite. Plot of stoichiometric calcium versus iron performed similar as Pezzotta (1998).

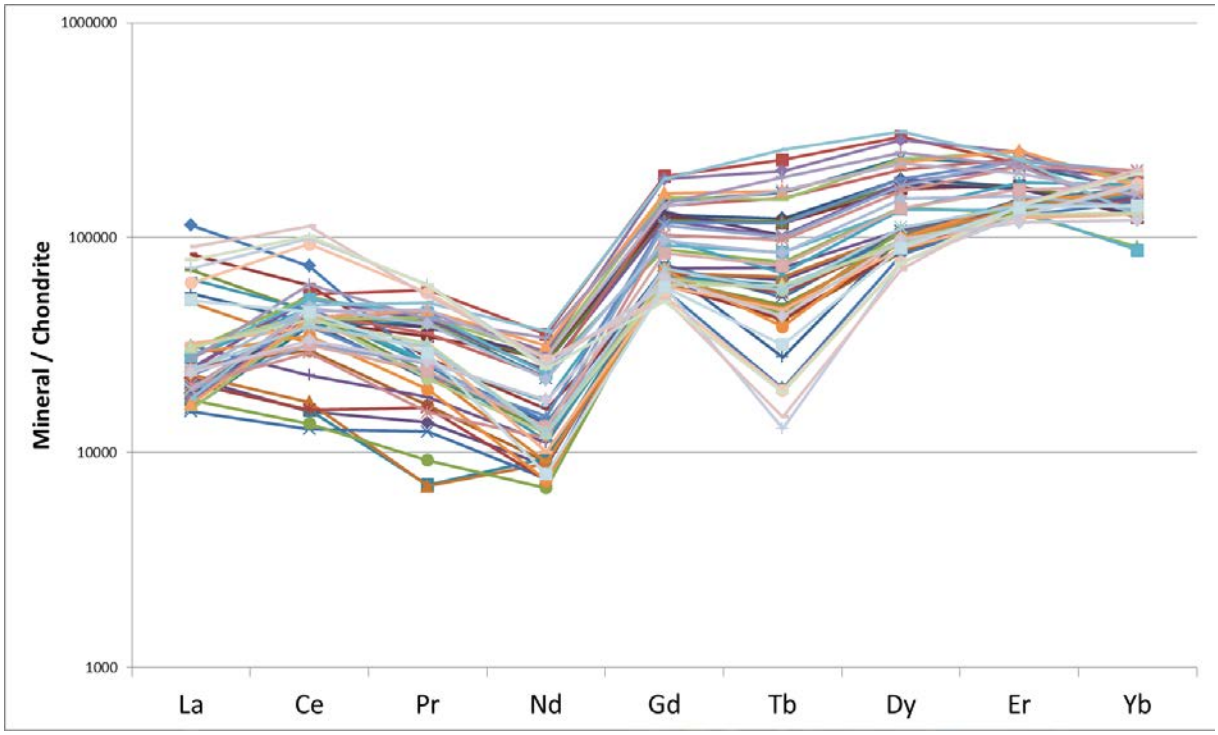

Figure 21 – Chondrite normalized REE pattern in gadolinite-(Y) (McDonough & Sun, 1995). The figure includes every analysis and a general pattern with relative enrichment of HREE versus LREE is observed. The observed spread within plot is possibly related to calcium versus REE dominated zones as seen in Figure 22.

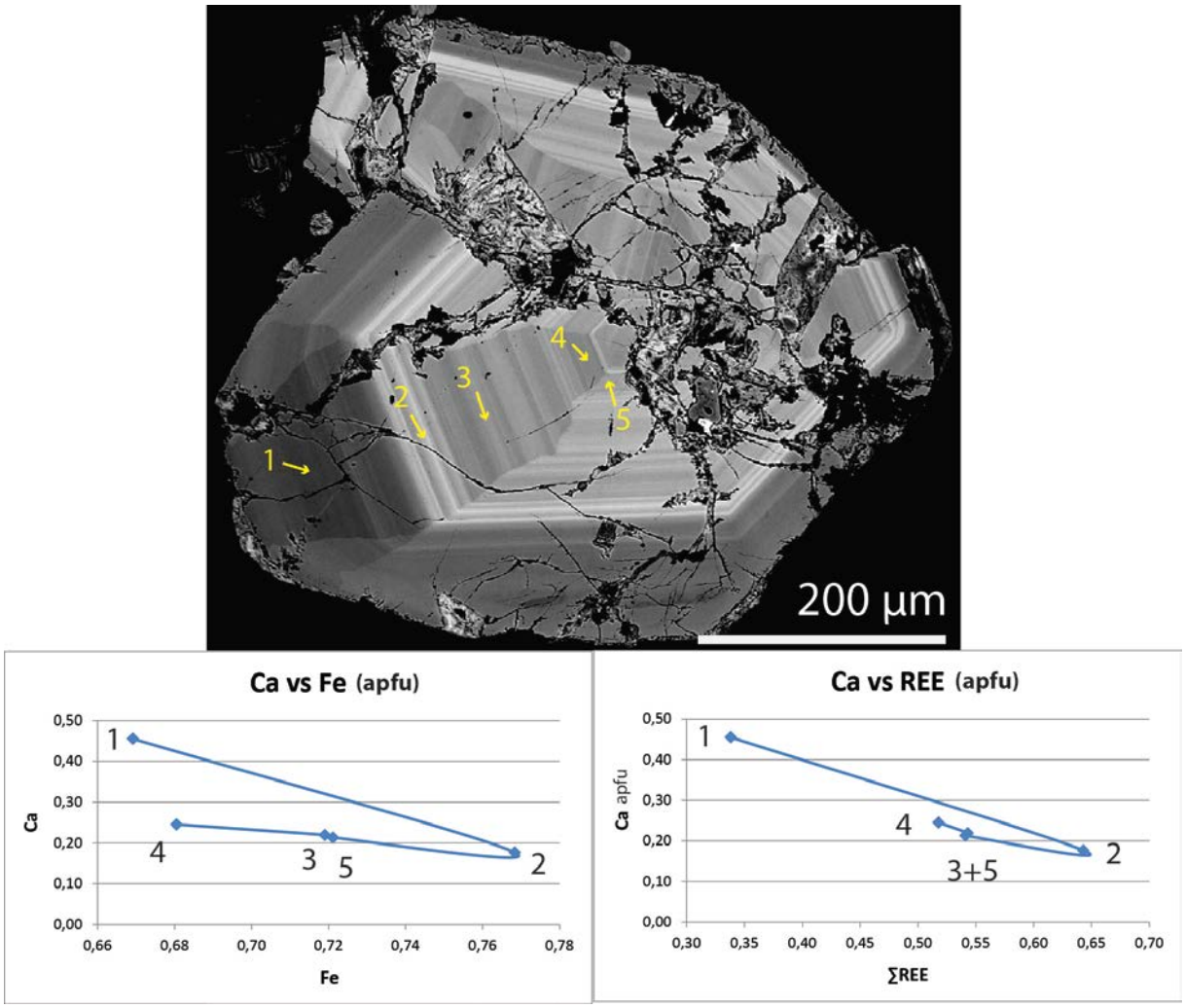

Figure 22 –BSE image of a gadolinite crystal with pristine zones showing alternating bright and dark zonation. Fractures are associated with metamictization induced by radioactive decay of thorium. EMPA analysis performed within selected zones indicated with numbers. Lower left: Calcium apfu plotted versus iron apfu. Bright zones contain elevated stoichiometric iron relative to calcium. Lower right: Similar plot with calcium apfu plotted versus REE apfu. Bright zones contain elevated stoichiometric REE relative to calcium.

Niobium and tantalum oxides

Columbite-(Fe), $FeNb_2O_6$

Complex oxides are observed in the samples and are primarily represented by columbite-(Fe) and pyrochlore group minerals. Columbite-(Fe) has previously been identified by X-ray powder diffraction (Jahren et al., 1998) however, based on EMP analysis the stoichiometry of the mineral is difficult to differentiate between ixiolite and columbite. This is due to a range of metals present in the analysis (i.e. Sb, W, Mn, Pb, Ti), and depending on calculated oxygen atoms. Recalculation based on 6 anions (columbite formula) yields a columbite-(Fe) formula. However, as seen in measurements along the rim (Table 7), EMP analysis yield low total

wt. %. All of the analyzed columbite-(Fe) grains contain a rim with different composition, which contains elevated lead- and lowered niobium- weight percent. These rims are possibly secondary alteration, and it is difficult to make an accurate measurement as the material is prone to beam penetration. The columbite-(Fe) is not observed with any mineral affinity, and appears both as local grains in the matrix and by clusters of danalite.

Table 7 - Selected chemical analysis of columbite-(Fe) from the amazonite pegmatite. Apfu calculated assuming 6 oxygen atoms. The high total wt. % value is produced by beam penetration, and low total values along the rim produced by elements not measured.

Wt. %	core	Core	core	core	rim	rim
FeO	16.66	16.46	16.75	16.39	0.37	0.10
Y_2O_3	0.36	0.413	0.39	0.44	0.12	22.15
ThO_2	0	0	0	0.09	1.22	4.17
Nb_2O_5	71.27	72.54	75.55	73.68	31.57	44.39
SnO	0.32	0.39	0.29	0.41	1.19	0.02
Sb_2O_3	0	0	0	0	4.17	0
Ta_2O_5	2.80	1.29	0.95	1.29	6.53	3.05
WO_3	2.66	1.13	1.62	1.28	4.97	0.54
PbO	0.38	0.48	0.30	0.32	37.25	0.44
UO_2	0.0129	0	0	0	1.75	0.57
MnO	3.95	2.77	2.99	2.89	0.25	0.05
CaO	0.06	0.27	0.07	0.22	1.68	0.89
TiO_2	2.36	2.83	2.74	3.09	6.96	0.57
Total	100.88	98.62	101.68	100.16	98.05	76.99
Formula proportions based on 6 oxygen atoms						
Fe	0.78	0,78	0.77	0.76	0.01	0
Y	0.01	0,01	0.01	0.01	0	0.32
Th	0.00	0,00	0	0	0.01	0.03
Nb	1.81	1,85	1.87	1.85	0.39	0.54
Sn	0.01	0,01	0.01	0.01	0.01	0
Sb	0.00	0,00	0	0	0.05	0
Ta	0.04	0,02	0.01	0.02	0.05	0.02
W	0.04	0,02	0.02	0.02	0.03	0
Pb	0.01	0,01	0	0	0.27	0
U	0.00	0,00	0	0	0.01	0
Mn	0.19	0,13	0.14	0.14	0.01	0
Ca	0	0.02	0	0.01	0.05	0.03
Ti	0.13	0.15	0.14	0.16	0.18	0.01
Total	3.01	3.00	2.98	2.99	1.06	0.95

Pyrochlore group

The pyrochlore group minerals have not been successfully analyzed on the EMP due to time constraints; however, when qualitatively analyzed with a scanning electron microscope (SEM) it appears to be a primary variation between niobium- and tantalum- dominated species (i.e. pyrochlore - microlite solution series; Hogarth, 1977). The pyrochlore is observed in thin-sections as masses of party overgrown grains (Fig. 23) with crystal faces at approximately 120^0. These pyrochlore grains are approximately 0.1 – 0.2 mm and subhedral to euhedral. The pyrochlore masses are associated with thorite and zircon, which are abundant across all observed thin-section samples and appear as a late stage.

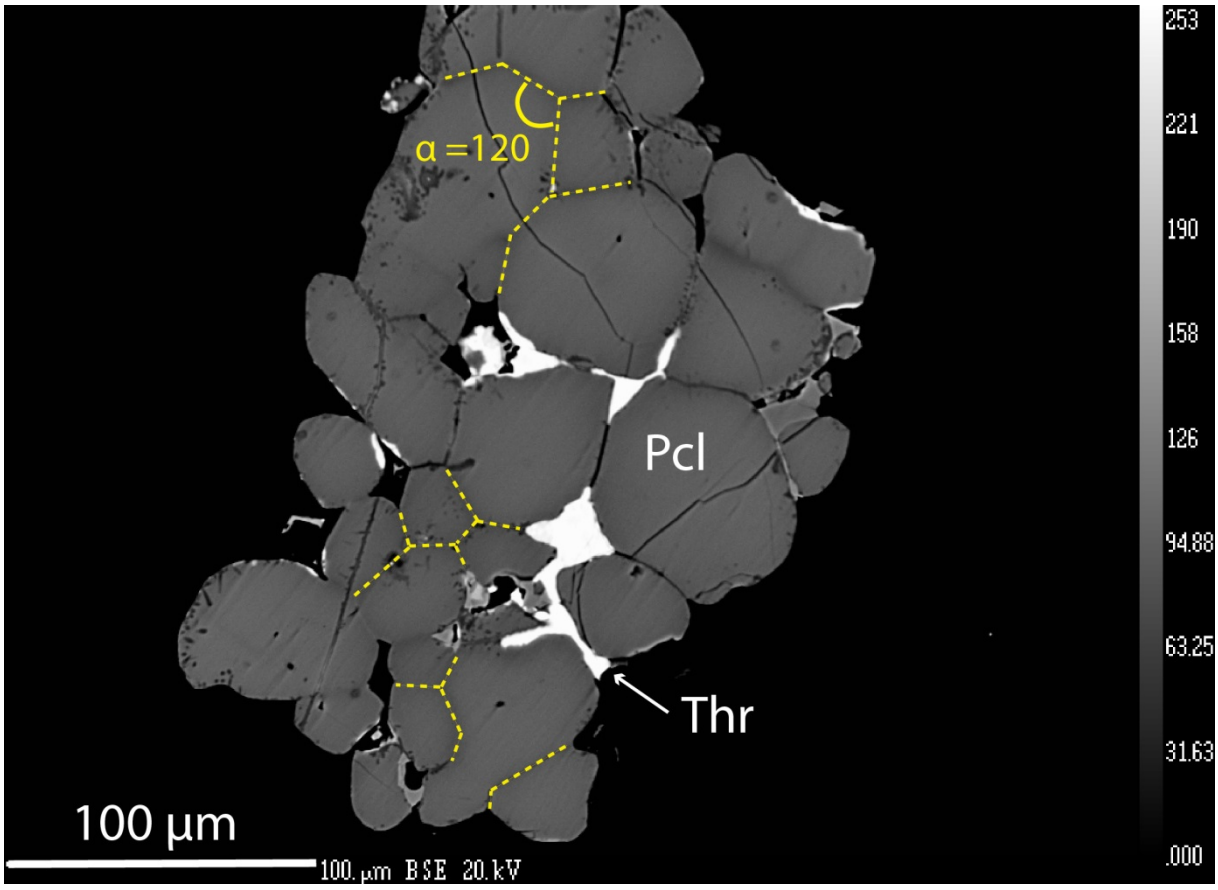

Figure 23 - BSE image of aggregate with pyrochlore (Pcl) group minerals and interstitial thorite (Thr). Dashed lines outline crystal grain boarders meeting at approximately 120 degree angle.

Other minerals not covered in this study

Initial studies of the amazonite pegmatite by Jahren et al (1998) performed XRD and microprobe analysis of several dark and visible indistinguishable minerals. Table 8 lists minerals from that study, which have not been investigated further. Hand-specimens contain powder-like material in several cavities and related to secondary alteration. Data from the EMPA has not been available (Jahren et al., 1998).

Table 8 - Additional minerals identified by Jahren et al (1998), but not analyzed in the current study. N.A = not available.

Mineral	**Chemical formula**	**Description**	**Identification**
Andradite	$Ca_3Fe_2Si_3O_{12}$	N.A.	EMPA
Allanite-(Ce)	$(Y,Ce,Ca)_2(Al,Fe)_3(SiO_4)_3(OH)$	N.A.	Not specified
Fergusonite-(Y)	$YNbO_4$	N.A.	Not specified
Sepiolite	$Mg_2Si_3O_8 \cdot 2\ H_2O$	Secondary	XRD
Halloysite	$Al_2Si_2O_5(OH)_4 \cdot 2\ H_2O$	Secondary	XRD
Tennantite	$(Cu,Fe)_{12}As_4S_{13}$	Secondary, inside cavity	XRD
Goethite	FeO(OH)	Secondary, inside cavity	XRD
Scheelite	$CaWO_4$	Microscopic grains	EMPA
Graphite	C	Amorphous carbon in transition to graphite	Reflective light microscopy
Halite	NaCl	Inclusion	Fluid inclusion
Sylvite	KCl	Inclusion	Fluid inclusion
Hematite	Fe_2O_3	Inclusion	Fluid inclusion
Hydrohalite	$NaCl \cdot 2\ H_2O$	Inclusion	Fluid inclusion

Element variation

The data pool for both major- and trace-element variations is represented by 15 samples as previously described in Table 4, and includes samples from the amazonite pegmatite, neighbor pegmatites, ekerite, and wall-rock. The limited dataset may not represent accurate variations, but it is possible to derive important differences primarily between the amazonite pegmatite and other pegmatites in the area, as they originate from a common source.

Major elements

Major elements plotted versus silica weight percent are presented in Fig. 24. Data on both major- and trace-element is presented in appendix 2. As seen in Figure 24 the amazonite pegmatite and neighbor pegmatites plot relatively close for all major elements. Al_2O_3, Na_2O, and TiO_2 appear stable in all samples while MnO shows a spread in the data. P_2O_5, K_2O, and CaO plot slightly higher for the amazonite pegmatite, but Fe_2O_3 is marginally higher in neighboring pegmatites.

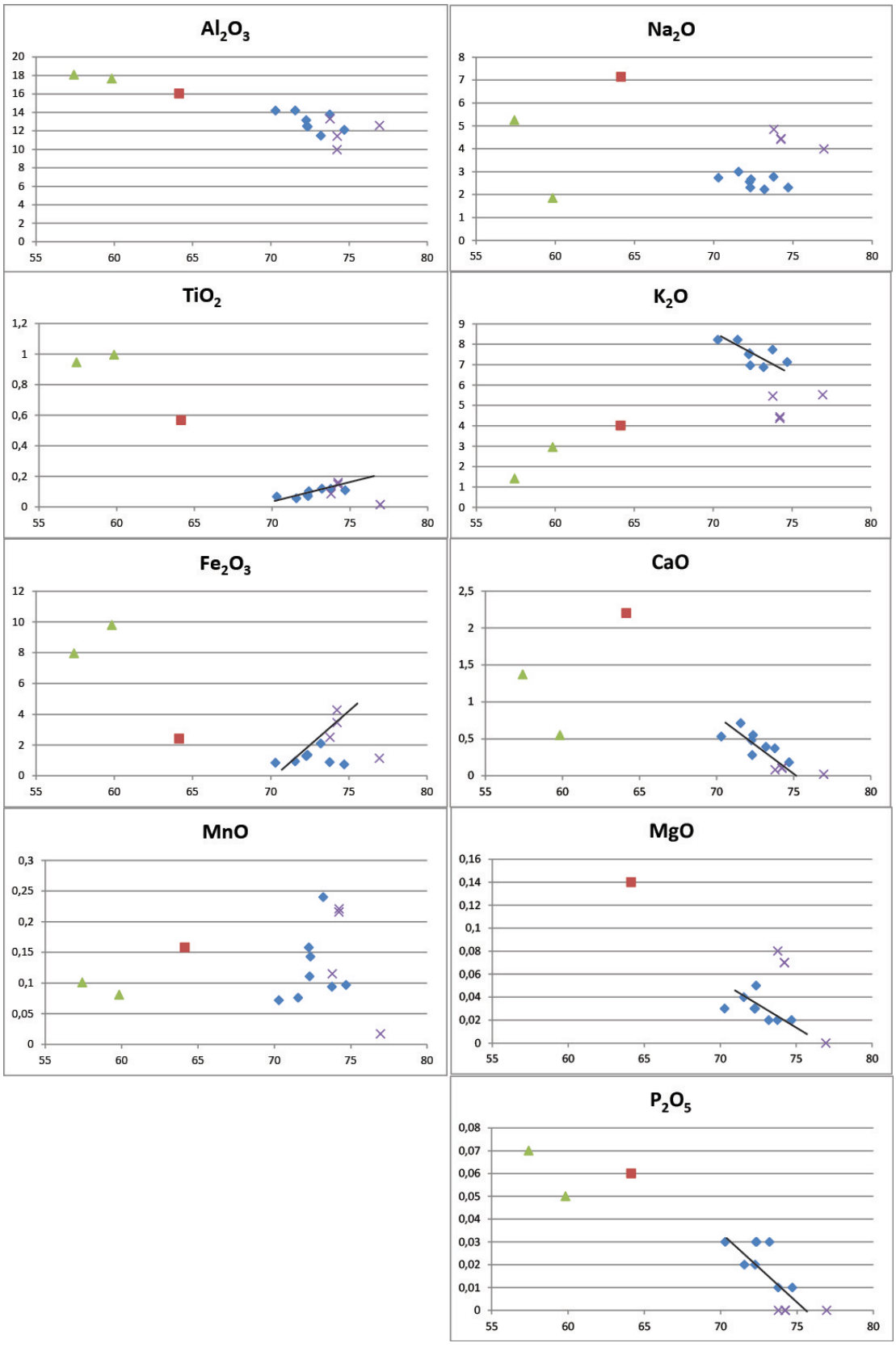

Figure 24 – Harker variation diagram of major element weight percent. Blue solid diamond: amazonite pegmatite, red square: ekerite, purple cross: other pegmatites in the region, green triangle: wall-rock of the amazonite pegmatite. Minor trend lines between the amazonite pegmatite and other pegmatites can be seen primarily in titanium, iron, and calcium. Titanium and iron increases while calcium decreases in the amazonite pegmatite, relative to other microcline pegmatites in the area. Plot of MgO in the wall-rock has been removed for visual purposes due to significant higher MgO.

Trace elements

The amazonite pegmatite at Bakstevalåsen show high contents of REE where the HREE are clearly enriched relative to LREE as seen in figure 25. This is very uncommon when compared to intrusive rocks in the Oslo Rift, which are in general LREE enriched (e.g. Neumann, 1976; Rasmussen, 1988). Most notably is the difference between the amazonite pegmatite and neighboring pegmatites in respect to trace elements as they cluster in two different groups (Fig. 26).

Rubidium and strontium are common trace-elements in feldspars (e.g. Iiyama, 1979); however, a discrepancy between the amazonite pegmatite and other microcline pegmatites in the area is observed (Fig. 26). Niobium exceeds the detection range with >1000 ppm in two samples which originate from the middle segment of the pegmatite, where boron mineralization is abundant (Fig. 9). Y versus REE shows a near linear correlation, and Nb - Ta ratios indicates different clustering between the amazonite- and neighbor-pegmatites. An interesting observation is the discrepancy between wall-rock material and the wall-rock reaction zone in respect to Nb and Ta content. The reaction zone contains relatively higher Nb than the wall-rock.

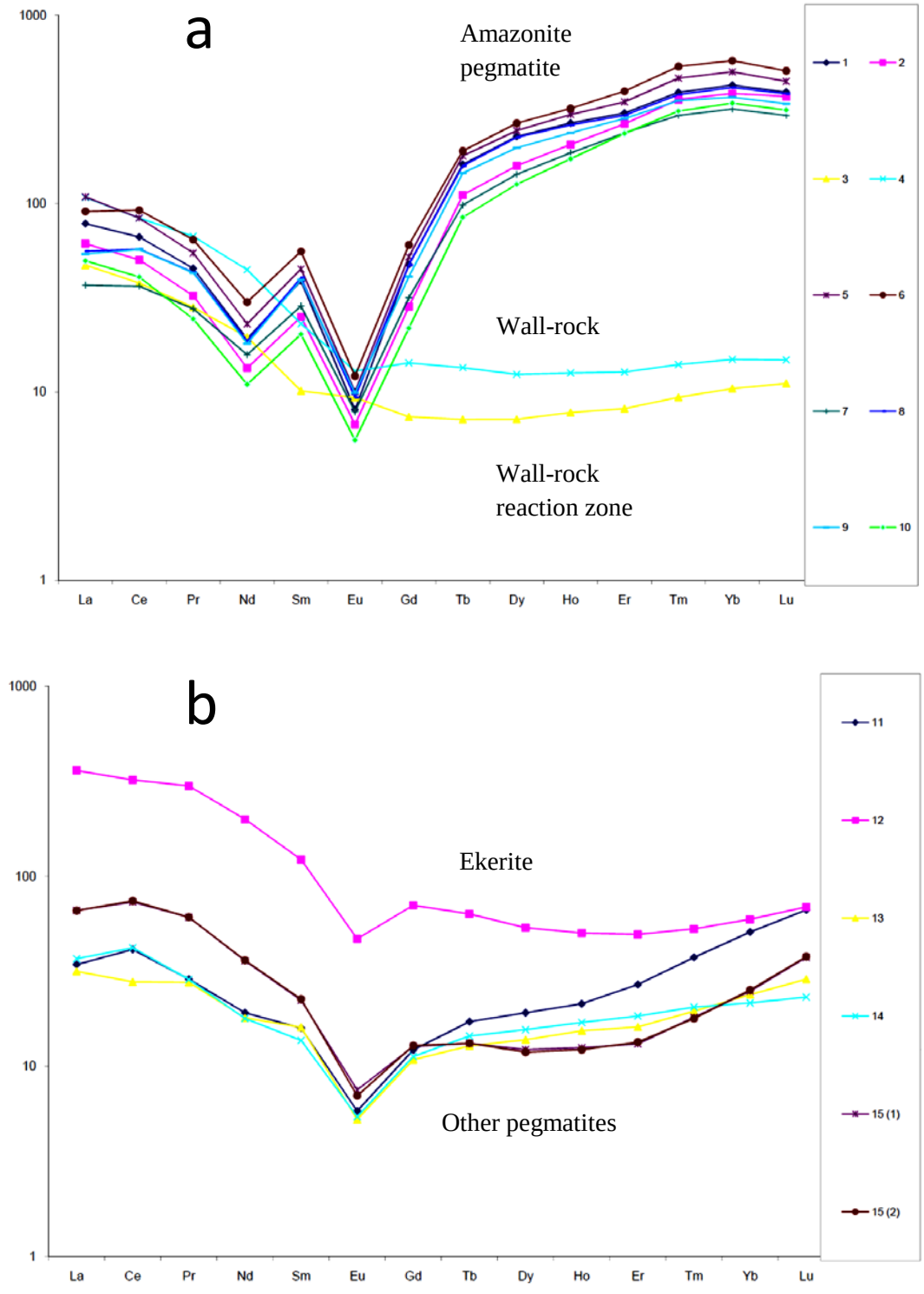

Figure 25 – REE chondrite normalized (McDonough & Sun, 1995) bulk-rock analysis from the amazonite pegmatite, neighbor pegmatite, and ekerite granitic intrusion. A: The samples 1,2,5,6,7,8,9 and 10 are from the amazonite pegmatite. Sample 3 and 4 are from the reaction zone and wall-rock respectively. B: Sample 12 is the ekerite granitic intrusion. Sample 11, 13, 14, and 15 are from other pegmatites in the area. The trend in elevated HREE relative to LREE in samples from the amazonite pegmatite is similar as seen in figure 8.

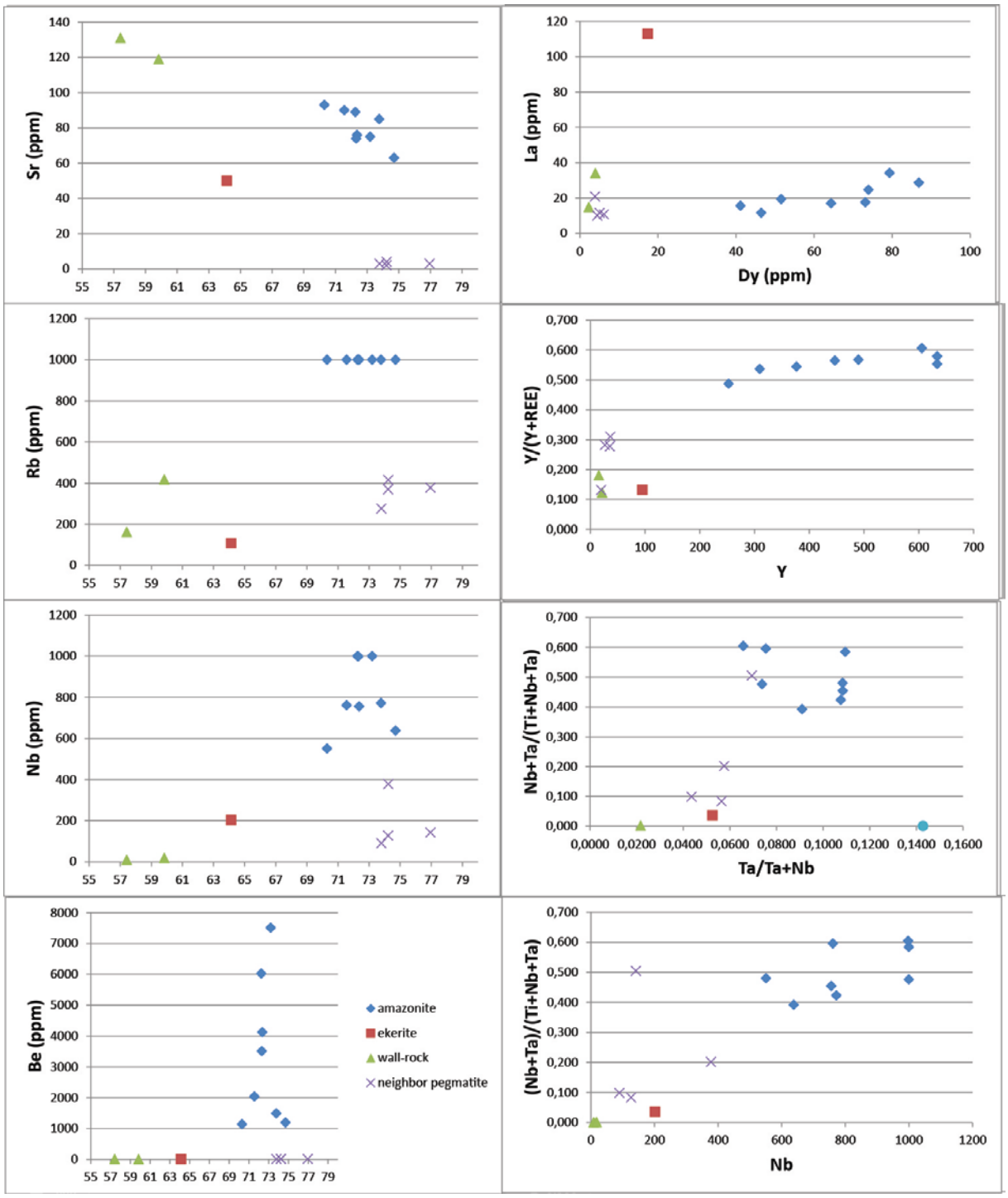

Figure 26 – Plot of trace element. Rb and Sr content with the same legend entry as in figure 8. Rubidium values for the amazonite pegmatite (blue diamond) exceed the equipment detection range (>1000 ppm) and therefore plot on a straight line. A noticeable difference between the microcline of the amazonite pegmatite and neighboring pegmatites can be observed. Niobium content (ppm) measures high in the amazonite pegmatite and two samples exceeds the detection limit of 1000 ppm and plot on a straight line. Nb – Ta ratios, and REE to Y relations are near linear, suggesting minor substitutions. LREE vs. HREE (La vs. Dy) show to trends from the ekerite source; both neighbor- and amazonite- pegmatite plot at low LREE values; however, the amazonite pegmatite has progressively increase in HREE.

Other pegmatites in the area

As seen in figure 5 (sample overview) several samples were collected from other pegmatites in the area between the ekerite granitic intrusion and the amazonite pegmatite at Bakstevalåsen. These pegmatites contain primarily microcline, quartz, amphibole, and accessory thorite and rutile minerals. The texture of these pegmatites is coarse grained where the amphibole crystals range between 2 and 5 cm. These pegmatites do not appear in the field with similar coarse- and fine-grained zones as the amazonite pegmatite. However, graphic granite intergrowth of microcline and quartz is clearly seen along the pegmatite margin. In polarized light the amphibole appear to be dominated by arfvedsonite, and the crystals are dominantly subhedral with secondary alteration. Figure 27 shows the observed pyroxene and amphibole which occur in the neighboring pegmatites in the area. Amphibole is the major mafic mineral with minor pyroxene, and almost all of the observed amphiboles contain secondary alteration.

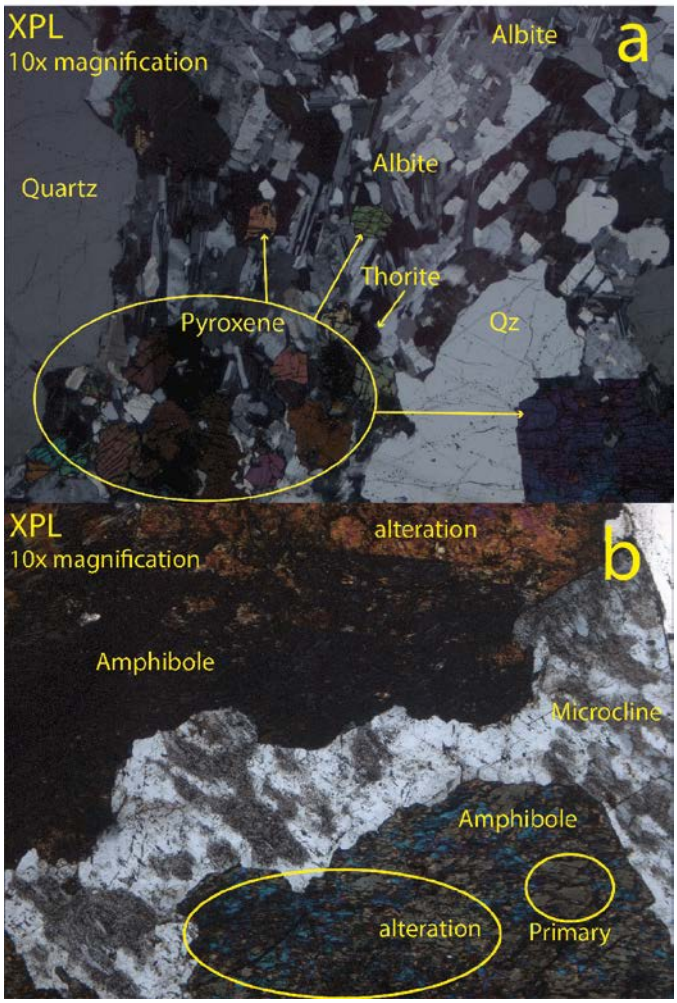

Figure 27 - Samples from amphibole pegmatite in the region viewed with crossed nicols (XPL) with 10x magnification (approximately FoW: 2x2 mm). Top: Subhedral to euhedral pryoxene in fine grained albite matrix. Bottom: Subhedral amphibole with an apparent secondary alteration).

Discussion

Pegmatite texture

The amazonite pegmatite contains a random zoning of coarse- and fine-grained texture (Fig. 6a, 7a, b). Factors which govern crystal growth and size in pegmatites depend on both undercooling of the rock-forming melt and fluxing of volatiles (H_2O, P, B, F) (Jahns & Burnham, 1969; Černy, 1992; London, 1990; 1996; 2008; 2009; London & Morgan, 2012; Linnen et al., 2012). The amazonite pegmatite is located approximately 700 meters away from the granitic host intrusion, but within the metamorphic aureole of the country rock. In addition the main pegmatite body has an alternating thickness between 10 – 30 cm, which could have implications on cooling rates and associated textures (i.e. zonation of a progressive growth front). A thorough fluid inclusion study might reveal accurate temperature ranges and the fluid medium which govern nucleation rates (halogen species). However, the classical model proposed by Jahns (1969) and refined by London (1984; 1990) for explaining pegmatite crystal growth, in terms of constitutional zone refinement, will not explain the coarse- and fine-grained texture (London & Morgan, 2012). The coarse grained texture is better explained by a first generation texture, which has been dissected in a later and secondary metasomatic stage. The striking diverging mineralogy within the two types of fabric strongly indicates a reducing fluid in respect to sulphides, with subsequent K auto metasomatism.

Amazonite coloring

Experimental work shows that the green amazonite color can be removed by heating up to 500 ^{o}C and re-introduced by irradiation (Hofmeister & Rossman, 1985a). Heating above 500 ^{o}C and subsequent radiation does not recover the amazonite color, but produce a smoky grey color due to disordered H centers (Hofmeister & Rossman, 1985a; 1985b). The intensity of green amazonite is related to the lead content (Foord & Martin, 1979) and the valence state (Pb^{+1}, Pb^{+2}) (Hofmeister & Rossman, 1985a). Recent studies indicate that a combined effect by lead and structural water govern the color intensity of amazonite (Hofmeister & Rossman, 1985a; Rein et al., 2004). The main mechanism behind amazonite coloring may be explained by three principal factors; irradiation invoked by ^{40}K which reduce Pb^{2+} to Pb^{1+}, and liberate hydroxyl radicals. These radicals may in turn oxidize Pb^{2+} to Pb^{3+} (Rein et al., 2004).

The amazonite color is not homogenous as described in the south- and middle-segment of the amazonite pegmatite at Bakstevalåsen. The amazonite in the south segment is observed with a uniform and crisp green color, but limited to the top layer adjacent to the sedimentary wall-

rock. However, in the middle segment the amazonite is only crisp green in the crystal core, and grades into a blue to faint grey variety towards the grain margin. This may imply that late circulating fluids altered the amazonite coloring by lead exchange, and not necessarily irradiation by radioactive decay.

Mineralogical associations

Danalite - genthelvite mineralization and element control

The helvite group is a beryllium silicate with minor sulphur, and composed of three end-members defined by manganese, iron, and zinc. There is complete miscibility between Mn – Fe and Zn – Fe (Hassan & Grundy, 1985). Pure end-member species are not found in nature, but average compositions contain varying amounts of zinc, iron, and manganese (Dunn, 1976). Danalite has not been reported from many Norwegian localities, however Høgtuva in the Nordland district contain a beryllium zone with accessory danalite crystals (Grauch et al, 1994).

Danalite is the rarest end-member of the helvite group, and the only end-member which was not successfully synthesized in the laboratory by Mel'nikov et al (1968), which is possibly explained by its narrow stability field in fO_2-fS_2 space (Burt, 1980), and the chalcophile-lithophile nature of manganese, zinc, and iron (Hassan & Grundy, 1985). In all the neighbor pegmatites observed in the study-area, iron appears to be controlled primarily by two mineral phases; amphibole (riebeckite and arfvedsonite) and accessory oxides (hematite, magnetite, and ilmenite). In the amazonite pegmatite iron is primarily controlled by magnetite and danalite in a succession where magnetite is abundant in the south segment, while danalite controls iron in the middle segment.

The magnetite in the south segment is accumulated along the bottom layer of the pegmatite body, which contains a narrow mineral assemblage (Fig. 9). At the middle segment of the amazonite pegmatite danalite is abundant in addition to a broad mineral assemblage. Figure 28 shows the hypothetical stability field of danalite, magnetite, pyrite, pyrrotite, and hematite in a $fS_2 – fO_2$ system (Burt, 1980). In addition to the narrow stability, Burt (1980) suggested danalite to be susceptible to supergene oxidation as it is not observed in coexistence with hematite (e.g. Glass et al., 1940; Oftedal & Sæbø, 1963; Kwak & Jackson, 1986). However, the fS_2 could possibly be buffered by graphite as indicated in Fig. 28, and provide a possible application on the observed danalite distribution in the studied amazonite pegmatite. Assuming the south segment represents an early consolidation phase of the pegmatite, the

middle- and north-segment might indicate a response from the pegmatite system to imposed geochemical changes.

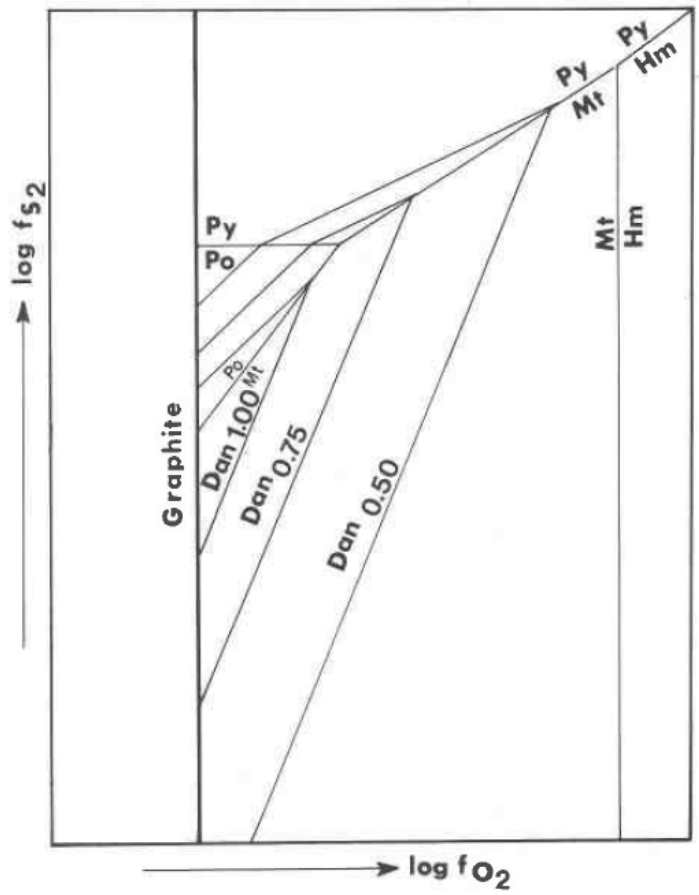

Figure 28 - Hypothetical fO_2 and fS_2 stability (Burt, 1980) in the system pyrite = Py, pyrrotite = Po, magnetite = Mt, and hematite = Hm. Danalite is susceptible to supergene oxidation and is not stable with hematite. Graphite may buffer sulphur fugacity.

In conjunction with the paragenetic sequence seen in Fig. 9 and the observed amazonite coloration, it is possible that late hydrothermal fluids were saturated with boron, sulphur, and/or calcium. Wall-rock derived carbon would thus provide graphite to buffer and possibly impair sulphur fugacity, promoting danalite stability in favor of magnetite. Burt (1980) suggested several breakdown reactions of danalite; however, these reactions could assumingly be equally danalite-forming under the right conditions. Based on the observed mineralogy of the amazonite pegmatite, the best suited reaction proposed by Burt (1980) is:

Reaction 1: 6 dan + 7 O_2 = 8 Mt + 9 Phe + 9 Qz + 2 S_2

Reaction 1 produces danalite and oxygen at the expense of magnetite, phenakite, quartz, and sulphur. Magnetite leaves the pegmatite system in the middle segment where danalite is most

abundant, and the supply of sulphur from the wall-rocks fit the reaction. Theoretically, oxygen provided by the reaction would be absorbed and/or transported away by circulating fluids, thus driving the reaction towards the left. However, phenakite occurs with a primary subhedral to euhedral crystal habit, and does not fit the reaction due to its abundance and near pristine crystals. Phenakite does not appear to be the Be source if danalite were to mineralize at a late stage. However, the abundance of danalite in the middle segment and the focused mineralization near wall-rock dilution into the pegmatite suggest some important aspects:

1) Indication of a secondary mineralization event due to increased circulation by fluxing fluids and the addition of chemical components.
2) Elevated sulphur fugacity buffered by graphite and promoting danalite stability.
3) Local phenakite crystals overgrown by danalite may represent a change in conditions which favor beryllium control by danalite.
4) Local grains of danalite – genthelvite in the south segment is restricted to the top layer, which is in contact with the wall-rock, and thus meets the assumptions of danalite stability induced by wall-rock derived fluids.

The most iron-rich danalite composition analyzed contains approximately Dan_{85}, but local variations do occur with a zinc dominated core and iron rich rim (Fig. 12 and 13). Similar variations are described by Kwak (1986), which were attributed simultaneous crystallization of iron-oxides, pyrite and sphalerite. If danalite crystallized simultaneously with other iron bearing minerals, the observed danalite compositions would not be expected due to the abundance of pyrite and biotite. Based on the observed relations in this study some possible mechanisms are proposed. The different crystal textures of danalite (Fig. 11) within coarse- and fine-grained zones may possibly reflect different growth rates governed by local volatile content and pegmatite thickness. The massive danalite grains observed within coarse grained zones could imply a steady-state growth rate, promoting rearrangement and partly resorbing nucleons along the growth-front interface, and thereby relatively enrich iron or zinc. The undefined and inconsistent danalite crystals which are associated with fine grained zones could reflect unsteady growth due to fluxing of fluids. Accordingly, the crystal textures which contain a homogeneous core or rim (Fig. 11 and 12) may reflect a change such growth condition. If the danalite crystals are a result from intergrowth of smaller grains, the local variations in iron-zinc ratios could simply reflect relict crystal cores and grain boundaries.

Helvite group minerals at other localities within the Oslo Region

The helvite and genthelvite members of the helvite group have been known in the Oslo region for a long time. Early observations were made in the syenite pegmatites in the Langesund area (Brøgger, 1890) and skarn deposits (Goldschmidt, 1911). Neumann (1950) and Oftedal & Sæbø (1963, 1965) reported findings of helvite in miarolitic cavities in the Grefsen and Nordmarka syenites. Oftedal (1963) gave a short review over the various localities where helvite were found and the accessory minerals in which it occurs. Based on his findings, Oftedal suggested the variations between the zinc (genthelvite) and manganese (helvite) end-members were attributed to temperature control and the availability of Zn. He proposed a general trend where genthelvite primarily occurs in equilibrium with sphalerite in skarn deposits, while helvite preferentially occur in syenite pegmatites where manganese saturation is more likely. The analytical data presented by Oftedal (1963) indicated helvite compositions with elevated zinc components. However, he did not fully recognize that there is no solid solution between zinc and manganese in the helvite group (Dunn, 1976; Hassan, 1985). Larsen (1988) published new chemical analyses from several of the helvite minerals in the syenite pegmatites of the Langesund area, and found the manganese components more in line with true helvites than the results of Oftedal (1963).

However, the majority of helvite localities in the Oslo region have a common mineral paragenesis: Quartz, biotite, muscovite, albite, zircon, sphene, pyroxene, allanite, amphibole, magnetite, calcite, molybdenite, galena, fluorite, astrophyllite, and monazite are reported as major phases occurring with helvite (Oftedal & Sæbø, 1963). The highest iron-% in genthelvite reported by Oftedal & Sæbø (1963) was from a skarn deposit near Grua with a 50% Mn and 45% Fe distribution. This genthelvite occurred in a matrix of pyroxene, magnetite, calcite, and minor fluorite.

Boron minerals

Boron is not associated with NYF type pegmatites (Černy & Ercit, 2005; Černy et al. 2012), but in the amazonite pegmatite boron is a major element occurring in schorl, danburite, nordenskiöldine, and possibly minor substitution with beryllium in the gadolinite-datolite solid solution series. Tourmaline and danburite is observed to mineralize along the wall-rock interface and into the pegmatite body, which further indicate a boron influx from the marine sediment wall-rock. Danburite and nordenskiöldine both contain calcium, with the former being abundant in the middle segment of the pegmatite (Fig. 9). Auto-metasomatism of

microcline and internal fractionation could enrich the residual fluid in respect to K and/or Ca, which would be highly reactive with boron. However, calcium could equally be derived from the calcareous wall-rock and explain mineralization of danburite and tourmaline along wall-rock material diluted into the pegmatite, and along microcline grain boundaries. London (1990) describes a similar process, however in the reverse order, where boron volatiles derived from the pegmatite body react with the wall-rock and deposit tourmaline outwards. The limited observation of boron minerals in the north segment is possibly related to a smaller sample pool due to limited exposure.

Gadolinite-(Y) and the calcium content

The measured gadolinite minerals contain substantial calcium relative to iron, while some individual crystal zonation are dominated by calcium (table 6); however, the name calcio-gadolinite was discredited by the IMA in 2006 (Burke, 2006). Figure 19 plots iron and calcium content according to the gadolinite – datolite solid solution series, where gadolinite-(Y) is the iron member. It is interesting to note that dysprosium is the dominant lanthanide element which is possibly related to a near ionic radius compared with Y, and thus promote a "camouflaged" substitution (Miyawaki et al., 1984). The observed enrichment in HREE relative to the LREE chondrite normalized pattern (Fig. 20) is commonly associated with rare element, gadolinite type pegmatite, and may be linked to partition of the REE into the late consolidation stage by F-complexing (Černy, 1997). Calcium-rich and iron-poor gadolinites are also found in miarolitic cavities at Cuasso al Monte, Italy (Pezzotta et al., 1999; Demartin & Minaglia, 2001).

Niobium and tantalum oxides

The primary carriers of Nb and Ta in granites and granitic pegmatites are columbite group minerals (Wise et al. 2012). This is also observed in the amazonite pegmatite with columbite-(Fe) and pyrochlore group minerals. In addition, fergusonite-(Y) was identified by Jahren et al. (1998). Trace-element analysis of the amazonite pegmatite measured Nb values above 1000 ppm (Fig. 26) with tantalum values below 100 ppm. The complex oxides are interpreted as a late phase; however, the geochemical control is not conclusive due to limited representative observations. The pyrochlore and columbite group minerals are possibly a late stage product, which mineralized by either metasomatic replacement or partition favoring the solid phase due to low temperature and consequent chemical quenching (e.g. London, 2008; Linnen et al, 2012).

Element distribution

Major elements

Figure 24 shows the major element variation versus silica weight percent; however, the number of samples is limited and may not reflect compositional variations precisely. The major elements do not show large discrepancies between the amazonite pegmatite and neighbor pegmatites. A slight decrease of calcium, phosphor, and potassium with increasing silica content can be seen. Calcium and potassium are associated with auto-metasomatism and the late mineralization of K-feldspar and albite, as seen in the north segment where cleavelandite partly replaces microcline. A slight increase in manganese may be linked to danalite being stable in favor of helvite, while iron appears to slightly decrease as expected during late mineralization of low temperature sulphides. Sodium, titanium, and alumina appear consistent, and are not observed in relation with any major mineralization trends.

Trace elements

Most REE deposits are situated in anorogenic extensional tectonics much similar to the tectonic setting of the Oslo Region (Chakhmouradian & Zaitsev, 2012). The REE chondrite normalized pattern from whole-rock analysis of the amazonite pegmatite (Fig. 25) shows a clear enrichment of HREE relative to LREE, which is unusual to rare element distribution in the Oslo Region (Neumann et al., 1974). The prominent europium anomaly is associated with the removal of plagioclase during fractional crystallization, where Eu^{2+} substitutes with Ca^{2+} (Winter, 2001). Despite this REE pattern being unusual for plutonic rocks in the Oslo Rift, it is normal for NYF family pegmatites to contain complex oxides which carry the heavy rare earths (Černy et al., 2012). On the contrary, elevated Rb and Sr (Rb exceeds detection limit), boron, and tantalum is not expected in a NYF suite pegmatite (Černy & Ercit, 2005; Černy et al., 2012). Figure 26 shows several interesting features; the amazonite pegmatite samples notably diverge from the plotted neighboring pegmatites in respect to Sr, Rb, and Nb with increasing silica. Rb^{+} and Sr^{+} are known to substitute with K^{+} in K-feldspar, but assuming a common genetic source for the pegmatites in the study area such discrepancies would not be expected. Lanthanum versus dysprosium shows notably divergence between the neighboring pegmatites and the amazonite pegmatite; however, the amazonite pegmatite shows an increase in dysprosium and is possibly related to accumulation of HREE into the residual volatile phase during internal fractionation. Nb-Ta and REE – Y variation appear semi-linear and could indicate substitution effects or late metasomatic remobilization. This is possibly indicated in the plot of Nb+Ta/Nb+Ti+Ta versus Nb+Ta where the wall-rock reaction zone

show a notably increase in Nb, and thus a potential Ta – Nb chemical exchange with pegmatite volatiles during metasomatic remobilization.

HFSE mobility

The post magmatic fluid which emplaced the amazonite pegmatite was likely saturated with fluorine, which is observed by fluorite and topaz mineralization, and was suggested by Hansteen & Burke (1990). In addition, Raade (1980) described several rare fluorides from miarolitic cavities within a separate ekerite intrusion further north. Fluorine increases the mobility of otherwise immobile elements (i.e. high field strength elements) by fluorine complexing (Salvi & William-Jones, 1996).

Implications to classification of the amazonite pegmatite

The amazonite pegmatite at Bakstevalåsen contain abundant Be-, Nb-, Y-, fluorine (in fluorite and topaz), and REE-minerals, which are characteristic for evolved NYF type pegmatites (Černy & Ercit, 2005). However, the amazonite pegmatite also contains abundant boron minerals, and pyrochlore which appear to be dominated by microlite (Hogarth, 1977). These elements are more characteristic for LCT- type pegmatites (Černy & Ercit, 2005; Černy et al., 2012) and may indicate an additional volatile influx or mixing of hydrothermal fluids during the late pegmatite consolidation stage. The amazonite pegmatite may potentially carry a weak LCT overprint on the original NYF signature, and thus indicate a mixed NYF + LCT pegmatite.

Conclusion

The amazonite pegmatite at Bakstevalåsen is classified as a rare-element class, gadolinite type pegmatite of the NYF family. The mineralogy of the pegmatite shows an internal zonation, which is related to one or several late- to post-magmatic hydrothermal alteration. The hydrothermal fluid must have interacted with the sedimentary wall-rocks by chemical exchange. This is best observed in the mineralogical difference between the south- and middle-segment, where early amazonite is localized near the wall-rock margin. Abundant boron and sulphide mineralization is observed in the middle segment, which also contain a thicker zone of the pegmatite body. The slightly thicker body in the middle segment may have facilitated longer cooling rates and volatile fluxing, resulting in a difference in texture fabric. The late hydrothermal stage imprinted the amazonite pegmatite with a weak LCT signature by the influx of primarily boron and possibly remobilization of niobium and tantalum. This influx also facilitated the narrow fO_2 – fS_2 stability field of danalite, which is observed to increase in abundance in the vicinity of diluted wall-rock. The lead and/or water content in the hydrothermal fluids also altered the amazonite coloring primarily along grain boundaries in the middle segment, where amazonite color appear bleached from crystal core and towards the rim.

The main element distribution of the amazonite pegmatite and neighboring pegmatite does not differ significantly; however, large discrepancies are observed in the trace-element distribution. Fractures and brittle defects in the initial pegmatite melt may have promoted permeability of fluids and accelerated chemical exchange.

Future work

This study merely scratches the surface on some of the petrogenetic processes of the amazonite pegmatite. At best, the results of this study manage to describe some of the many peculiar traits observed in the amazonite pegmatite. Additional substance to the initial observations would be provided by a few complementary studies:

1) Stable isotope analysis on primarily S and O, and investigate the scope of sedimentary influx and possible mixing with meteoric water.
2) A systematic bulk-rock analysis with a larger sample pool from the entire pegmatite and wall-rock profile, and perform trace-element analysis of the three main segments of the pegmatite to constrain and verify the ideas put forth in this study.
3) Chemical analysis and identify the composition of the abundant pyrochlore group minerals.
4) Investigate possible the zircon population and their Lu – Hf ages, and how these signatures correlate with “normal” Oslo Rift patterns.
5) Investigate the biotite group minerals and their iron component.

References

Alderton, D., H., M., Pearce, J., A., Potts, P., J. 1980. Rare earth element mobility during granite alteration: Evidence from southwest England. *Earth and Planetary Science Letters*, **49**, 149 – 165.

Andersen, T., Griffin, W., L., Jackson, S., E., Knudsen, T-L., Pearson, N., J. 2004. Mid-Proterozoic magmatic arc evolution at the southwest margin of the Baltic shield. *Lithos*, **73**, 289 – 318.

Andersen, T., Erambert, M., Larsen, A., O., Selbekk, R., S. 2010. Petrology of nepheline syenite pegmatites in the Oslo Rift, Norway: Zirconium silicate mineral assemblages as indicators of alkalinity and volatile fugacity in mildly agpaitic magma. *Journal of Petrology*, **51**, 2303 – 2325.

Barth, F., W., T. 1945. An account of the principal types of igneous rocks in the Oslo region, Norway, with special reference to essexites. *Geological Society of Denmark, Bulletin*, **10**, 636 – 641.

Brøgger, W., C. 1890. Die Mineralien der Syenitpegmatitgänge der südnorwegischen Augit- und Nephelinsyenite. *Zeitschrift fur Krystallographie*, **16**, 898 p.

Burke, A., J., E. 2006. A mass discreditation of GQN minerals. *The Canadian Mineralogist*, **44**, 1557 – 1560.

Burt, D., M. 1980. The stability of danalite, $Fe_4Be_3(SiO_4)_3S$. *American Mineralogist*, **65**, 355 – 360.

Cámara, F., Berti, R., Ottolini, L., Della-Ventura, G., Bellatreccia, F. 2008. The crystal chemistry of Li in gadolinite. *American Mineralogist*, **93**, 996 – 1004.

Chakhmouradian, R., A., Zaitsev, N., A. 2012. Rare earth mineralization in igneous rocks: Sources and processes. *Elements*, **8**, 347 – 353.

Černy, P. 1997. REE trends in rare-element granitic pegmatites; Enrichment vs. depletion in granite-to-pegmatite sequences. *Journal of the Czech Geological Society*, **42**, 34.

Černy, P., London, D., Novak, M. 2012. Granitic pegmatites as reflections of their sources. *Elements*, **8**, 289 – 294.

Černy, P. 1992. Geochemical and petrogenetic features of mineralization in rare-element granitic pegmatites in the light of current research. *Applied Geochemistry*, **7**, 393 – 416.

Černy, P., Meintzer, E., R., Anderson, J. A. 1985. Extreme fractionation in rare-element granitic pegmatites: Selected examples of data and mechanisms. *Canadian Mineralogist*, **23**, 381 – 421.

Černy, P., Ercit, S.T. 2005. The classification of granitic pegmatites revisited. *The Canadian Mineralogist*, **43**, 2005 – 2026.

Demartin, F., Minaglia, A. 2001. Characterization of gadolinite-group minerals using crystallographic data only: The case of hingganite-(Y) from Cuasso Al Monte, Italy. *The Canadian Mineralogist*, **39**, 1105 – 1114.

Dons, A., J. 1978. Terminology and history of investigations. *Norges Geologiske Undersøkelse, Bulletin*, **337**, 9 – 16.

Dunn, J., P. 1976. Genthelvite and the helvine group. *Mineralogical Magazine*, 40, 627 – 636.

Foord, E. E., Martin, F., R., 1979. Amazonite from the Pike's Peak batholith. *Mineralogical Record*, **10**, 373 – 382

Glass, J., J., Jahns, H., R., Stevens, E., R. 1944. Helvite and danalite from New Mexico and the helvite group. *The American Mineralogist*, **29**, 163 – 191.

Goldschmidt, V., M. 1911. Die Kontaktmetamorphose im Kristianiagebiet, *Videnskapsselskapets Skrifter. I. Matematisk-Naturvidenskapelig Klasse 1911. No*. **1**. 483 p.

Grauch, R., I., Lindahl, I., Evans, Jr., T., H., Burt, M., D., Fitzpatrick, J., J., Foord, E., E., Graff, P-R., Hysingjord, J. 1994. Høgtuvaite, a new beryllian member of the aenigmatite group from Norway, with new X-ray data on aenigmatite. *The Canadian Mineralogist*, **32**, 439 – 448.

Hansteen, T. H. Burke, E., A., J. 1990. Melt-mineral-fluid interaction in peralkaline silicic intrusions in the Oslo Rift, southeast Norway. II. High-temperature fluid inclusions in the Eikeren-Skrim complex. *Norges Geologiske Undersøkelse, Bulletin*, **417**, 15 – 32.

Hassan, I., Grundy, D., H. 1985. The crystal structures of helvite group minerals, $(Mn,Fe,Zn)_8(Be_6Si_6O_{24})S_2$. *American Mineralogist*, **70**, 186 – 192.

Hogarth, D., D. 1977. Classification and nomenclature of the pyrochlore group. *American Mineralogist*, **62**, 403 – 410.

Hofmeister, M., A., Rossman, R., G. 1985 a. A spectroscopic study of irradiation coloring of amazonite: structurally hydrous, Pb-bearing feldspar. *American Mineralogist*, **70**, 794 – 804.

Hofmeister, M., A., Rossman, R., G. 1985 b. A Model for the irradiative coloration of smoky feldspar and the inhibiting influence of water. *Physics and Chemistry of Minerals*, **12**, 324 – 332.

Hurum, J. Jahren, J. Berg, H-J. Bjerkgård, T. 1997. En eksotisk pegmatitt i Kambrosiluren ved Eikeren, Buskerud. *Norsk Bergverksmuseum Skrift*, **12**, 31-33.

Husebye, S., E., Ramberg, B., I. 1978. Geophysical investigations. *Norges Geologiske Undersøkelse, Bulletin*, **337**, 41 – 54.

Henningsmoen, G. 1978. Sedimentary rocks associated with the Oslo Region lavas. *Norges Geologiske Undersøkelse, Bulletin*, **337**, 17 – 24.

Iiyama, J., T. 1979. Trace element distribution in rock-forming silicates. The alkali and alkaline earths. *Physics and chemistry of the earth*, **11**, 161 – 174.

Ihlen, M., P., Vokes, M., F. 1978. Metallogeny. *Norges Geologiske Undersøkelse, Bulltein*, **337**, 75 – 90.

Jahns, H., R., Burnham, C., W. 1969. Experimental studies of pegmatite genesis: I. A model for the derivation and crystallization of granitic pegmatites. *Economic Geology*, **64**, 843 – 864.

Jahren, J., Hurum, J. 1997. Kambrosilurbergartene på Fiskum, øvre Eiker. *Norsk Bergverksmuseum Skrift*, **12**, 26 – 30.

Jahren, J., Berg, H.J. Hurum, J.H., Wulff-Pedersen, E. 1998. Nye undersøkelser av amazonitt-genthelvin pegmatitten fra Fiskum, Øvre Eiker. *Norsk Bergverksmuseum Skrift*, **13**, 13 – 15.

Jarosewich, E., Boatner, L., A. 1991. Rare-earth element reference samples for electron microprobe analysis. *Geostandards Newsletter*, **15**, 397 – 399.

Kwak, T., A., P., Jackson, P., G. 1986. The compositional variation and genesis of danalite in Sn-F–W skarns, NW Tasmania, Australia. *Neues Jahrbuch für Mineralogie. Monatshefte*, **10**, 452 – 462.

Larsen, A., O. 1988. Helvite group minerals from syenite pegmatites in the Oslo Region, Norway. Contribution to the mineralogy of Norway. *Norsk Geologisk Tidsskrift*, **68**, 119 – 124.

Larsen, A., O. 2010. The Langesundsfjord; History, geology, pegmatites, minerals. *Salzhemmerdorf, Germany: Bode*, 239 p.

Larsen, T., B., Olaussen, S., Sundvoll, B., Heeremans, M. 2008. The Permo-Carboniferous Oslo Rift through six stages and 65 million years. *Episodes*, **31**, 52 – 58.

Linnen, L., R., Van-Lichtervelde, M., Cerny, P. 2012. Granitic pegmatites as sources of strategic metals. *Elements*, **8**, 275 – 280.

Le Maitre, R., W. 2002. International union of geological sciences. Subcommission on systematics of igneous rocks. Igneous Rocks: A classification and glossary of terms. *Cambridge: Cambridge University Press*, 236 p.

London, D. 1990. Internal differentiation of rare-element pegmatites: A synthesis of recent research. *Geological Society of America Special Paper*, **246**, 35 – 50.

London, D. 1996. Granitic pegmatites. *Geological Society of America Special Papers*, **315**, 305 – 319.

London, D. 2008. Pegmatites. *Canadian Mineralogist Special Publication*, **10**, 347 p.

London, D. 2009. The origin of primary textures in granitic pegmatites. *The Canadian Mineralogist*, **47**, 697 – 724.

London, D., Morgan, IV., B., G. 2012. The pegmatite puzzle. *Elements*, **8**, 263 – 268.

Lutro, O., Nordgulen, Ø. 2008. Oslofeltet, berggrunnskart M 1:250 000. *Norges Geologiske Undersøkelse*.

McDonough, W., F., Sun, S., S. (1995): The composition of the earth. *Chemical Geology* **120**, 113-253.

Mel'nikov, O., K., Latvin, B., M., Fedosova, S., P. 1968. Production of helvite-group compounds. A. M. Lobacher, Ed. Gidrotermal'nyi Sintez Kristallov, Nauka Press, Moscov, 167 – 174.

Miyawaki, R., Nakai, I., Nagashima, K. 1984. A refinement of the crystal structure of gadolinite. *American Mineralogist*, **69**, 948 – 953.

Neumann, H., 1950. A new find of helvite in the Oslo area. *Norsk Geologisk Tidsskrift*, **28**, 234.

Neumann, E-R. 1976. Compositional relations among pyroxenes, amphiboles and other mafic phases in the Oslo Region plutonic rocks. *Lithos*, **9**, 85 – 109.

Neumann, E-R., Brunfelt, A., O., Finstad, G., K. 1977. Rare earth elements in some igneous rocks in the Oslo rift, Norway. *Lithos*, **10**, 311 – 319.

Neumann, E.-R., Wilson, M., Heermans, M., Spencer, E. A., Obst, K., Timmerman, M. J. Kirstein, L. 2004. Carboniferous-Permian rifting and magmatism in southern Scandinavia, the North Sea and northern Germany: a review. *Geological Society, London, special publication*, **223**, 11 – 41.

Oftedal, I., Sæbø, P., C. 1963. No. 18. Classification of some Norwegian members of the helvine Group. Contributions to the mineralogy of Norway. *Norsk Geologisk Tidsskrift*, **43**, 405 – 409.

Oftedal, I., Sæbø, P., C. 1965. Minerals from nordmarkite druses. Contributions to the mineralogy of Norway, No. 30. *Norsk Geologisk Tidsskrift*, **45**, 171 – 175.

Orlaussen, S., Larsen, T., B., Steel, R. 1994. The upper Carboniferous-Permian Oslo Rift; Basin fill in relation to tectonic development. *Canadian Society of Petroleum Geologists, Memoir*, **17**, 175 – 197.

Owen, A., W., Bruton, D., L., Bockelie, J., F., Bockelie, T. 1990. The Ordovician successions of the Oslo Region, Norway. *Norges Geologiske Undersøkelse, Special Publication*, **4**, 3 – 54.

Pezzotta, F., Diella, V., Guastoni, A. 1999. Chemical and paragenetic data on gadolinite-group minerals from Baveno and Cuasso al Monte, southern Alps, Italy. *American Mineralogist*, **84**, 782 – 789.

Raade, G. 1972. Mineralogy of the miarolitic cavitites in the plutonic rocks of the Oslo Region, Norway. *The Mineralogical Record*, **3**, 7 – 11.

Raade, G. 1980. Rare fluorides from a soda granite in the Oslo Region, Norway. The Mineralogical Record, 11, 83 – 91.

Ramberg, B. I., Larsen, T., B. 1978. Tectonomagmatic evolution. *Norges Geologiske Undersøkelse, Bulltein*, **337**, 55 – 73.

Rasmussen, E., Neumann, E-R., Andersen, T., Sundvoll, B., Fjerdingstad, V., Stabel, A. 1988. Petrogenetic processes associated with intermediate and silicic magmatism in the Oslo Rift, south-east Norway. *Mineralogical Magazine*, **365**, 293 – 307.

Rein, E., P., Simmons, B., W., Falster, U., A., Wise, A., M., Nizamoff, W., J. 2004. The cooperative effects of lead and structural water on color intensity of microcline, var. amazonite. *30th Rochester Mineralogical Symposium: Contributed Papers in Specimen Mineralogy: Part 3, Rocks and Minerals*, **79:5**, 341 – 345.

Salvi, S., Williams-Jones, E., A. 1996. The role of hydrothermal processes in concentrating high-field strength elements in the Strange Lake peralkaline complex, northeastern Canada. *Geochimica et Cosmochimica Acta*, **60**, 1917 – 1932.

Shmakin, B., M. 2007. Diversity of accessory minerals in rare-metal-rare earth pegmatites. *Geology of Ore Deposits*, **50**, 518 – 523.

Trønnes, G., R., Brandon, D., A. 1992. Mildly peraluminous high-silica granites in a continental rift: the Drammen and Finnemarka batholiths, Oslo Rift, Norway. *Contributions to Mineralogy and Petrology*, **109**, 275 – 294.

Whitney, L., D., Evans, W., B. 2010. Abbreviations for names of rock-forming minerals. *American Mineralogist*, **95**, 185 – 187.

Winter, D., J. 2001. Principles of igneous and metamorphic petrology, 2nd edition. *Pearson Prentice Hall*, 693 p.

Wise, A., M., Francis, A., C., Cerny, P. 2012. Compositional and structural variations in columbite-group minerals from granitic pegmatites of the Brunswick and Oxford fields, Maine: differential trends in F-poor and F-rich environments. *The Canadian Mineralogist*, **50**, 1515 – 1530.

Zagorsky, V., Ye., Makagon, V., M., Shmakin, B., M. 2003. Systematics of granitic pegmatites. *Russian Geology and Geophysics*, **44**, 422 – 435.

Appendix 1: EMP data

- Danalite
- Gadolinite-(Y)
- Cassiterite and nordenskiöldine

Danalite	**B-0**	1	2	3	4	5	6	7	8	9	10	11	12	13	14	15
wt. %	SiO_2	31.65	31.66	32.15	31.71	31.85	31.85	32.28	31.99	32.18	32.11	31.95	31.37	31.94	31.94	32.04
	S	5.70	5.62	5.65	5.78	5.70	5.59	5.77	5.83	5.73	5.79	5.69	5.56	5.77	5.67	5.66
	MnO	7.29	11.38	7.81	6.06	7.90	11.37	6.89	6.34	6.78	5.91	6.55	11.13	7.04	6.34	6.22
	FeO	25.44	19.60	30.47	29.09	23.42	18.49	31.11	27.51	29.68	30.04	29.27	17.54	21.43	27.36	30.27
	ZnO	19.41	22.16	14.08	17.30	21.57	22.96	14.18	18.75	16.26	16.01	16.16	23.68	24.23	18.31	15.85
	BeO	13.10	12.30	12.60	12.90	12.40	12.50	12.60	12.40	12.20	13.00	13.20	13.40	13.20	13.20	12.70
	Total	99.75	99.91	99.93	99.96	99.99	99.97	99.94	99.92	99.97	99.97	99.97	99.90	100.73	99.99	99.91
apfu	Si	3.01	3.04	3.05	3.02	3.05	3.05	3.06	3.06	3.07	3.04	3.02	2.99	3.02	3.02	3.04
	S	1.02	1.01	1.00	1.03	1.02	1.00	1.02	1.04	1.03	1.03	1.01	0.99	1.02	1.01	1.01
	Mn	0.59	0.93	0.63	0.49	0.64	0.92	0.55	0.51	0.55	0.47	0.52	0.90	0.56	0.51	0.50
	Fe	2.03	1.58	2.42	2.31	1.88	1.48	2.47	2.20	2.37	2.38	2.31	1.40	1.70	2.17	2.40
	Zn	1.36	1.57	0.99	1.22	1.53	1.62	0.99	1.32	1.15	1.12	1.13	1.66	1.69	1.28	1.11
	Be	3.00	2.84	2.87	2.95	2.85	2.88	2.87	2.85	2.80	2.95	3.00	3.07	3.00	3.00	2.90
		16	17	18	19	20	21	22	23	24	25	26	27	28	29	30
wt. %	SiO_2	30.42	30.48	30.96	30.74	30.73	30.90	30.76	30.75	30.75	30.96	30.83	30.63	30.91	31.15	31.45
	S	5.68	5.87	5.84	5.76	5.88	5.74	5.91	5.85	5.74	5.70	5.76	5.74	5.84	5.82	5.71
	MnO	5.98	6.17	6.09	6.09	6.44	6.33	6.17	5.97	6.11	6.19	5.98	6.81	6.85	6.07	6.06
	FeO	24.61	28.51	30.14	30.73	30.83	31.20	30.81	30.71	29.90	30.20	30.16	22.51	23.16	30.35	30.69
	ZnO	21.52	18.43	16.06	16.09	15.73	15.74	15.50	16.10	16.32	16.57	16.39	23.64	23.61	16.11	16.08
	BeO	13.60	13.40	13.80	13.40	13.30	12.90	13.70	13.50	14.00	13.20	13.70	13.50	12.50	13.40	12.80
	Total	98.96	99.93	99.98	99.94	99.98	99.95	99.90	99.96	99.95	99.98	99.95	99.96	99.96	99.99	99.95
apfu	Si	2.93	2.92	2.93	2.93	2.93	2.96	2.92	2.93	2.91	2.95	2.93	2.93	2.99	2.96	3.00
	S	1.02	1.05	1.04	1.03	1.05	1.03	1.05	1.04	1.02	1.02	1.02	1.03	1.06	1.04	1.02
	Mn	0.49	0.50	0.49	0.49	0.52	0.51	0.50	0.48	0.49	0.50	0.48	0.55	0.56	0.49	0.49
	Fe	1.98	2.28	2.39	2.45	2.46	2.50	2.45	2.44	2.37	2.41	2.39	1.80	1.87	2.41	2.45
	Zn	1.53	1.30	1.12	1.13	1.11	1.11	1.09	1.13	1.14	1.17	1.15	1.67	1.69	1.13	1.13
	Be	3.15	3.08	3.14	3.07	3.05	2.97	3.13	3.09	3.18	3.02	3.12	3.11	2.90	3.06	2.93

B-0 continued		31	32	33	34	35	36	37	38	39	40	41	42	43	44	45
wt. %	SiO_2	31.30	29.49	29.29	29.75	29.30	29.69	29.50	29.53	29.85	29.83	30.10	29.85	29.87	29.89	31.96
	S	5.72	5.89	5.82	5.75	5.86	5.90	5.82	5.85	5.78	5.69	5.63	5.67	5.84	5.73	5.65
	MnO	6.35	6.51	6.39	6.48	6.54	6.46	6.44	6.35	6.13	6.53	6.26	6.30	6.39	6.32	6.37
	FeO	29.64	27.92	27.66	27.79	27.76	27.64	28.17	27.85	26.98	23.62	27.48	26.01	26.91	27.14	27.22
	ZnO	17.01	18.42	18.56	18.87	18.22	18.72	18.10	18.74	18.85	23.17	19.43	20.40	18.91	18.63	18.82
	BeO	12.80	14.60	15.10	14.20	15.20	14.50	14.80	14.50	15.20	14.00	13.90	14.50	14.90	15.10	12.80
	Total	99.96	99.90	99.91	99.96	99.96	99.97	99.93	99.90	99.91	100.00	100.00	99.90	99.91	99.96	99.99
apfu	Si	2.99	2.81	2.78	2.84	2.77	2.82	2.80	2.81	2.81	2.86	2.87	2.84	2.83	2.82	3.04
	S	1.02	1.05	1.04	1.03	1.04	1.05	1.03	1.04	1.02	1.02	1.01	1.01	1.04	1.01	1.01
	Mn	0.51	0.53	0.51	0.52	0.52	0.52	0.52	0.51	0.49	0.53	0.51	0.51	0.51	0.50	0.51
	Fe	2.37	2.22	2.19	2.22	2.20	2.20	2.24	2.22	2.13	1.89	2.19	2.07	2.13	2.14	2.16
	Zn	1.20	1.29	1.30	1.33	1.27	1.31	1.27	1.32	1.31	1.64	1.37	1.43	1.32	1.30	1.32
	Be	2.94	3.34	3.44	3.25	3.46	3.31	3.38	3.32	3.44	3.22	3.19	3.31	3.39	3.42	2.92
		46	47	48	49	50	51	52	53	54	55	56	57	58	59	60
wt. %	SiO_2	32.13	32.07	32.04	31.91	32.03	32.02	32.31	32.03	32.21	31.95	31.49	31.80	32.19	31.64	31.85
	S	5.75	5.64	5.69	5.65	5.69	5.61	5.55	5.70	5.68	5.59	5.63	5.53	5.62	5.50	5.62
	MnO	5.81	6.32	6.38	6.87	6.53	6.51	6.03	6.12	6.28	5.61	5.29	5.45	5.84	5.40	5.62
	FeO	26.55	26.79	27.49	26.53	25.65	27.80	27.33	26.39	26.55	24.52	23.67	24.42	26.20	23.48	24.23
	ZnO	19.89	19.10	18.22	19.55	20.52	18.32	18.98	20.12	19.83	22.41	23.28	22.58	20.65	22.92	22.07
	BeO	12.70	12.80	13.00	12.30	12.40	12.50	12.50	12.40	12.20	12.70	13.40	12.90	12.30	13.80	13.40
	Total	99.96	99.91	99.98	99.99	99.98	99.97	99.94	99.92	99.92	99.98	99.95	99.92	99.99	100.00	99.98
apfu	Si	3.06	3.05	3.04	3.05	3.06	3.05	3.07	3.06	3.08	3.05	3.00	3.03	3.08	2.99	3.02
	S	1.03	1.00	1.01	1.01	1.02	1.00	0.99	1.02	1.02	1.00	1.00	0.99	1.01	0.97	1.00
	Mn	0.47	0.51	0.51	0.56	0.53	0.53	0.49	0.50	0.51	0.45	0.43	0.44	0.47	0.43	0.45
	Fe	2.11	2.13	2.18	2.12	2.05	2.22	2.17	2.11	2.12	1.96	1.88	1.95	2.09	1.86	1.92
	Zn	1.40	1.34	1.27	1.38	1.45	1.29	1.33	1.42	1.40	1.58	1.63	1.59	1.46	1.60	1.54
	Be	2.90	2.92	2.96	2.83	2.85	2.86	2.86	2.85	2.80	2.91	3.06	2.96	2.82	3.13	3.05

B-0 continued		61	62	63	64	65	66	67	68	69	70
wt. %	SiO_2	31.73	31.68	31.79	32.05	32.12	31.75	32.09	32.07	32.22	32.09
	S	5.69	5.58	5.67	5.70	5.72	5.73	5.62	5.59	5.96	5.89
	MnO	5.42	5.52	5.79	6.68	5.53	5.27	6.44	6.72	6.50	5.36
	FeO	25.20	24.49	26.02	27.32	24.77	23.86	26.05	28.16	27.32	31.08
	ZnO	22.14	22.43	21.24	18.83	22.20	24.24	19.89	17.42	18.05	15.12
	BeO	12.60	13.00	12.30	12.20	12.50	12.00	12.70	12.80	12.90	13.30
	Total	99.94	99.92	99.97	99.93	99.98	100.00	100.00	99.96	99.98	99.91
apfu	Si	3.04	3.02	3.05	3.07	3.07	3.07	3.05	3.04	3.06	3.03
	S	1.02	1.00	1.02	1.02	1.02	1.04	1.00	0.99	1.06	1.04
	Mn	0.44	0.45	0.47	0.54	0.45	0.43	0.52	0.54	0.52	0.43
	Fe	2.02	1.95	2.09	2.19	1.98	1.93	2.07	2.24	2.17	2.45
	Zn	1.56	1.58	1.50	1.33	1.57	1.73	1.40	1.22	1.26	1.05
	Be	2.90	2.98	2.84	2.81	2.87	2.78	2.90	2.92	2.94	3.01

	B3-1	71	72	73	74	75	76	77	78	79	80	81	82	83	84	85
wt. %	SiO_2	31.82	31.36	31.49	31.74	31.63	31.62	31.66	31.46	31.74	31.94	31.90	32.10	32.23	32.05	31.25
	S	5.64	5.64	5.66	5.62	5.51	5.66	5.71	5.66	5.66	5.60	5.81	5.59	5.63	5.62	5.79
	MnO	5.67	4.65	5.22	5.40	4.72	6.03	5.71	5.65	5.54	5.98	6.20	5.94	5.30	5.87	6.51
	FeO	24.00	17.58	22.60	22.36	20.70	24.34	23.82	23.65	25.82	25.52	25.52	25.74	25.61	25.26	24.03
	ZnO	23.20	31.22	24.51	24.66	27.91	22.92	23.53	23.29	21.63	21.19	21.25	20.90	21.36	21.77	22.41
	BeO	12.40	12.30	13.30	13.00	12.20	12.20	12.40	13.10	12.40	12.50	12.20	12.50	12.60	12.20	12.80
	Total	99.91	99.94	99.97	99.97	99.93	99.94	99.99	99.98	99.95	99.94	99.97	99.98	99.91	99.97	99.91
apfu	Si	3.05	3.04	3.00	3.03	3.06	3.05	3.04	3.00	3.04	3.05	3.06	3.06	3.07	3.07	3.00
	S	1.01	1.03	1.01	1.00	1.00	1.02	1.03	1.01	1.02	1.00	1.04	1.00	1.00	1.01	1.04
	Mn	0.46	0.38	0.42	0.44	0.39	0.49	0.46	0.46	0.45	0.48	0.50	0.48	0.43	0.48	0.53
	Fe	1.93	1.43	1.80	1.79	1.67	1.96	1.91	1.89	2.07	2.04	2.05	2.05	2.04	2.03	1.93
	Zn	1.64	2.24	1.72	1.74	1.99	1.63	1.67	1.64	1.53	1.50	1.51	1.47	1.50	1.54	1.59
	Be	2.86	2.87	3.05	2.98	2.83	2.82	2.86	3.01	2.86	2.87	2.81	2.87	2.89	2.81	2.95

B3-1 continued		86	87	88	89	90	91	92	93	94	95	96	97	98	99	100
wt. %	SiO_2	31.75	31.58	31.20	31.28	31.56	31.07	31.62	32.14	31.51	31.70	31.93	32.24	31.32	31.03	31.28
	S	5.58	5.61	5.57	5.49	5.48	5.60	5.59	5.60	5.68	5.60	5.61	5.67	5.61	5.65	5.66
	MnO	5.84	7.10	3.93	3.96	5.41	4.55	5.50	5.31	6.14	6.85	4.89	5.48	5.44	5.31	5.50
	FeO	23.82	22.19	10.59	18.87	22.99	15.45	23.10	22.64	13.59	20.42	20.87	22.69	21.45	11.69	21.73
	ZnO	23.29	23.82	39.02	30.60	23.94	33.74	24.74	25.03	33.25	25.25	26.88	24.43	25.57	36.75	25.20
	BeO	12.50	12.50	12.40	12.50	13.30	12.30	12.20	12.00	12.60	12.90	12.60	12.30	13.40	12.30	13.40
	Total	99.99	100.00	99.93	99.96	99.94	99.92	99.96	99.93	99.94	99.93	99.98	99.98	99.99	99.91	99.95
apfu	Si	3.04	3.03	3.05	3.03	3.00	3.03	3.05	3.09	3.05	3.03	3.06	3.09	2.99	3.03	2.99
	S	1.00	1.01	1.02	1.00	0.98	1.02	1.01	1.01	1.03	1.00	1.01	1.02	1.00	1.04	1.01
	Mn	0.47	0.58	0.32	0.32	0.44	0.38	0.45	0.43	0.50	0.56	0.40	0.44	0.44	0.44	0.44
	Fe	1.91	1.78	0.86	1.53	1.83	1.26	1.86	1.82	1.10	1.63	1.67	1.82	1.71	0.96	1.73
	Zn	1.65	1.69	2.81	2.19	1.68	2.43	1.76	1.78	2.37	1.78	1.90	1.73	1.80	2.65	1.78
	Be	2.88	2.88	2.91	2.91	3.04	2.88	2.83	2.78	2.93	2.96	2.90	2.83	3.07	2.89	3.07

		101	102	103	104	105	106	107
Wt. %	SiO_2	31.57	31.68	31.66	31.90	31.04	31.93	31.71
	S	5.73	5.70	5.58	5.73	5.71	5.80	5.71
	MnO	5.14	5.35	7.78	5.45	5.70	5.49	5.14
	FeO	21.64	21.55	16.77	22.41	11.93	22.65	13.26
	ZnO	26.03	25.25	28.90	24.83	36.11	25.04	35.71
	BeO	12.70	13.30	12.00	12.50	12.30	11.90	11.30
	Total	99.95	99.99	99.91	99.95	99.94	99.91	99.97
apfu	Si	3.03	3.02	3.07	3.06	3.03	3.09	3.11
	S	1.03	1.02	1.01	1.03	1.05	1.05	1.05
	Mn	0.42	0.43	0.64	0.44	0.47	0.45	0.43
	Fe	1.74	1.72	1.36	1.80	0.97	1.83	1.09
	Zn	1.85	1.78	2.07	1.76	2.60	1.79	2.59
	Be	2.93	3.04	2.79	2.88	2.89	2.76	2.67

	B5-1	108	109	110	111	112	113	114	115	116	117	118	119	120	121	122
wt. %	SiO_2	32.42	32.51	32.19	32.22	32.33	32.22	32.28	32.38	32.51	32.37	32.53	32.39	32.56	32.30	32.43
	S	5.88	5.76	5.73	5.84	5.80	5.77	5.86	5.75	5.78	5.86	5.75	5.82	5.79	5.77	5.77
	MnO	5.67	5.36	5.22	5.38	5.51	5.73	5.67	5.49	5.52	5.36	5.53	5.47	5.62	5.58	5.53
	FeO	34.89	34.63	33.98	33.70	35.02	34.91	35.64	34.30	33.61	33.96	35.61	34.77	35.31	34.82	34.38
	ZnO	11.47	11.74	13.16	13.07	11.53	11.78	10.33	11.62	13.25	13.06	10.97	11.07	10.51	11.34	12.29
	BeO	12.60	12.80	12.50	12.70	12.70	12.40	13.10	13.30	12.20	12.30	12.40	13.30	13.00	13.00	12.40
	Total	100.00	99.93	99.92	100.00	99.99	99.93	99.95	99.97	99.99	99.98	99.92	99.91	99.90	99.93	99.92
apfu	Si	3.06	3.06	3.06	3.05	3.05	3.06	3.04	3.04	3.09	3.07	3.08	3.04	3.06	3.04	3.07
	S	1.04	1.02	1.02	1.04	1.03	1.03	1.03	1.01	1.03	1.04	1.02	1.02	1.02	1.02	1.02
	Mn	0.45	0.43	0.42	0.43	0.44	0.46	0.45	0.44	0.44	0.43	0.44	0.43	0.45	0.44	0.44
	Fe	2.76	2.73	2.70	2.67	2.77	2.77	2.80	2.69	2.67	2.70	2.82	2.73	2.77	2.74	2.72
	Zn	0.80	0.82	0.92	0.91	0.80	0.83	0.72	0.80	0.93	0.92	0.77	0.77	0.73	0.79	0.86
	Be	2.86	2.90	2.85	2.89	2.88	2.83	2.96	3.00	2.78	2.81	2.82	3.00	2.93	2.94	2.82
		123	124	125	126	127	128	129	130	131	132	133	134	135		
wt. %	SiO_2	31.86	31.74	31.87	32.21	32.17	31.93	32.36	32.03	32.13	32.26	32.55	32.35	32.35		
	S	5.81	5.71	5.61	5.74	5.79	5.82	5.76	5.76	5.78	5.77	5.74	5.79	5.74		
	MnO	5.85	5.83	5.81	5.83	5.80	6.10	5.83	5.87	6.17	5.82	5.72	5.91	5.60		
	FeO	35.48	33.69	35.53	35.34	33.67	27.30	30.75	35.61	33.72	36.58	36.21	36.89	36.95		
	ZnO	10.86	12.66	10.66	11.39	12.36	19.17	15.39	10.06	12.56	9.59	9.85	8.97	9.24		
	BeO	13.00	13.20	13.30	12.30	13.00	12.50	12.70	13.50	12.50	12.80	12.70	12.90	12.90		
	Total	99.96	99.98	99.97	99.94	99.91	99.92	99.93	99.95	99.97	99.94	99.91	99.91	99.92		
apfu	Si	3.01	3.00	3.00	3.06	3.04	3.05	3.07	3.00	3.05	3.04	3.07	3.04	3.04		
	S	1.03	1.01	0.99	1.02	1.02	1.04	1.02	1.01	1.03	1.02	1.01	1.02	1.01		
	Mn	0.47	0.47	0.46	0.47	0.46	0.49	0.47	0.47	0.50	0.46	0.46	0.47	0.45		
	Fe	2.80	2.66	2.80	2.81	2.66	2.18	2.44	2.79	2.68	2.88	2.85	2.90	2.91		
	Zn	0.76	0.88	0.74	0.80	0.86	1.35	1.08	0.70	0.88	0.67	0.68	0.62	0.64		
	Be	2.95	2.99	3.01	2.81	2.95	2.87	2.89	3.04	2.85	2.90	2.87	2.92	2.92		

	B5-2	136	137	138	139	140	141	142	143	144	145	146	147	148	149	150
wt. %	SiO_2	31.90	31.76	31.81	32.35	32.40	32.20	32.48	31.89	32.10	32.33	32.31	31.48	31.92	32.25	31.93
	S	5.87	5.95	5.88	5.78	5.92	5.85	5.85	5.87	5.85	5.86	5.77	5.69	5.82	5.92	5.92
	MnO	6.57	6.84	6.07	7.12	6.64	8.15	5.64	5.97	5.72	5.56	8.17	5.59	5.66	5.56	5.45
	FeO	28.23	30.40	31.24	25.53	27.29	22.18	30.03	29.74	30.15	29.93	21.49	30.45	28.60	30.88	30.77
	ZnO	18.51	15.28	15.61	20.61	18.67	22.36	16.66	17.18	16.25	16.72	23.66	15.61	18.66	16.36	16.12
	BeO	11.80	12.70	12.30	11.40	12.00	12.10	12.20	12.20	12.80	12.50	11.40	14.00	12.20	11.90	12.70
	Total	99.94	99.97	99.96	99.91	99.97	99.93	99.94	99.92	99.95	99.97	99.93	99.98	99.95	99.91	99.93
apfu	Si	3.07	3.02	3.04	3.12	3.10	3.09	3.09	3.05	3.05	3.07	3.13	2.96	3.06	3.09	3.04
	S	1.06	1.06	1.05	1.05	1.06	1.05	1.04	1.05	1.04	1.04	1.05	1.00	1.04	1.06	1.05
	Mn	0.54	0.55	0.49	0.58	0.54	0.66	0.46	0.48	0.46	0.45	0.67	0.45	0.46	0.45	0.44
	Fe	2.27	2.42	2.50	2.06	2.18	1.78	2.39	2.38	2.39	2.38	1.74	2.39	2.29	2.47	2.45
	Zn	1.32	1.07	1.10	1.47	1.32	1.58	1.17	1.21	1.14	1.17	1.69	1.08	1.32	1.16	1.13
	Be	2.73	2.91	2.83	2.64	2.76	2.79	2.79	2.81	2.92	2.85	2.65	3.16	2.81	2.74	2.90

		151	152	153	154	155	156	157	158	159	160
wt. %	SiO_2	31.93	31.96	32.02	31.97	32.31	32.59	31.32	31.57	31.49	32.06
	S	5.87	5.74	5.86	5.79	5.77	5.87	5.85	5.81	5.76	5.77
	MnO	5.67	6.50	5.71	7.55	8.14	6.87	6.27	5.82	7.38	6.31
	FeO	30.51	26.11	30.56	19.82	22.69	28.51	27.04	28.22	21.19	27.02
	ZnO	17.01	19.70	16.13	25.93	22.26	17.37	19.97	18.35	24.74	19.07
	BeO	11.90	12.80	12.60	11.80	11.70	11.70	12.40	13.10	12.30	12.60
	Total	99.96	99.95	99.96	99.98	99.99	99.98	99.93	99.97	99.98	99.95
apfu	Si	3.07	3.04	3.05	3.09	3.11	3.12	3.01	3.00	3.04	3.06
	S	1.06	1.02	1.05	1.05	1.04	1.05	1.05	1.04	1.04	1.03
	Mn	0.46	0.52	0.46	0.62	0.66	0.56	0.51	0.47	0.60	0.51
	Fe	2.45	2.08	2.43	1.60	1.83	2.28	2.18	2.24	1.71	2.15
	Zn	1.21	1.38	1.13	1.85	1.58	1.23	1.42	1.29	1.76	1.34
	Be	2.75	2.93	2.88	2.74	2.71	2.69	2.87	2.99	2.85	2.88

	B11-1	161	162	163	164	165	166	**B12-1**	167	168	169	170	171	172	173
wt. %	SiO_2	31.75	31.83	32.01	32.51	31.71	31.46	SiO_2	32.15	32.11	31.90	32.37	32.40	32.46	32.55
	S	5.66	5.75	5.77	5.59	5.62	5.54	S	5.61	5.59	5.58	5.75	5.73	5.63	5.73
	MnO	6.79	6.84	6.03	6.34	6.51	5.28	MnO	12.19	4.16	3.92	6.94	6.89	7.27	6.98
	FeO	20.69	22.10	26.32	27.71	21.23	12.12	FeO	20.08	30.06	29.42	34.27	35.68	34.98	34.70
	ZnO	25.65	24.38	19.35	18.51	25.31	36.26	ZnO	20.61	18.51	19.38	10.47	8.92	9.71	10.00
	BeO	12.20	11.90	13.40	12.10	12.40	12.10	BeO	12.10	12.30	12.50	13.00	13.20	12.70	12.90
	Total	99.91	99.94	100.00	99.97	99.98	99.98	Total	99.93	99.94	99.91	99.93	99.97	99.94	100.00
apfu	Si	3.06	3.08	3.02	3.10	3.05	3.07	Si	3.08	3.07	3.05	3.04	3.04	3.06	3.06
	S	1.02	1.04	1.02	1.00	1.01	1.01	S	1.01	1.00	1.00	1.01	1.01	0.99	1.01
	Mn	0.55	0.56	0.48	0.51	0.53	0.44	Mn	0.99	0.34	0.32	0.55	0.55	0.58	0.56
	Fe	1.67	1.79	2.08	2.21	1.71	0.99	Fe	1.61	2.40	2.35	2.70	2.80	2.76	2.73
	Zn	1.83	1.74	1.35	1.30	1.80	2.61	Zn	1.46	1.30	1.37	0.73	0.62	0.68	0.69
	Be	2.83	2.76	3.04	2.77	2.86	2.83	Be	2.78	2.82	2.87	2.94	2.97	2.87	2.91

	B14-1	174	175	176	177	178	179
Wt. %	SiO_2	32.20	32.04	32.35	32.59	31.89	32.21
	S	5.90	5.98	5.92	5.77	5.84	6.02
	MnO	6.59	6.59	6.70	6.77	7.77	6.59
	FeO	39.09	33.88	36.15	37.90	30.20	38.02
	ZnO	6.26	11.70	8.60	7.09	14.65	7.56
	BeO	12.90	12.70	13.20	12.70	12.50	12.60
	Total	99.99	99.90	99.97	99.93	99.94	100.00
apfu	Si	3.03	3.04	3.03	3.06	3.04	3.04
	S	1.04	1.06	1.04	1.02	1.04	1.07
	Mn	0.52	0.53	0.53	0.54	0.63	0.53
	Fe	3.07	2.69	2.83	2.98	2.41	3.00
	Zn	0.43	0.82	0.59	0.49	1.03	0.53
	Be	2.91	2.89	2.97	2.87	2.86	2.86

Gadolinite-(Y)

		B-0				B3-2	
		1	2	3	4	5	6
wt. %	CaO	5.56	6.29	5.26	6.50	3.78	5.13
	SiO_2	24.70	25.27	24.48	25.06	24.83	25.00
	FeO	9.93	9.48	10.00	9.57	10.65	11.17
	MnO	0.19	0.23	0.17	0.19	0.34	0.27
	BeO	10.30	10.50	10.10	10.40	10.30	10.40
	Y_2O_3	19.91	19.72	17.72	18.31	30.03	25.56
	La_2O_3	1.71	2.01	2.52	2.20	0.65	1.42
	Ce_2O_3	6.71	7.11	8.13	7.28	2.39	3.23
	Dy_2O_3	2.26	2.27	2.09	2.24	2.90	2.63
	Gd_2O_3	1.23	1.37	1.20	1.16	1.50	1.35
	Yb_2O_3	3.27	3.20	3.79	3.65	2.21	2.58
	ThO_2	4.91	3.95	5.52	3.64	2.90	4.30
	Pr_2O_3	0.60	0.66	0.58	0.65	0.29	0.31
	Nd_2O_3	1.45	1.35	1.45	1.32	0.94	0.42
	Tb_2O_3	0.08	0.05	0.06	0.08	0.18	0.13
	Er_2O_3	2.33	2.31	2.61	2.58	2.15	2.54
	Total	95.13	95.78	95.69	94.82	96.03	96.47
apfu	Ca	0.51	0.57	0.49	0.59	0.34	0.46
	Si	2.12	2.13	2.12	2.14	2.08	2.09
	Fe	0.71	0.67	0.72	0.68	0.74	0.78
	Mn	0.01	0.02	0.01	0.01	0.02	0.02
	Be	2.12	2.13	2.10	2.13	2.07	2.09
	Y	0.91	0.88	0.82	0.83	1.34	1.14
	La	0.05	0.06	0.08	0.07	0.02	0.04
	Ce	0.21	0.22	0.26	0.23	0.07	0.10
	Dy	0.06	0.06	0.06	0.06	0.08	0.07
	Gd	0.03	0.04	0.03	0.03	0.04	0.04
	Yb	0.09	0.08	0.10	0.09	0.06	0.07
	Th	0.10	0.08	0.11	0.07	0.06	0.08
	Pr	0.02	0.02	0.02	0.02	0.01	0.01
	Nd	0.04	0.04	0.04	0.04	0.03	0.01
	Tb	0.00	0.00	0.00	0.00	0.00	0.00
	Er	0.06	0.06	0.07	0.07	0.06	0.07

		B5-1							
		1	2	3	4	5	6	7	8
wt. %	CaO	2.80	2.46	2.39	1.93	5.37	7.04	8.08	7.62
	SiO_2	24.47	24.00	24.04	23.47	25.36	25.29	25.97	25.50
	FeO	9.96	10.32	10.36	10.74	10.12	9.76	9.18	9.69
	MnO	0.42	0.38	0.40	0.32	0.39	0.21	0.23	0.26
	BeO	10.20	10.00	10.00	9.70	10.50	10.50	10.80	10.70
	Y_2O_3	27.17	26.53	26.52	24.50	27.86	20.96	19.47	19.28
	La_2O_3	0.50	0.56	0.53	0.45	0.70	1.53	2.33	1.97
	Ce_2O_3	2.97	2.98	3.02	2.80	2.15	2.90	4.32	3.23
	Dy_2O_3	4.97	5.23	5.22	6.86	2.52	2.96	2.59	2.77
	Gd_2O_3	2.86	2.76	3.04	3.40	1.42	1.67	1.39	1.47
	Yb_2O_3	2.28	2.67	2.35	3.07	2.91	3.11	2.97	2.99
	ThO_2	1.62	2.17	2.50	1.78	2.74	5.30	3.66	5.88
	Pr_2O_3	0.38	0.45	0.42	0.44	0.18	0.24	0.30	0.25
	Nd_2O_3	1.47	1.40	1.49	1.19	0.48	0.73	0.85	0.68
	Tb_2O_3	0.49	0.49	0.43	0.67	0.17	0.12	0.17	0.20
	Er_2O_3	3.19	3.12	3.09	3.97	2.44	2.76	2.45	2.46
	Total	95.75	95.52	95.80	95.29	95.32	95.09	94.75	94.95
apfu	Ca	0.26	0.23	0.22	0.18	0.48	0.64	0.72	0.68
	Si	2.09	2.08	2.08	2.07	2.11	2.13	2.16	2.14
	Fe	0.71	0.75	0.75	0.79	0.70	0.69	0.64	0.68
	Mn	0.03	0.03	0.03	0.02	0.03	0.02	0.02	0.02
	Be	2.09	2.08	2.08	2.06	2.10	2.12	2.15	2.15
	Y	1.24	1.22	1.22	1.15	1.23	0.94	0.86	0.86
	La	0.02	0.02	0.02	0.01	0.02	0.05	0.07	0.06
	Ce	0.09	0.09	0.10	0.09	0.07	0.09	0.13	0.10
	Dy	0.14	0.15	0.15	0.20	0.07	0.08	0.07	0.07
	Gd	0.08	0.08	0.09	0.10	0.04	0.05	0.04	0.04
	Yb	0.06	0.07	0.06	0.08	0.07	0.08	0.08	0.08
	Th	0.03	0.04	0.05	0.04	0.05	0.10	0.07	0.11
	Pr	0.01	0.01	0.01	0.01	0.01	0.01	0.01	0.01
	Nd	0.04	0.04	0.05	0.04	0.01	0.02	0.03	0.02
	Tb	0.01	0.01	0.01	0.02	0.00	0.00	0.00	0.01
	Er	0.09	0.08	0.08	0.11	0.06	0.07	0.06	0.06

	B11-1					
		9	10	11	12	13
wt. %	CaO	9.96	9.16	9.45	9.25	10.51
	SiO_2	26.67	26.22	26.35	25.97	26.68
	FeO	9.49	9.56	9.42	9.61	9.20
	MnO	0.27	0.24	0.26	0.23	0.26
	BeO	11.10	10.90	10.90	10.80	11.10
	Y_2O_3	20.16	20.97	20.01	20.08	19.67
	La_2O_3	0.62	0.59	0.64	0.43	0.58
	Ce_2O_3	1.11	1.13	1.24	0.93	1.14
	Dy_2O_3	3.03	3.06	3.09	3.15	2.86
	Gd_2O_3	1.60	1.66	1.58	1.72	1.57
	Yb_2O_3	3.08	3.10	2.78	2.91	2.76
	ThO_2	3.86	3.99	4.97	5.66	3.96
	Pr_2O_3	0.15	0.08	0.08	0.14	0.18
	Nd_2O_3	0.46	0.50	0.47	0.40	0.40
	Tb_2O_3	0.26	0.24	0.27	0.22	0.23
	Er_2O_3	2.61	2.69	2.67	2.57	2.57
	Total	94.43	94.07	94.17	94.05	93.66
apfu	Ca	0.87	0.81	0.83	0.82	0.92
	Si	2.17	2.16	2.17	2.15	2.17
	Fe	0.64	0.66	0.65	0.67	0.63
	Mn	0.02	0.02	0.02	0.02	0.02
	Be	2.17	2.15	2.15	2.15	2.17
	Y	0.87	0.92	0.88	0.89	0.85
	La	0.02	0.02	0.02	0.01	0.02
	Ce	0.03	0.03	0.04	0.03	0.03
	Dy	0.08	0.08	0.08	0.08	0.08
	Gd	0.04	0.05	0.04	0.05	0.04
	Yb	0.08	0.08	0.07	0.07	0.07
	Th	0.07	0.07	0.09	0.11	0.07
	Pr	0.00	0.00	0.00	0.00	0.01
	Nd	0.01	0.01	0.01	0.01	0.01
	Tb	0.01	0.01	0.01	0.01	0.01
	Er	0.07	0.07	0.07	0.07	0.07

B11-1 continued

		14	15	16	17	18
wt. %	CaO	9.16	8.91	7.71	7.97	7.09
	SiO_2	25.81	26.23	25.66	25.93	25.05
	FeO	9.70	9.48	9.45	9.69	9.67
	MnO	0.25	0.27	0.24	0.22	0.22
	BeO	10.70	10.90	10.50	10.80	10.40
	Y_2O_3	20.42	20.11	20.88	20.38	18.22
	La_2O_3	0.49	0.88	1.79	1.39	3.17
	Ce_2O_3	0.98	1.65	3.30	2.31	5.30
	Dy_2O_3	3.15	3.19	2.80	2.91	2.44
	Gd_2O_3	1.57	1.65	1.52	1.47	1.32
	Yb_2O_3	2.99	2.81	2.93	2.99	2.69
	ThO_2	5.52	4.99	4.07	5.28	6.01
	Pr_2O_3	0.10	0.20	0.28	0.26	0.27
	Nd_2O_3	0.37	0.59	0.61	0.48	0.75
	Tb_2O_3	0.18	0.30	0.25	0.20	0.08
	Er_2O_3	2.62	2.60	2.54	2.53	2.32
	Total	94.01	94.76	94.52	94.81	95.00
apfu	Ca	0.82	0.79	0.69	0.71	0.65
	Si	2.15	2.16	2.15	2.15	2.13
	Fe	0.67	0.65	0.66	0.67	0.69
	Mn	0.02	0.02	0.02	0.02	0.02
	Be	2.14	2.15	2.11	2.15	2.12
	Y	0.90	0.88	0.93	0.90	0.82
	La	0.02	0.03	0.06	0.04	0.10
	Ce	0.03	0.05	0.10	0.07	0.16
	Dy	0.08	0.08	0.08	0.08	0.07
	Gd	0.04	0.05	0.04	0.04	0.04
	Yb	0.08	0.07	0.07	0.08	0.07
	Th	0.10	0.09	0.08	0.10	0.12
	Pr	0.00	0.01	0.01	0.01	0.01
	Nd	0.01	0.02	0.02	0.01	0.02
	Tb	0.01	0.01	0.01	0.01	0.00
	Er	0.07	0.07	0.07	0.07	0.06

		B16-1						
		19	20	21	22	23	24	25
wt. %	CaO	1.23	2.40	1.36	1.83	3.30	2.34	1.74
	SiO_2	22.70	24.03	22.99	23.51	24.93	23.62	23.25
	FeO	9.95	11.24	11.05	11.22	10.17	10.45	10.50
	MnO	0.33	0.25	0.31	0.30	0.46	0.35	0.35
	BeO	9.40	10.00	9.60	9.80	10.30	9.80	9.60
	Y_2O_3	21.08	28.45	24.83	27.63	30.17	24.94	24.87
	La_2O_3	0.67	0.84	0.69	0.77	0.80	0.64	0.56
	Ce_2O_3	3.90	3.82	3.74	3.37	2.52	2.78	3.18
	Dy_2O_3	8.68	4.09	5.29	3.97	2.94	5.54	6.11
	Gd_2O_3	4.43	2.03	2.74	2.25	1.63	2.71	3.24
	Yb_2O_3	2.37	1.66	3.48	3.25	2.99	3.55	3.53
	ThO_2	2.06	3.38	3.45	3.09	1.73	2.46	1.84
	Pr_2O_3	0.62	0.44	0.45	0.29	0.21	0.25	0.39
	Nd_2O_3	1.89	1.29	1.27	0.92	0.40	0.79	1.19
	Tb_2O_3	0.96	0.32	0.42	0.28	0.16	0.49	0.64
	Er_2O_3	4.06	2.37	3.91	3.29	2.72	4.18	4.27
	Total	94.33	96.62	95.59	95.77	95.42	94.90	95.25
apfu	Ca	0.12	0.22	0.13	0.17	0.30	0.22	0.17
	Si	2.07	2.05	2.05	2.05	2.09	2.08	2.06
	Fe	0.76	0.80	0.82	0.82	0.71	0.77	0.78
	Mn	0.03	0.02	0.02	0.02	0.03	0.03	0.03
	Be	2.06	2.05	2.05	2.05	2.08	2.07	2.05
	Y	1.03	1.29	1.18	1.28	1.35	1.17	1.18
	La	0.02	0.03	0.02	0.02	0.02	0.02	0.02
	Ce	0.13	0.12	0.12	0.11	0.08	0.09	0.10
	Dy	0.26	0.11	0.15	0.11	0.08	0.16	0.17
	Gd	0.13	0.06	0.08	0.07	0.05	0.08	0.10
	Yb	0.07	0.04	0.09	0.09	0.08	0.10	0.10
	Th	0.04	0.07	0.07	0.06	0.03	0.05	0.04
	Pr	0.02	0.01	0.01	0.01	0.01	0.01	0.01
	Nd	0.06	0.04	0.04	0.03	0.01	0.02	0.04
	Tb	0.03	0.01	0.01	0.01	0.00	0.01	0.02
	Er	0.12	0.06	0.11	0.09	0.07	0.12	0.12

B16-1 continued

		26	27	28	29	30	31
wt. %	CaO	1.35	0.90	2.42	1.39	2.18	3.16
	SiO_2	22.96	22.45	24.12	23.07	23.51	24.28
	FeO	10.31	10.85	11.32	10.24	11.02	10.24
	MnO	0.40	0.32	0.23	0.41	0.35	0.41
	BeO	9.50	9.30	10.00	9.60	9.80	10.10
	Y_2O_3	23.69	21.51	27.67	23.97	25.87	26.70
	La_2O_3	0.44	0.49	0.78	0.47	0.54	0.57
	Ce_2O_3	2.99	3.05	3.72	3.04	2.29	2.10
	Dy_2O_3	6.83	8.37	3.98	6.58	5.13	4.84
	Gd_2O_3	3.54	4.29	2.11	3.70	2.62	2.36
	Yb_2O_3	3.30	2.77	1.60	3.17	3.74	3.76
	ThO_2	1.60	2.89	3.44	1.71	3.08	1.76
	Pr_2O_3	0.46	0.49	0.48	0.50	0.28	0.17
	Nd_2O_3	1.53	1.57	1.23	1.68	0.69	0.62
	Tb_2O_3	0.63	0.85	0.36	0.69	0.42	0.41
	Er_2O_3	4.56	4.57	2.45	4.64	4.19	3.91
	Total	94.09	94.67	95.93	94.86	95.70	95.38
apfu	Ca	0.13	0.09	0.22	0.13	0.20	0.29
	Si	2.07	2.06	2.07	2.07	2.06	2.09
	Fe	0.78	0.83	0.81	0.77	0.81	0.74
	Mn	0.03	0.02	0.02	0.03	0.03	0.03
	Be	2.06	2.05	2.06	2.07	2.06	2.08
	Y	1.14	1.05	1.26	1.14	1.21	1.22
	La	0.01	0.02	0.02	0.02	0.02	0.02
	Ce	0.10	0.10	0.12	0.10	0.07	0.07
	Dy	0.20	0.25	0.11	0.19	0.14	0.13
	Gd	0.11	0.13	0.06	0.11	0.08	0.07
	Yb	0.09	0.08	0.04	0.09	0.10	0.10
	Th	0.03	0.06	0.07	0.03	0.06	0.03
	Pr	0.02	0.02	0.02	0.02	0.01	0.01
	Nd	0.05	0.05	0.04	0.05	0.02	0.02
	Tb	0.02	0.03	0.01	0.02	0.01	0.01
	Er	0.13	0.13	0.07	0.13	0.12	0.11

		B3-1								
		32	33	34	35	36	37	38	39	40
wt. %	CaO	2.61	1.51	0.68	3.11	1.93	3.94	3.26	1.79	2.88
	SiO_2	24.26	23.08	22.48	24.64	23.70	24.76	24.85	23.37	24.47
	FeO	11.01	10.05	11.13	10.99	10.85	10.44	10.95	10.39	10.61
	MnO	0.32	0.36	0.32	0.34	0.35	0.36	0.36	0.36	0.37
	BeO	10.10	9.60	9.30	10.20	9.90	10.30	10.30	9.70	10.20
	Y_2O_3	30.12	23.13	22.37	30.29	27.94	27.65	30.74	24.34	30.62
	La_2O_3	0.86	0.75	0.50	0.89	0.66	0.67	0.86	0.55	0.68
	Ce_2O_3	3.17	4.34	3.49	2.75	3.42	2.28	2.98	3.26	2.79
	Dy_2O_3	2.88	7.32	9.16	2.62	4.45	4.03	2.75	6.50	3.27
	Gd_2O_3	1.49	3.31	4.31	1.37	2.22	1.94	1.38	3.22	1.65
	Yb_2O_3	2.38	2.39	2.31	2.35	2.53	3.16	2.38	2.91	2.57
	ThO_2	3.14	1.84	1.51	3.28	2.96	1.89	1.89	3.00	1.66
	Pr_2O_3	0.24	0.45	0.54	0.34	0.43	0.26	0.35	0.50	0.34
	Nd_2O_3	0.65	1.82	1.96	0.54	1.16	0.70	0.66	1.48	0.66
	Tb_2O_3	0.24	0.79	1.07	0.19	0.35	0.31	0.25	0.69	0.24
	Er_2O_3	2.34	3.96	4.24	2.27	2.87	3.06	2.35	3.64	2.61
	Total	95.80	94.70	95.38	96.16	95.73	95.76	96.32	95.70	95.60
apfu	Ca	0.24	0.15	0.07	0.28	0.18	0.36	0.29	0.17	0.26
	Si	2.06	2.07	2.05	2.07	2.06	2.09	2.07	2.07	2.07
	Fe	0.78	0.75	0.85	0.77	0.79	0.74	0.76	0.77	0.75
	Mn	0.02	0.03	0.02	0.02	0.03	0.03	0.03	0.03	0.03
	Be	2.06	2.07	2.03	2.06	2.06	2.09	2.07	2.06	2.07
	Y	1.36	1.10	1.08	1.36	1.29	1.24	1.37	1.15	1.38
	La	0.03	0.02	0.02	0.03	0.02	0.02	0.03	0.02	0.02
	Ce	0.10	0.14	0.12	0.08	0.11	0.07	0.09	0.11	0.09
	Dy	0.08	0.21	0.27	0.07	0.12	0.11	0.07	0.19	0.09
	Gd	0.04	0.10	0.13	0.04	0.06	0.05	0.04	0.09	0.05
	Yb	0.06	0.07	0.06	0.06	0.07	0.08	0.06	0.08	0.07
	Th	0.06	0.04	0.03	0.06	0.06	0.04	0.04	0.06	0.03
	Pr	0.01	0.01	0.02	0.01	0.01	0.01	0.01	0.02	0.01
	Nd	0.02	0.06	0.06	0.02	0.04	0.02	0.02	0.05	0.02
	Tb	0.01	0.02	0.03	0.01	0.01	0.01	0.01	0.02	0.01
	Er	0.06	0.11	0.12	0.06	0.08	0.08	0.06	0.10	0.07

Cassiterite and Nordenskiöldine

Cassiterite

		1	2	3	4	5
wt. %	CaO	0.27	0.20	0.45	0.23	0.23
	SnO_2	97.22	97.12	97.34	95.40	97.77
	Total	97.49	97.32	97.78	95.63	98.00
apfu	CaO	0.01	0.01	0.01	0.01	0.01
	SnO_2	1.00	1.00	0.99	1.00	1.00
	sum	1.00	1.00	1.01	1.00	1.00

Nordenskiöldine

		1	2	3	4	5	6	7	8	9	10
wt. %	CaO	19.68	19.33	19.53	20.05	19.98	19.67	20.00	19.85	20.27	20.59
	SnO_2	53.49	54.73	54.09	53.89	53.44	53.58	54.78	54.88	54.80	53.67
	B_2O_3	26.80	25.90	26.30	26.00	26.50	26.70	25.20	25.20	24.90	25.70
	Total	99.97	99.96	99.92	99.94	99.92	99.95	99.98	99.93	99.97	99.97
apfu	CaO	0.95	0.95	0.95	0.98	0.97	0.95	0.99	0.98	1.00	1.01
	SnO_2	0.96	1.00	0.98	0.98	0.96	0.96	1.01	1.01	1.01	0.98
	B_2O_3	2.08	2.04	2.06	2.04	2.07	2.08	2.00	2.00	1.99	2.03
	Total	4.00	3.98	3.99	4.00	4.00	4.00	3.99	3.99	4.00	4.01

Appendix 2: Major- and trace-elements

Major elements

Wt. %	1	2	3	4	5	6	7	8	9	10	11	12	13	14	15
SiO_2	73.2	71.56	57.42	59.84	72.26	72.36	74.7	72.31	73.77	70.3	74.23	64.14	73.79	76.95	74.24
Al_2O_3	11.47	14.2	18.07	17.65	13.15	12.45	12.1	12.5	13.77	14.18	9.96	16.04	13.3	12.57	11.43
Fe_2O_3(T)	2.1	0.94	7.96	9.8	1.29	1.36	0.74	1.32	0.89	0.85	4.27	2.42	2.5	1.14	3.46
MnO	0.24	0.076	0.101	0.081	0.158	0.143	0.097	0.111	0.094	0.072	0.216	0.158	0.115	0.017	0.221
MgO	0.02	0.04	3.96	4.81	0.03	0.05	0.02	0.03	0.02	0.03	0.07	0.14	0.08	< 0.01	0.07
CaO	0.39	0.71	1.37	0.55	0.48	0.55	0.18	0.28	0.37	0.53	0.1	2.2	0.08	0.02	0.11
Na_2O	2.22	3	5.25	1.85	2.56	2.67	2.31	2.31	2.77	2.73	4.41	7.14	4.84	3.99	4.44
K_2O	6.87	8.22	1.41	2.95	7.5	6.96	7.12	7.56	7.73	8.22	4.36	4.01	5.45	5.52	4.44
TiO_2	0.119	0.056	0.946	0.995	0.08	0.102	0.109	0.07	0.118	0.067	0.148	0.568	0.086	0.015	0.159
P_2O_5	0.03	0.02	0.07	0.05	0.02	0.03	0.01	0.03	0.01	0.03	< 0.01	0.06	< 0.01	< 0.01	< 0.01
LOI	0.02	0.27	3.27	1.5	0.17	0.13	0.14	0.01	0.21	0.2	0.14	2.18	0.22	0.16	0.15
Total	96.68	99.09	99.83	100.1	97.7	96.8	97.53	96.53	99.77	97.2	97.91	99.06	100.4	100.4	98.73

Trace elements

ppm	1	2	3	4	5	6	7	8	9	10	11	12	13	14	15
Sc	2	1	27	30	1	1	2	1	1	< 1	4	3	2	< 1	1
Be	7507	2036	10	5	6025	4126	1194	3510	1495	1143	17	10	10	14	12
V	6	6	184	196	6	6	6	6	6	< 5	7	16	7	5	6
Ba	352	453	165	510	448	343	328	361	372	467	18	172	13	14	11
Sr	75	90	131	119	89	76	63	74	85	93	2	50	3	3	4
Y	606	377	16	22	634	634	310	490	447	253	36	95	27	37	20
Zr	1953	3456	151	154	3496	5984	3144	2998	2564	3381	587	1371	537	244	549
Cr	230	230	210	280	190	170	220	200	220	180	170	40	230	260	220
Co	1	< 1	19	31	2	1	< 1	< 1	< 1	< 1	< 1	< 1	< 1	1	< 1
Ni	< 20	< 20	90	110	< 20	< 20	< 20	< 20	< 20	< 20	< 20	< 20	< 20	< 20	< 20
Cu	< 10	< 10	20	40	< 10	< 10	< 10	< 10	< 10	< 10	< 10	< 10	< 10	< 10	< 10
Zn	3470	1930	50	100	3360	2880	1980	1570	1700	1940	380	150	110	60	260
Ga	49	58	22	21	51	59	56	57	61	59	39	33	39	36	39
Ge	13	11	3	3	12	11	9	12	12	13	5	2	3	2	4
As	486	520	28	< 5	305	632	10	495	435	227	< 5	< 5	< 5	< 5	< 5
Rb	> 1000	> 1000	162	418	> 1000	> 1000	> 1000	> 1000	> 1000	> 1000	370	108	276	378	415
Nb	> 1000	761	9	18	> 1000	756	638	998	772	551	127	202	90	142	378
Mo	> 100	24	< 2	< 2	> 100	> 100	12	> 100	90	20	< 2	< 2	2	3	3
Ag	13.4	24.5	0.6	1.1	23.9	23.4	13.7	22.4	18	12.6	4.9	9.3	4.1	1	4
In	< 0.2	< 0.2	< 0.2	< 0.2	< 0.2	< 0.2	< 0.2	< 0.2	< 0.2	< 0.2	0.2	< 0.2	< 0.2	< 0.2	< 0.2
Sn	189	118	26	15	123	71	61	177	86	106	19	8	< 1	2	4
Sb	16.8	16.1	0.6	1.6	15.7	11.2	16.7	11.2	13.4	13.1	1	< 0.5	< 0.5	< 0.5	< 0.5
Cs	92.1	83.7	8.4	32.9	78.2	98.8	112	84.5	113	91	2	0.7	1.9	2.3	1.8

Trace elements continued

ppm	1	2	3	4	5	6	7	8	9	10	11	12	13	14	15
La	24.7	19.3	14.9	34	34.2	28.7	11.6	17.6	17	15.6	10.8	113	10	11.6	20.8
Ce	54.1	40.9	30.8	68.2	68.2	75	29.6	46.7	46.5	33.2	33.4	260	22.6	34.1	59.9
Pr	5.07	3.63	3.15	7.51	6.13	7.21	3.09	4.83	4.8	2.74	3.22	33.4	3.1	3.2	6.81
Nd	11.4	8	11.7	26.6	13.7	17.9	9.4	11.1	10.8	6.5	11.4	119	10.7	10.7	21.5
Sm	7.5	4.8	1.9	4.4	8.6	10.7	5.5	7.8	7.6	3.9	3.1	23.4	3.1	2.6	4.3
Eu	0.58	0.48	0.67	0.93	0.72	0.88	0.57	0.68	0.71	0.4	0.42	3.38	0.38	0.39	0.52
Gd	12.3	7.3	1.9	3.7	13.5	15.6	8.2	12.3	10.6	5.7	3.2	18.2	2.8	2.9	3.3
Tb	7.9	5.4	0.3	0.7	8.8	9.3	4.8	7.8	7.1	4.1	0.8	3.1	0.6	0.7	0.6
Dy	74	51.6	2.3	4	79.4	86.9	46.5	73.2	64.4	41.2	6.2	17.4	4.5	5.1	3.9
Ho	18.8	14.4	0.5	0.9	20.8	22.5	13	18.3	16.6	12.1	1.5	3.5	1.1	1.2	0.9
Er	64.6	56.5	1.7	2.7	74	84.2	50.6	62.9	60.3	50.3	5.7	10.5	3.4	3.9	2.8
Tm	12.5	11.5	0.3	0.45	14.9	17.2	9.42	12.1	11.3	9.93	1.2	1.69	0.62	0.66	0.57
Yb	88.6	80	2.2	3.1	104	120	66.2	86.1	76.4	71.1	10.6	12.3	5	4.5	5.2
Lu	12.6	12	0.36	0.48	14.4	16.4	9.51	12.4	11	10.2	2.14	2.22	0.93	0.75	1.21
Hf	269	318	3.8	4.3	509	575	216	424	259	289	22.8	30.3	17.9	7.9	21.1
Ta	79.7	62.1	1.5	0.4	123	92	63.9	70.3	93.1	67	7.6	11.2	4.1	10.6	23.1
Tl	8.9	11.8	0.3	1.5	10.8	10.8	10.5	11.6	11.8	12.7	0.7	0.6	0.7	1.1	0.8
Pb	3760	1350	129	24	1160	1260	1190	4430	1410	1530	48	19	11	28	14
Bi	2.2	< 0.4	< 0.4	< 0.4	< 0.4	< 0.4	< 0.4	2.4	0.9	< 0.4	< 0.4	< 0.4	< 0.4	< 0.4	< 0.4
Th	530	459	8.2	9.9	599	488	253	447	320	494	28.1	25.3	11.2	17.7	5.3
U	8.5	9.3	2	2.7	10.5	16.2	11.5	10.4	9.6	12.5	6.2	9	3.8	12.4	35.3
W	43	32	2	1	60	35	23	37	35	26	2	1	1	2	2

Appendix 3: Thin section images

Scans and polarized scans to supplement mineral descriptions

B-0

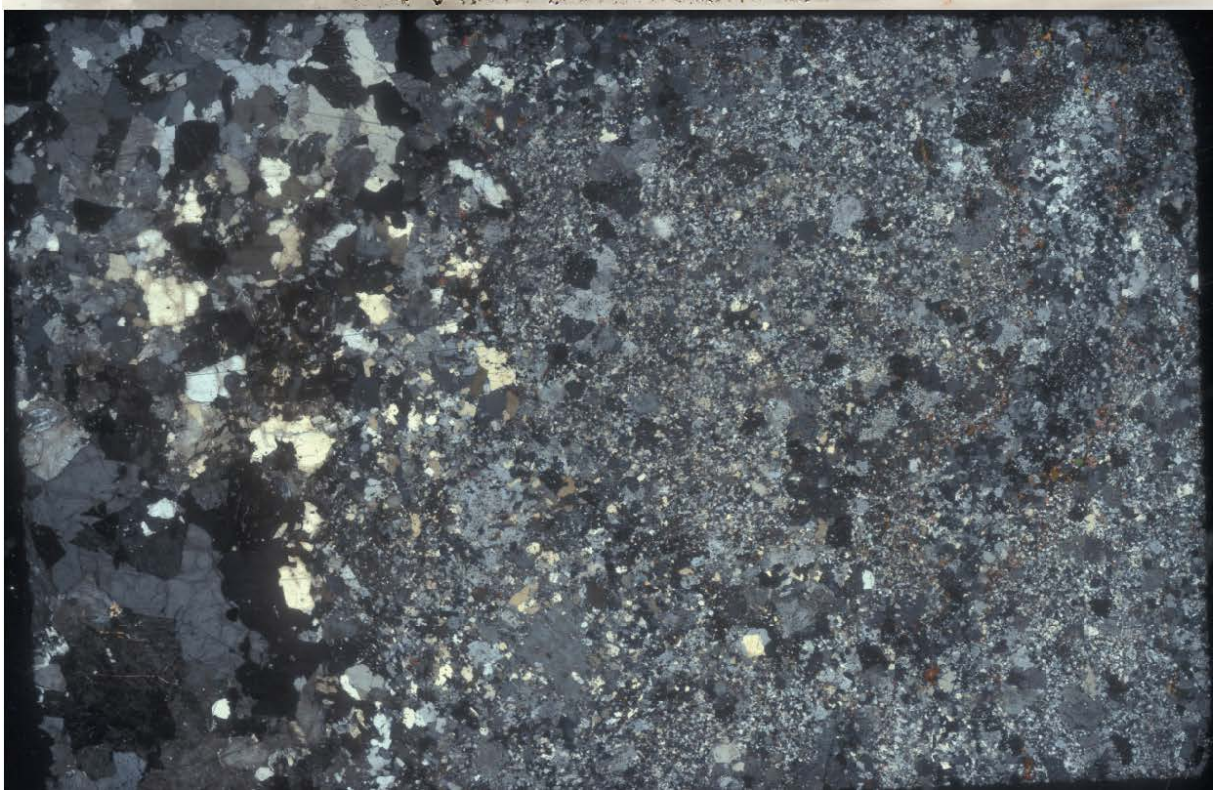

B1-1

B1-2

B1-3

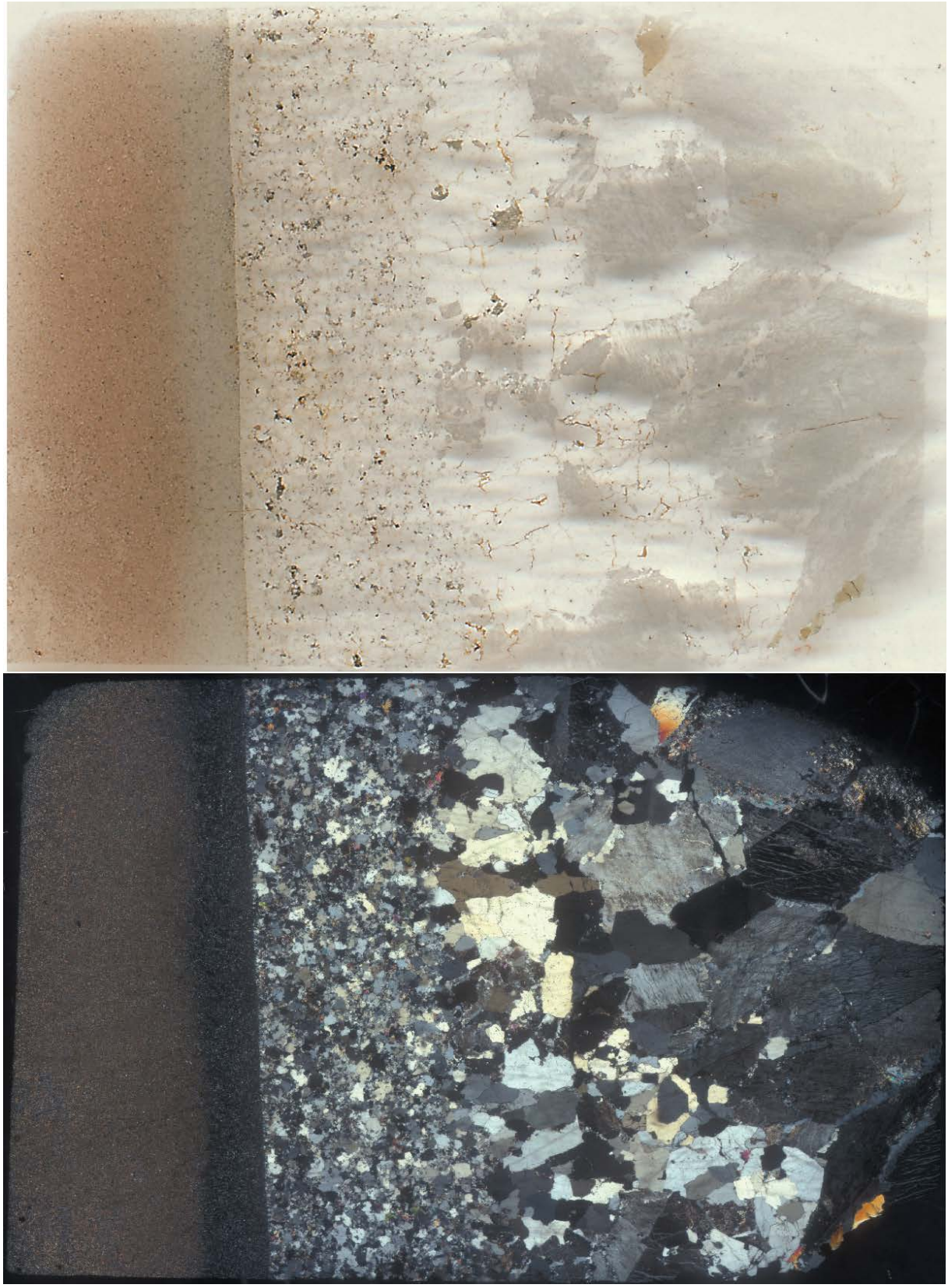

B2-1

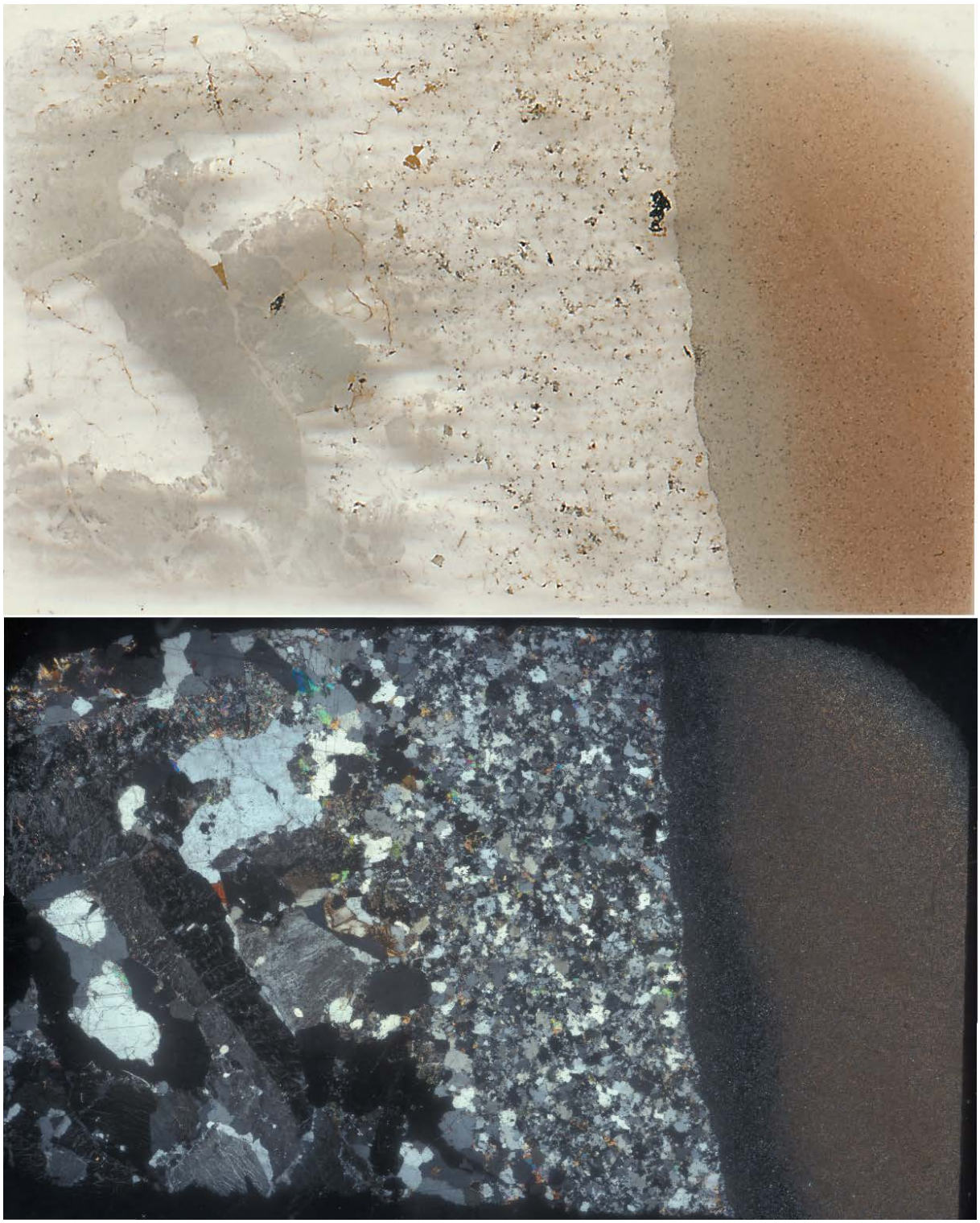

B3-1

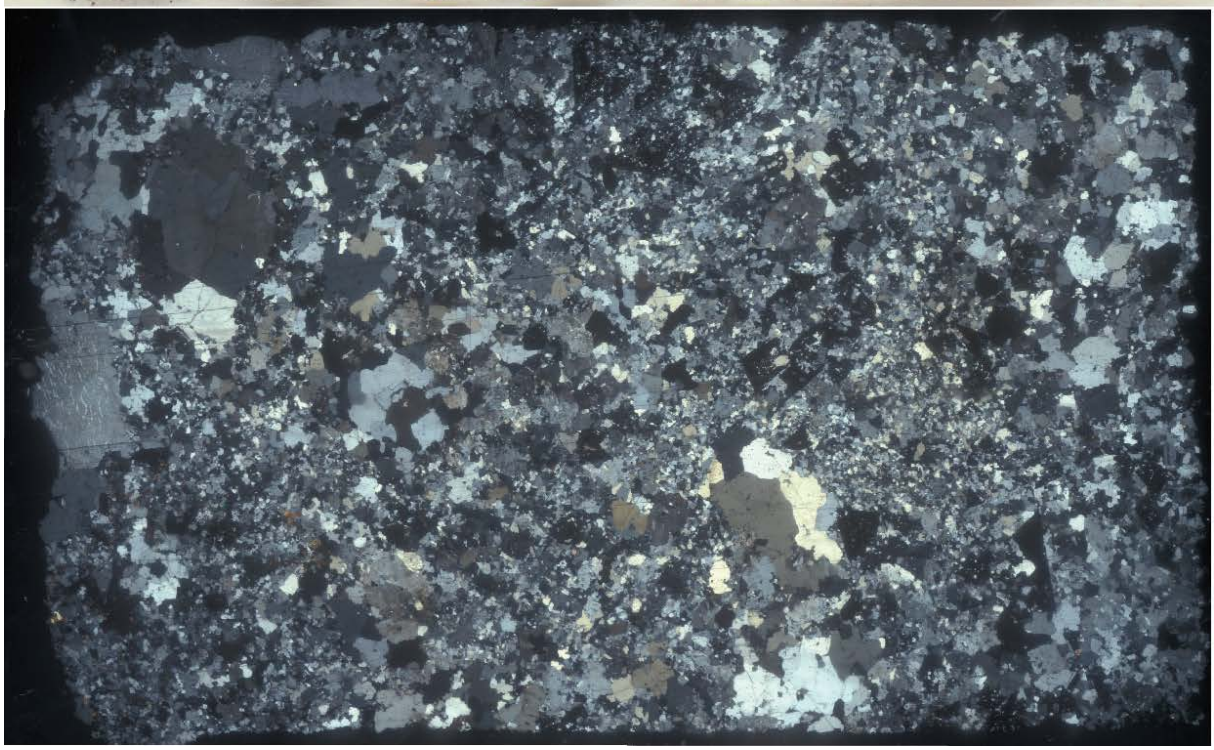

B3-2

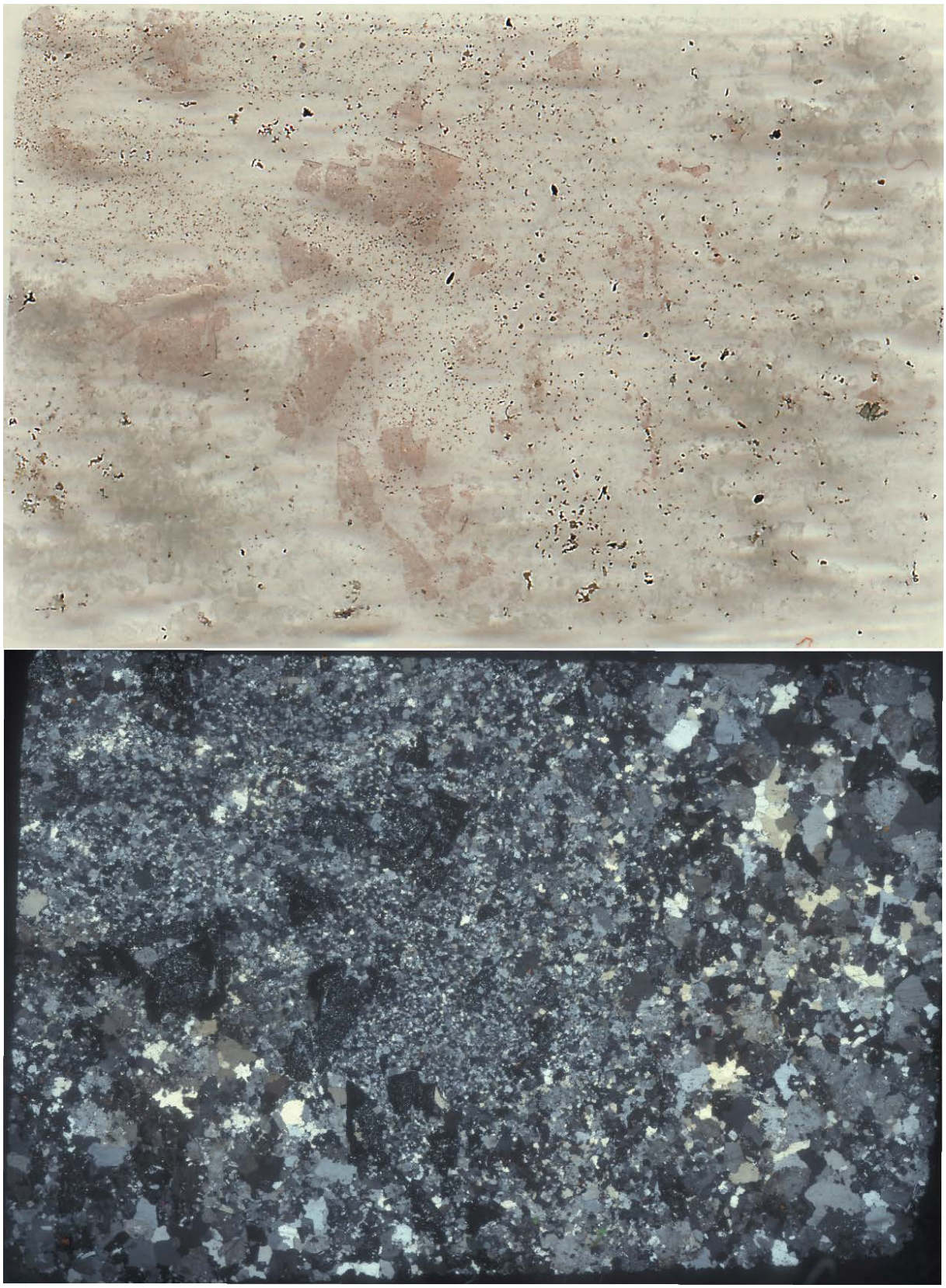

B4-1

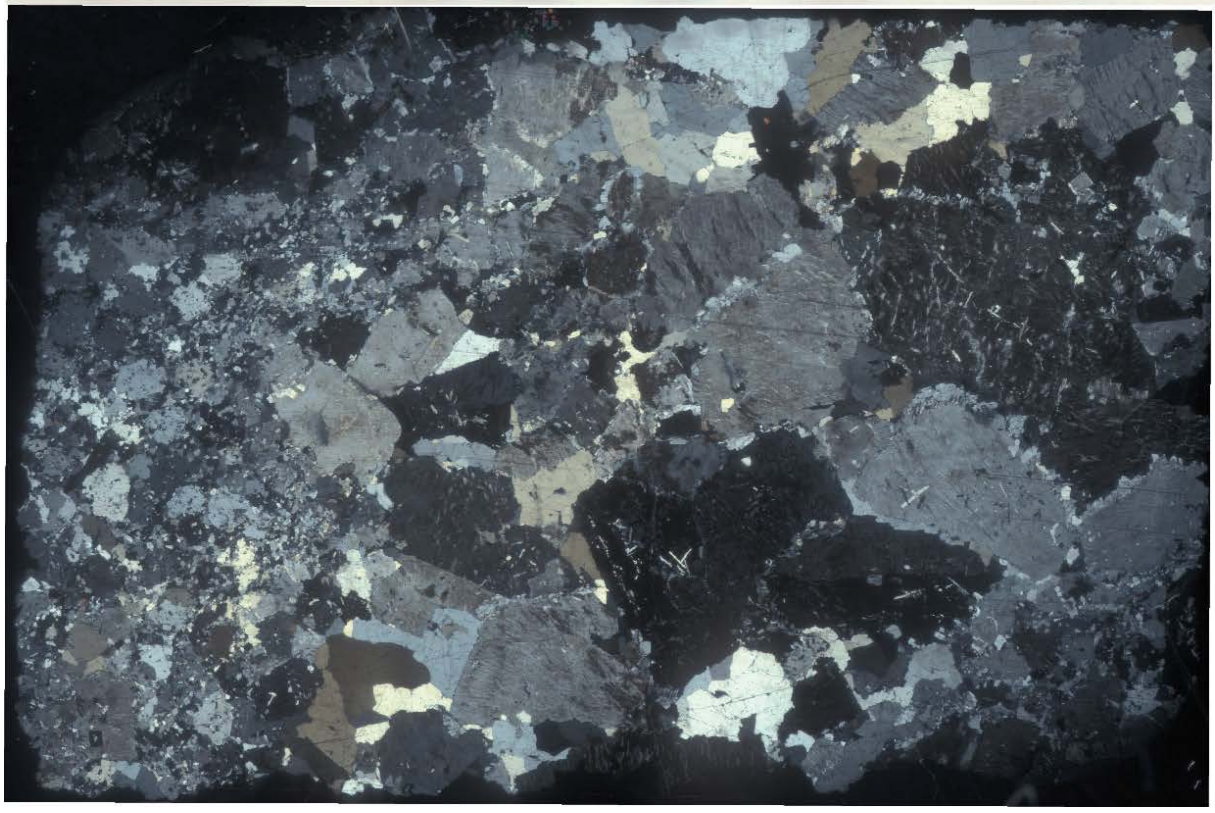

B5-1

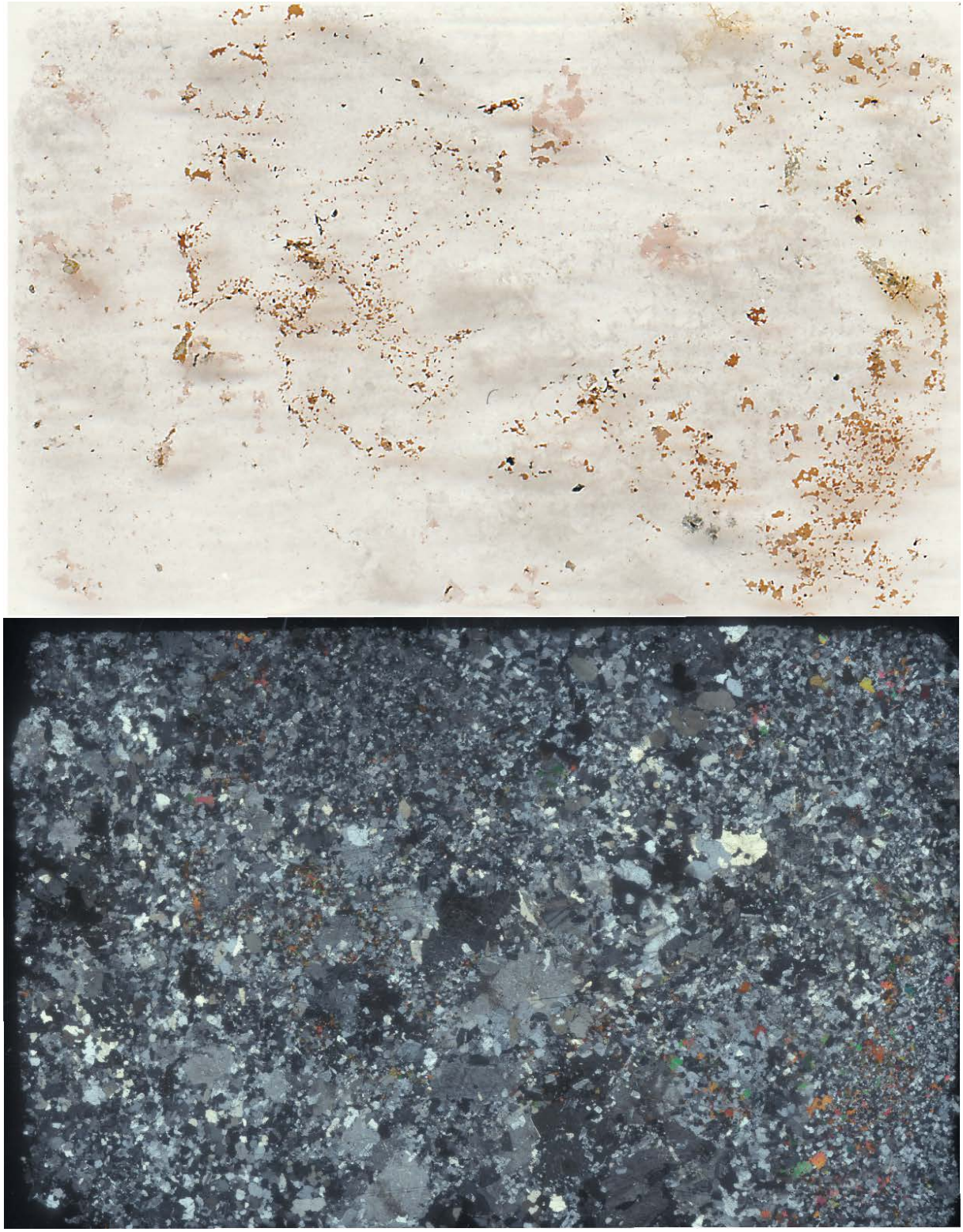

B5-2

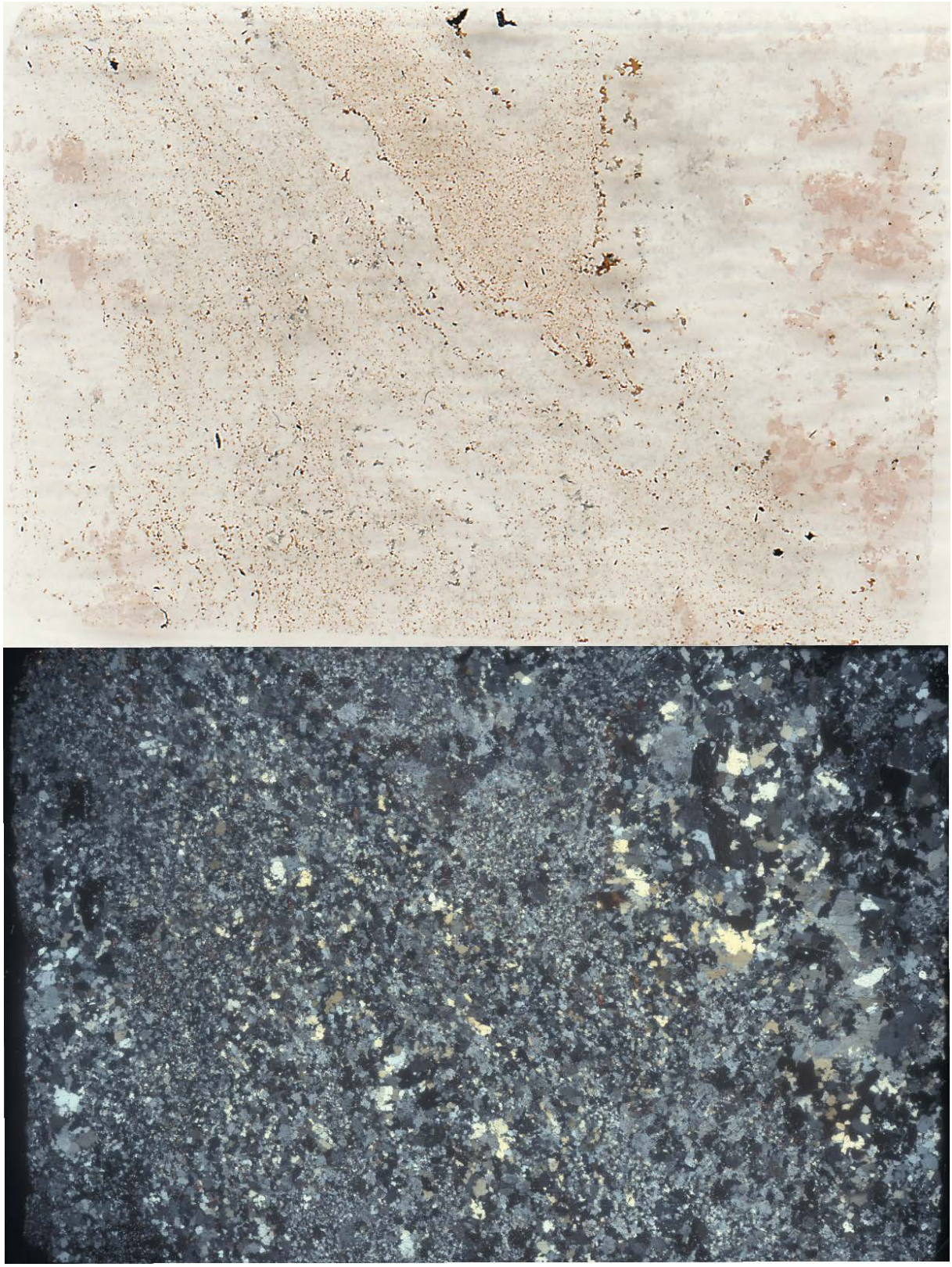

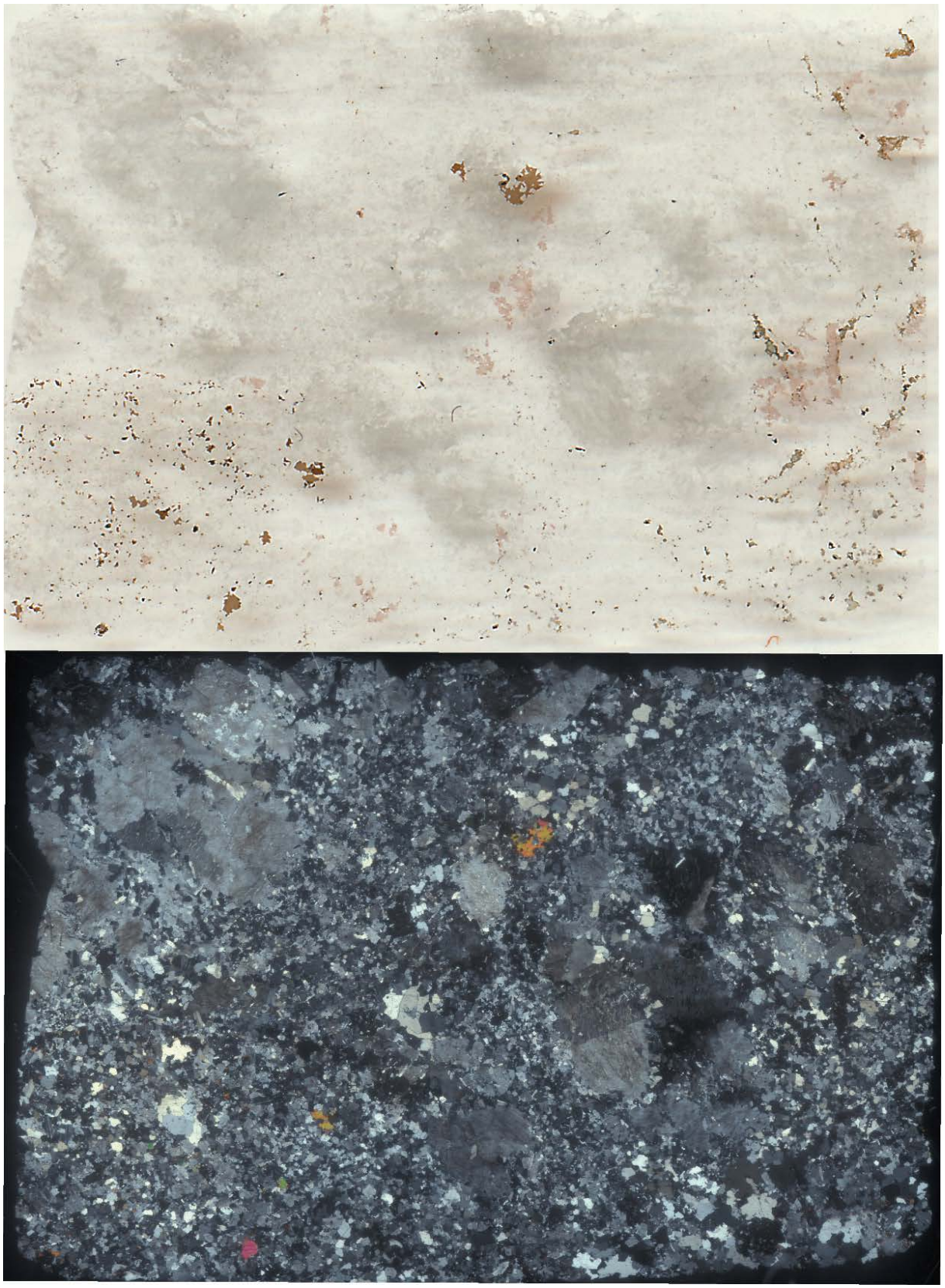

B9-1

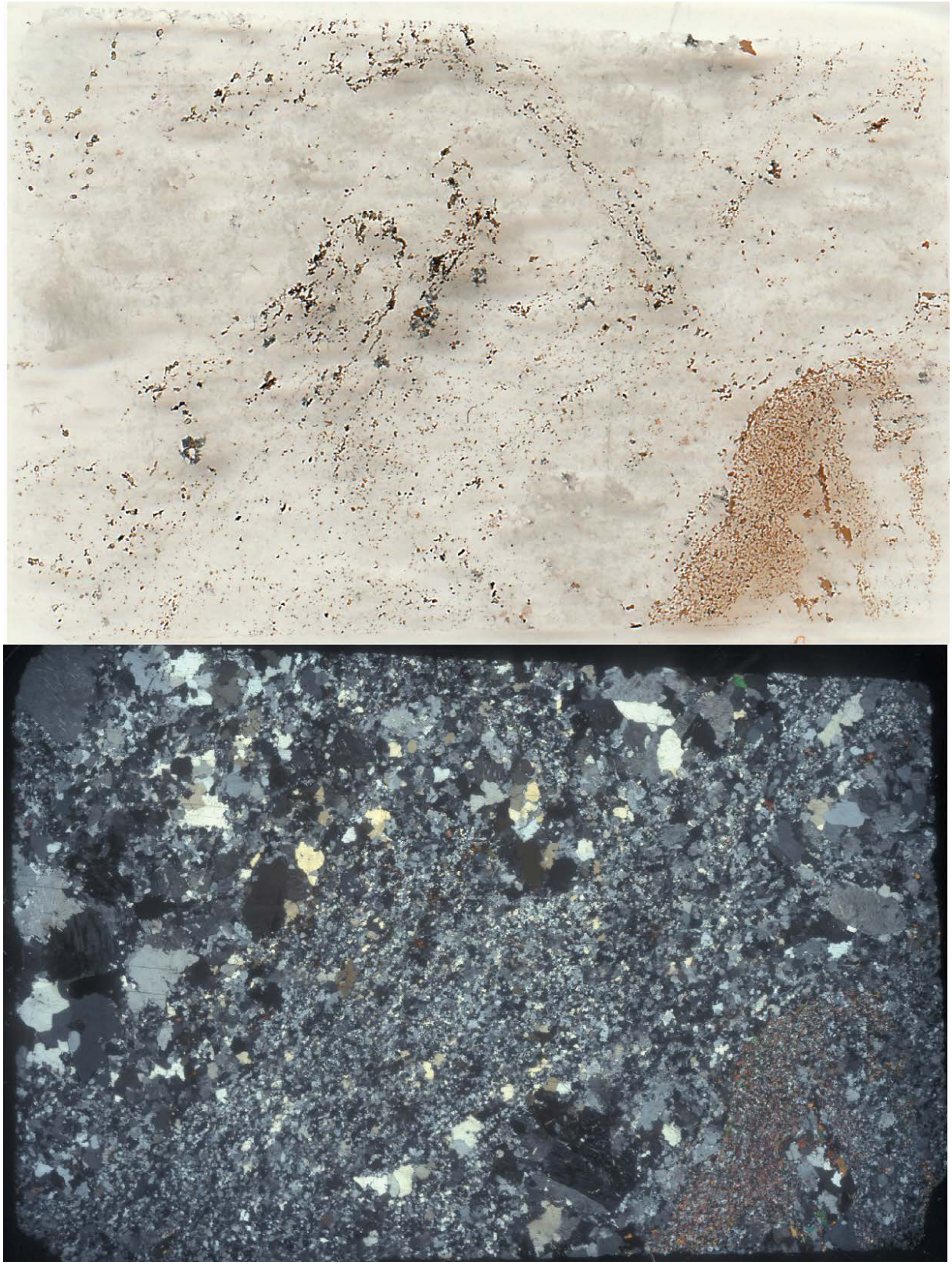

B10-1

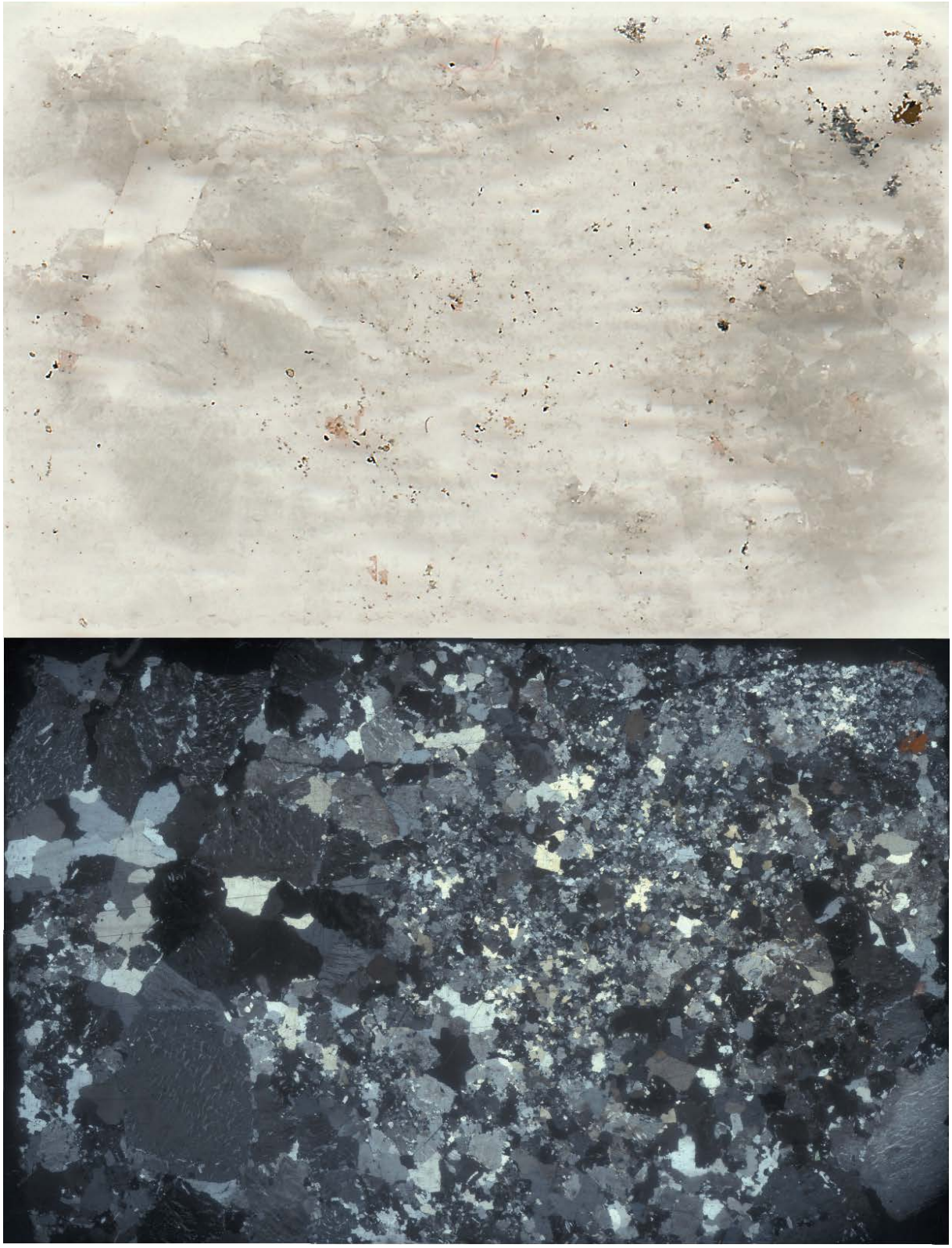

B10-2

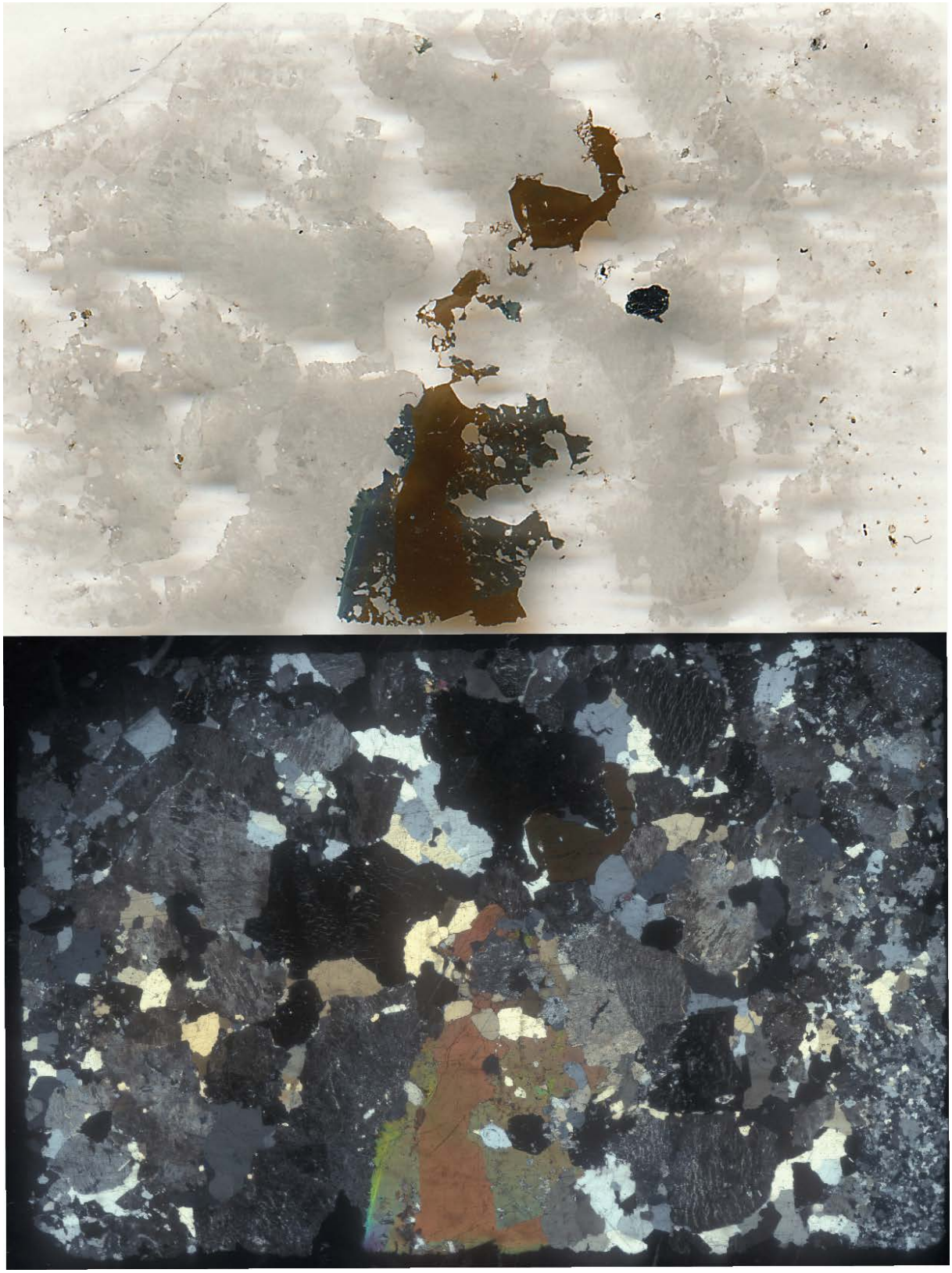

B11-1

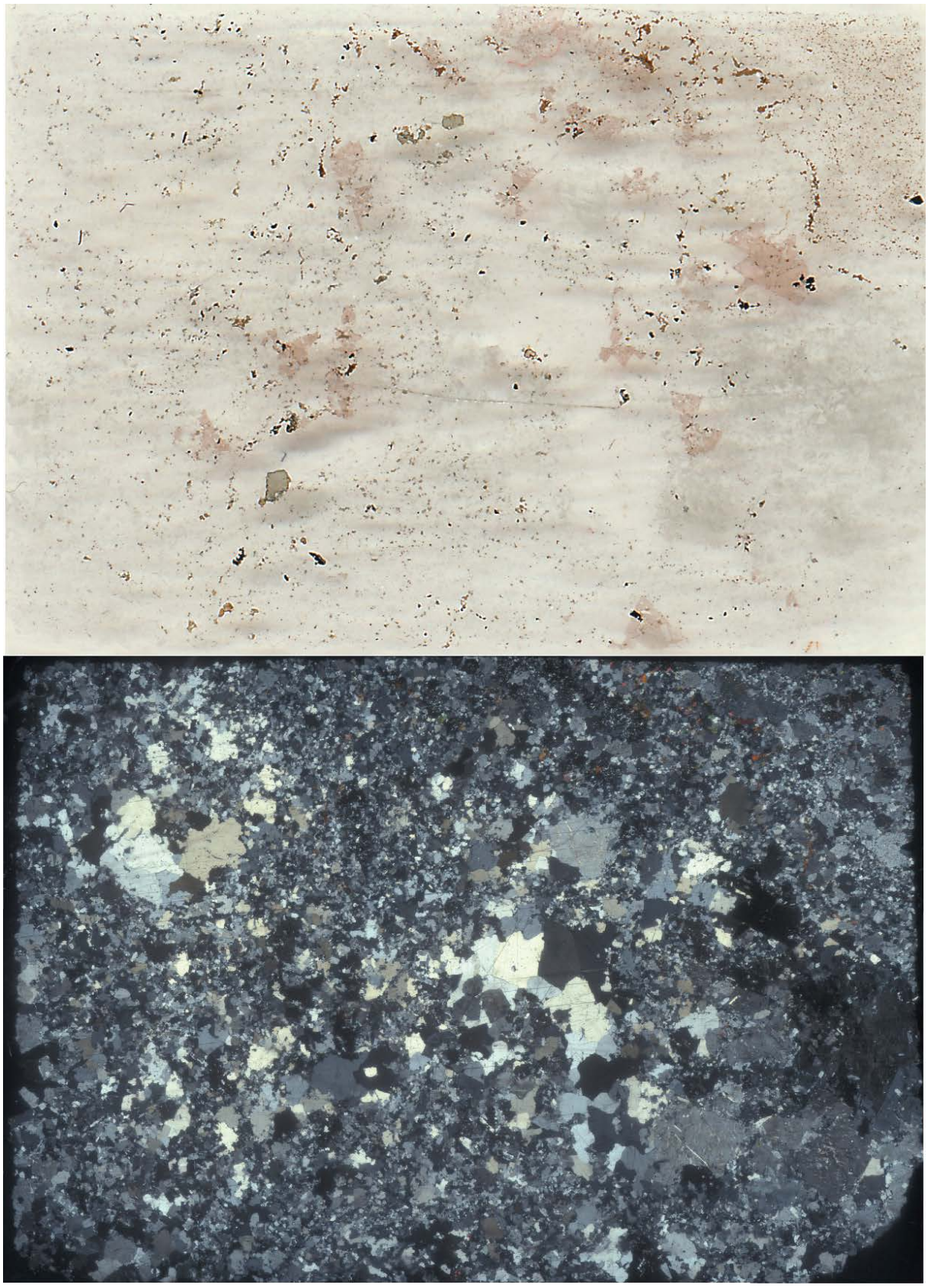

B12-1

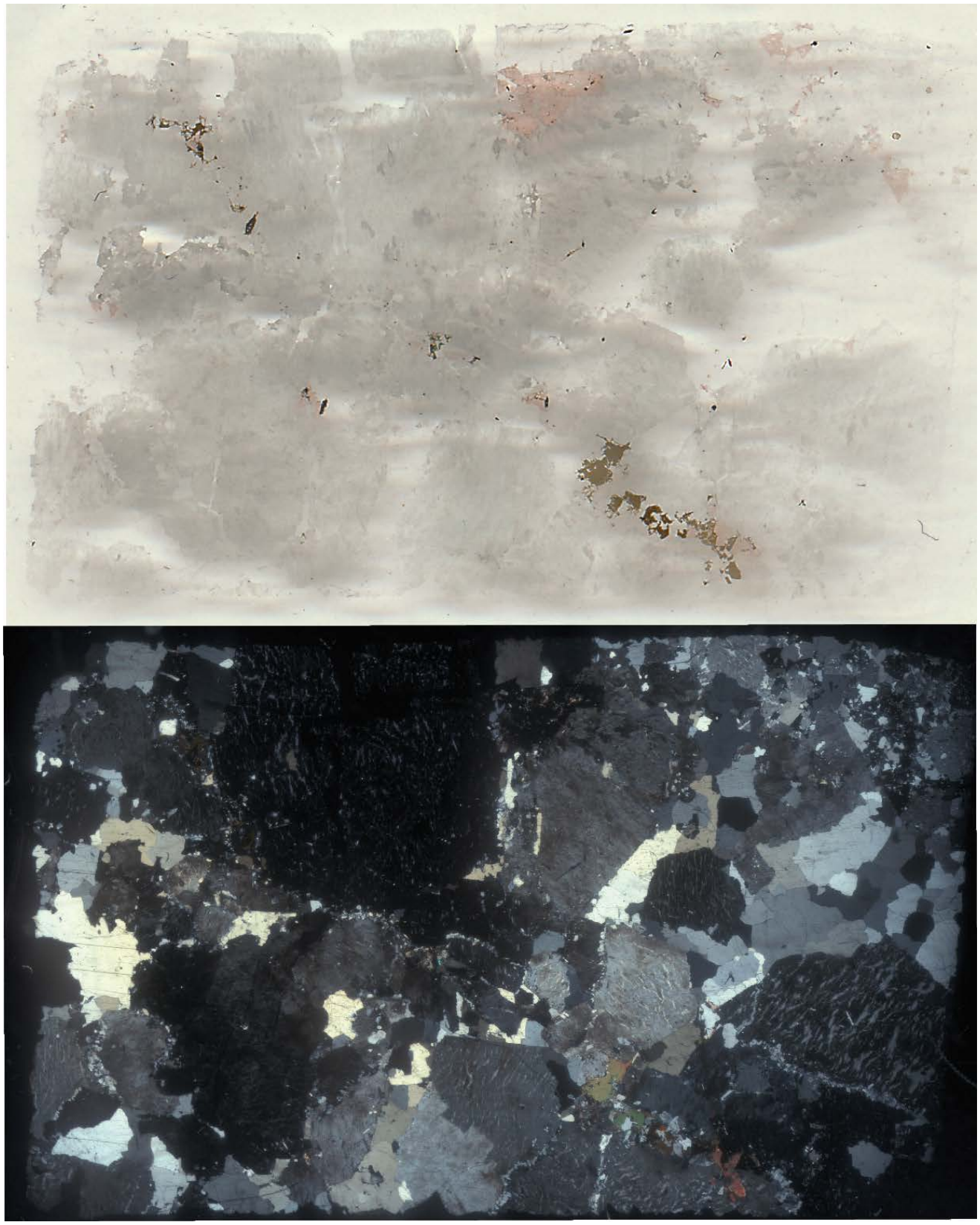

B13-1

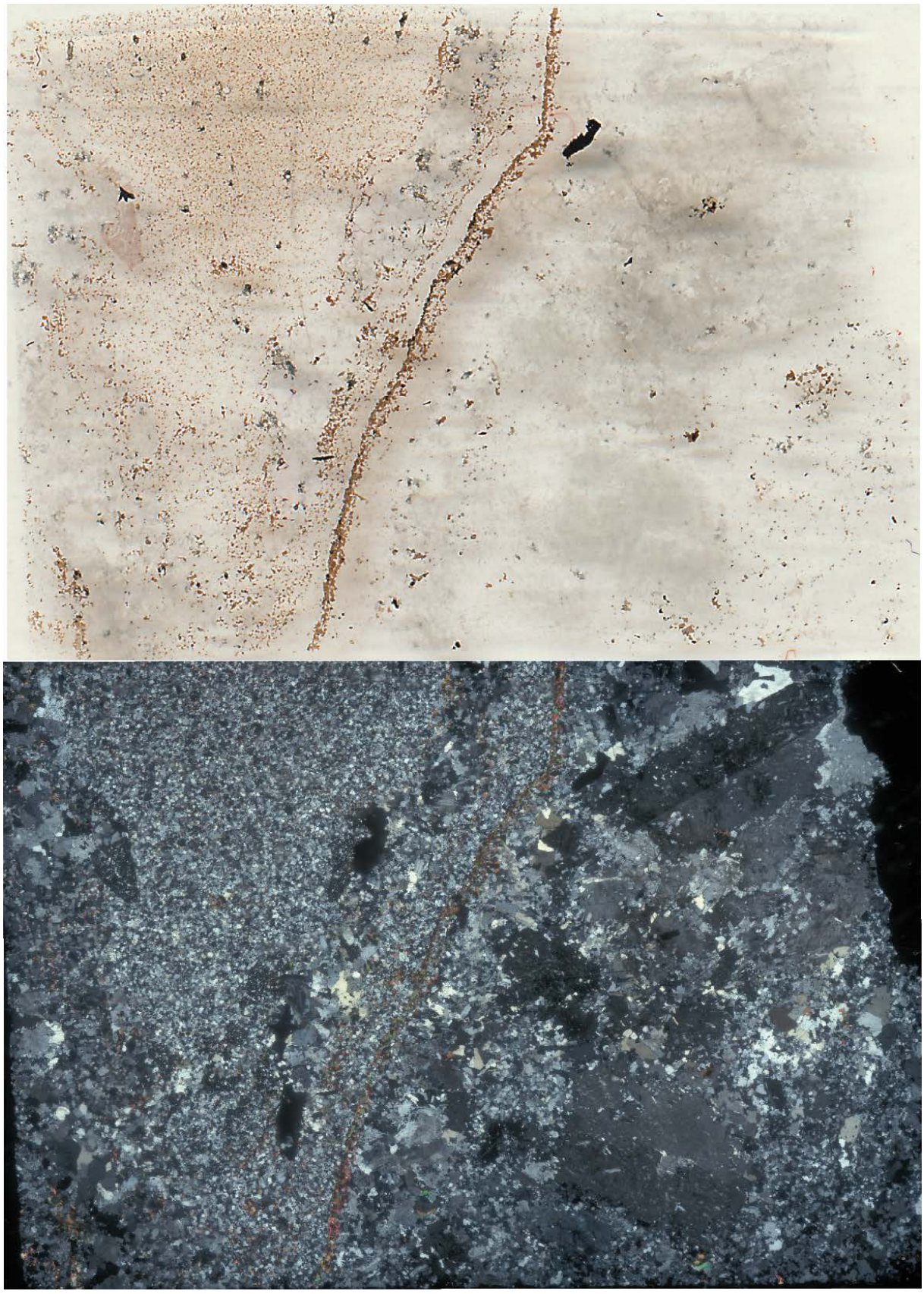

B14-1

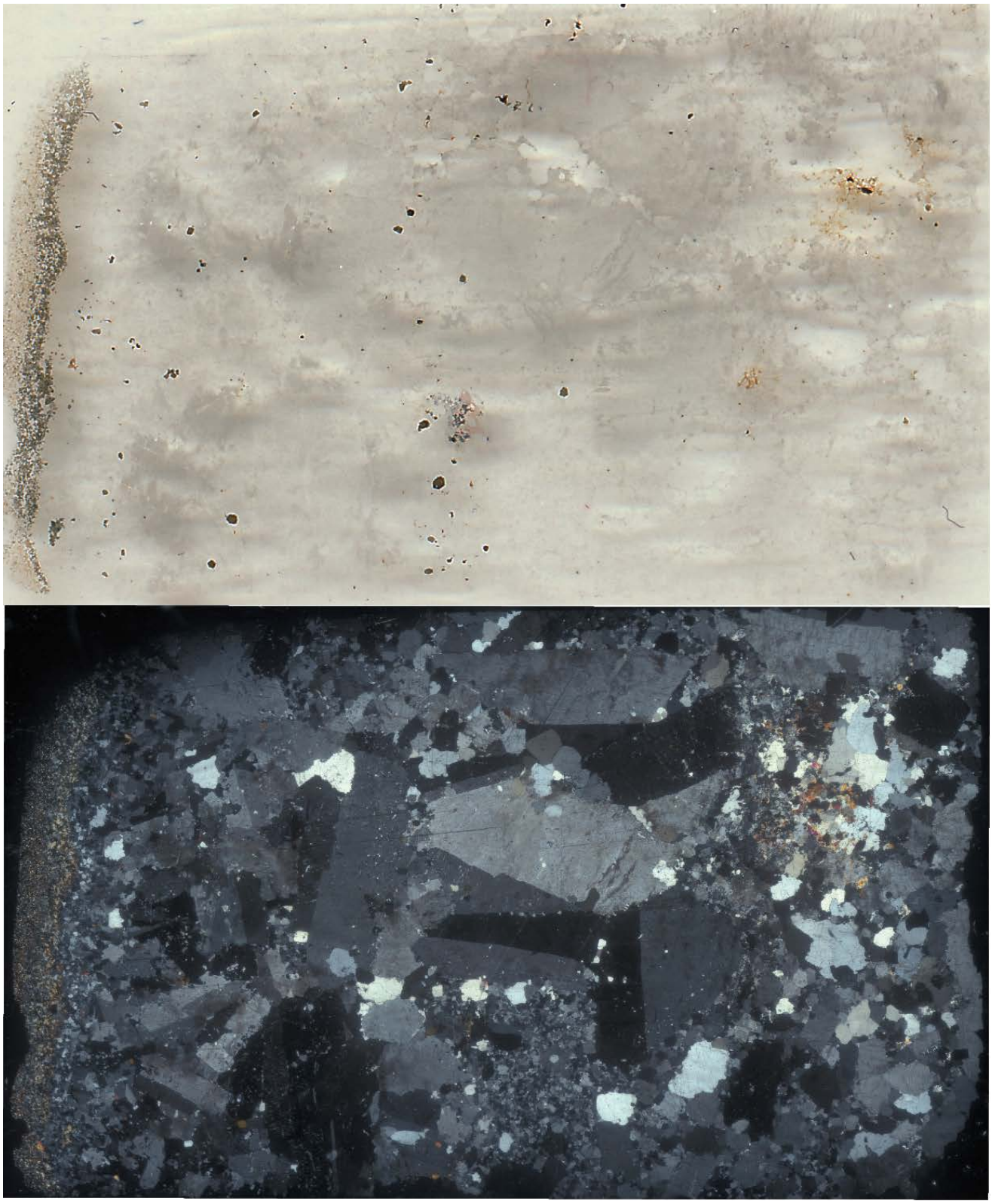

B16-1

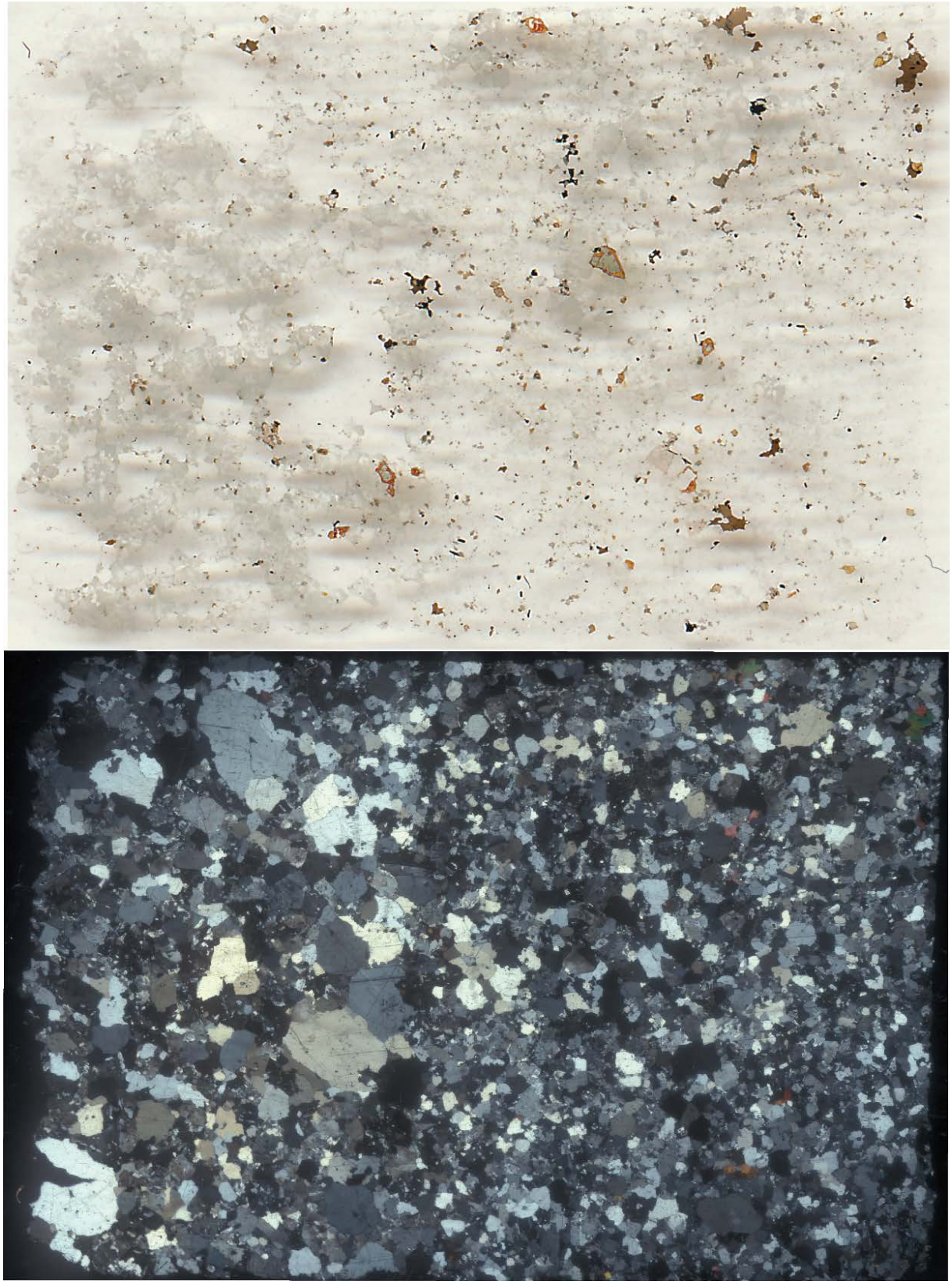

B21-1